

Final Report

on

**Corrosion Assessment Criteria: Rationalizing Their Use
for Vintage vs. Modern Pipelines**

Prepared for

**U. S Department of Transportation
Research and Special Projects Agency
Contract No. DTRS56-03-T-0014**

by

B. N. Leis and X. -K. Zhu

September 2005

BATTELLE
505 King Avenue
Columbus, Ohio, 43201-2693

Acknowledgements

This work was prepared under contract to the Research and Special Projects Agency U. S Department of Transportation, under Contract No. DTRS56-03-T-0014, with Mr. James Merritt serving as the contracting officer's technical representative. Cost-share for this project came through funding from the Pipeline Research Council International (PRCI), associated with their project on Guidelines for Assessing Corrosion Associated with Girth and Long-Seam Welds. Cost share also derived from the Southern California (SoCal) Gas Company (part of Sempra). The PRCI cost share project was directed by their project working group managed on behalf of PRCI by Mr. Damodaran Raghu (Shell Global Solutions US). SoCal's interest was represented by Mr. William Amend (since resigned) and Mr Tom Ishi.

Neither Battelle nor the Government, nor PRCI through its cost-share involvement, nor any person acting on their behalf:

Makes any warranty or representation, expressed or implied, with respect to the accuracy, completeness or usefulness of any information contained in this report or that the use of any information, apparatus, method, or process disclosed in this report may not infringe privately owned rights.

Assumes any liabilities with the respect to the use of, or for damages resulting from the use of any information, apparatus, method or process disclosed in this report.

REPORT DOCUMENTATION PAGE			<i>Form Approved</i> <i>OMB No. 0704-0188</i>		
Public reporting burden for this collection of information is estimated to average 1 hour per response, including the time for reviewing instructions, searching existing data sources, gathering and maintaining the data needed, and completing and reviewing this collection of information. Send comments regarding this burden estimate or any other aspect of this collection of information, including suggestions for reducing this burden to Department of Defense, Washington Headquarters Services, Directorate for Information Operations and Reports (0704-0188), 1215 Jefferson Davis Highway, Suite 1204, Arlington, VA 22202-4302. Respondents should be aware that notwithstanding any other provision of law, no person shall be subject to any penalty for failing to comply with a collection of information if it does not display a currently valid OMB control number. PLEASE DO NOT RETURN YOUR FORM TO THE ABOVE ADDRESS.					
1. REPORT DATE (DD-MM-YYYY) 30-09-2005		2. REPORT TYPE Final		3. DATES COVERED (From - To) 9/9/2003 – 9/8/2005	
4. TITLE AND SUBTITLE: Corrosion Assessment Criteria: Rationalizing Their Use for Vintage vs. Modern Pipelines			5a. CONTRACT NUMBER DTRS56-03-T-0014		
			5b. GRANT NUMBER		
			5c. PROGRAM ELEMENT NUMBER		
6. AUTHOR(S) B. Leis and X. Zhu			5d. PROJECT NUMBER G004831		
			5e. TASK NUMBER 22		
			5f. WORK UNIT NUMBER		
7. PERFORMING ORGANIZATION NAME(S) AND ADDRESS(ES) AND ADDRESS(ES) Battelle 505 King Avenue Columbus, OH 43201			8. PERFORMING ORGANIZATION REPORT		
9. SPONSORING / MONITORING AGENCY NAME(S) AND ADDRESS(ES) US Department of Transportation Research and Special Programs Administration Office of Contracts and Procurement, DMA-30 400 7th Street, SW, Room 7104 Washington, DC 20590			10. SPONSOR/MONITOR'S ACRONYM(S)		
			11. SPONSOR/MONITOR'S REPORT NUMBER(S)		
12. DISTRIBUTION / AVAILABILITY STATEMENT Unlimited					
13. SUPPLEMENTARY NOTES None					
14. ABSTRACT The appearance in the 1990s of corrosion severity assessment criteria derived consistent with plastic-collapse theory presented the industry with an alternative to the criteria empirically evolved beginning in the 1970s. While the industry now had a less conservative alternative to their empirical counterparts, there was no basis to identify which criterion was appropriate. This project has quantitatively evaluated these two sets of criteria to establish which is valid as a function of characteristic geometric features of the corrosion, as well as the vintage, grade and other metrics of the line pipe and the pipeline's service and loading. Consideration was given to the mathematical form of these criteria, their "validation" databases, the corrosion geometry, the line-pipe properties, and other factors through use of numerical and analytical techniques and demonstration full-scale testing.					
15. SUBJECT TERMS corrosion, corrosion severity criteria, line-pipe steel, vintage pipelines, SMYS, UTS, SMTS, plastic-collapse, fracture, fracture mechanics, constraint					
16. SECURITY CLASSIFICATION OF: Unclassified			17. LIMITATION OF ABSTRACT	18. NUMBER OF PAGES 96	19a. NAME OF RESPONSIBLE PERSON
a. REPORT Final	b. ABSTRACT	c. THIS PAGE iii			19b. TELEPHONE NUMBER (include area code) 614-424-4421 or -3976

Standard Form 298 (Rev. 8-98)
Prescribed by ANSI Std. Z39.18

Table of Contents

	Page
Report Documentation Page	iii
Executive Summary	ix
Introduction.....	1
Objectives and Scope.....	3
Definitions.....	3
Approach.....	4
Technical Background and Issues.....	4
Approach Adopted.....	6
Task Descriptions and Report Organization.....	6
Results – Task One: Flow-Stress and Format of the Criteria	8
Format of the 1970s Family of Criteria – NG-18 Equations	8
Format of the 1970s Family of Criteria – B31G.....	8
Format of the 1970s Family of Criteria – API 579.....	9
Format of the 1970s Family of Criteria – Modified B31G and RSTRENG.....	9
Predictive Differences for B31G versus Modified B31G.....	10
Evolution of the 1990s Criteria.....	12
Format of the 1990s Set of Criteria – PCORRC.....	13
Format of the 1990s Set of Criteria – British Gas (BG) LPC-1.....	14
Format of the 1990s Set of Criteria – Det Norske Veritas (DNV) RP-F101	14
Contrasting Predictions for the 1990s Criteria.....	15
Generic Format of the 1970s and 1990s Criteria.....	16
Failure Stress of Defect-Free Line Pipe.....	16
Summary for Task One.....	21
Results – Task Two: Empirical Aspects	22
Implications of Prior Work and Task One.....	22
Early Vintage Database and the Effect of Repeat-Testing	25
Trends in Line Pipe Mechanical Properties	26
Trends in Line Pipe Fracture Properties	30
Trends in Defect Geometry and Measurement Accuracy.....	30
Accounting for Defect Geometry and Implications of Y/T	31

Table of Contents

	Page
Role of Flow-Stress in Lieu of UTS	33
Summary for Task Two	33
Results – Task Three: Analytical Aspects	34
Implications of Prior Work and Task Two	34
Background to Numerical Analyses to Characterize the Role of Constraint.....	35
Numerical Calculations and Constraint Analyses.....	39
The J-A ₂ Solution.....	39
Constraint Correction of <i>J-R</i> Curves for Ductile Crack Growth	44
Application to Prediction Failure Pressure of a Cracked Pipeline.....	46
Implications for High-Constraint Scenarios	51
Summary for Task Three	53
Results – Task Four: Guidelines for Using the 1970s versus the 1990s Criteria	54
Implications of Prior Work	55
Guidelines for Using 1970s versus 1990s Criteria	56
Summary for Task Four	60
Results – Task Five: Full-Scale Demonstration Testing.....	61
Experimental Approach	62
The SSAW Line-Pipe and its Properties.....	62
Line-Pipe Inspection and the Test Pipe	64
The Simulated Corrosion	66
The Experimental Setup.....	67
The Results.....	69
Fractographic Implications of Constraint and Crack-Like Defects	72
Summary for Task Five	78
Summary, Commentary, and Conclusions.....	79
Recommendations.....	81
References.....	82

Table of Contents

List of Figures

	Page
Figure 1. Metal-loss corrosion typical of the extremes found during rehabilitation underway in the 1970s.....	2
Figure 2. Comparison of Modified B31G with B31G illustrating relative conservatism.....	10
Figure 3. Actual failure stress compared to the actual UTS	17
a) early vintage Gr B through X52	
b) 1960s and 1970s line pipe along with recent vintage pipe	
Figure 4. Definitions of flow-stress compared to actual failure stress	18
a) 1.1 x SMYS definition	
b) SMYS + 10 ksi definition	
Figure 5. Trends in predicted failure pressure and defect shape and size.....	20
a) impact of conservative pressure predictions	
b) sensitivity of predicted pressure with defect depth and length	
Figure 6. PCORRC predictions of burst-test failure pressure referenced to the UTS	23
a) database but excluding Gr A and Gr B steels	
b) early vintage database including Gr A and Gr B steels	
Figure 7. Analysis of the vintage database in terms of PCORRC referenced to the UTS	27
a) vintage database including early Gr A and Gr B line pipes	
b) vintage database including early Gr A and Gr B line pipes – but excluding repeat-test cases	
Figure 8. Trends in mechanical properties for vintage large-diameter line pipe.....	28
a) distribution of UTS for some 1950s production	
b) Y/T for the vintage database, excluding repeat-test cases, and archived results	
Figure 9. UTS-based comparison of geometry effects for Modified B31G and PCORRC.....	32
Figure 10. True stress-strain curve of X80 pipeline steel	38
Figure 11. Experimental J-R curves for SENB specimens	38
Figure 12. Experimental J-R curves for SENT specimens	40
Figure 13. Typical finite element mesh for test specimens	40

Table of Contents

List of Figures (continued)

	Page
Figure 14. Distribution of opening stress $\sigma_{\theta\theta}$ along the distance from the crack tip (symbols are FEA results, the lines reflect asymptotic solutions).....	41
a) $a/W = 0.24$	
b) $a/W = 0.42$	
Figure 15. Variation of A_2 with J for SENB specimens considering global bending.....	43
a) the J - A_2 solution without global bending	
b) the modified J - A_2 solution with global bending	
Figure 16. Variation of $J_{0.2\text{mm}}$ and $J_{1.0\text{mm}}$ with constraint parameter A_2 for SENB specimens	46
Figure 17. Comparison of predicted and experimental J - R curves for SENB specimens	47
Figure 18. Comparison of predicted and experimental J - R curves for SENT specimens	47
Figure 19. Finite element mesh for 762mm x 23mm pipe with an axial surface crack of $a/t = 0.5$	48
Figure 20. Distribution of the opening stress determined from the FEA and J - A_2 solution along the distance from the crack tip.....	49
Figure 21. Predicted J - R curve for X80 pipe with a surface crack and compared with those for SENB specimens.....	50
Figure 22. Variation of J -integral with internal pressure for the cracked pipe	51
Figure 23. J - R curve for early-vintage line pipe	52
Figure 24. SYMS and functions of SMYS as a failure criterion for line pipe.....	56
Figure 25. Trends in failure predictions based on SMTS	58
a) actual failure stress vs SMTS for defect-free line pipe	
b) SMTS-based PCORRC predictions for the vintage corrosion database	
Figure 26. Y/T for the pipe (squares) and weld (triangles) compared to typical trends	63
Figure 27. FSE CVN results for the pipe body used in the test vessel	63
Figure 28. Features typical of the SSAW used in early pipe making	65
a) view of the ID surface centered along the weld – a defect and flash are evident	
b) cross-section showing the structure of the SSAW – flash and slight under-fill are evident	
Figure 29. Overview of the three areal defects prior to the first test	65

Table of Contents

List of Figures (continued)

	Page
Figure 30. The three patches of simulated areal corrosion targeted to fail at 1346 psi	68
a) #1 - 1.6-inch long, 70-percent deep	
b) #2 - 2.6-inch long, 50-percent deep	
c) #3 - 10-inches long, 30-percent deep	
Figure 31. Overview of the test vessel prior to adding the pressure transducers.....	68
Figure 32. Modified B31G predictions in comparison to PCORRC in Figure 6a.....	71
Figure 33. Features of the origins for the leak through corrosion defect #1	73
a) view of the leak-path (circled)	
b) detail of the leak-path (circled) from the ID	
c) view of the leak-path broken-open	
d) details of the leak path and opened crack	
e) leak path after opening to illustrate origins (circled) in net wall (dashed lines)	
Figure 34. Features of the origins for the rupture at corrosion defect #2	75
a) view of the rupture from the simulated corrosion defect	
b) fracture plane and cracking (thumbnail feature in rightmost circle – voids in the other circle	
c) voids and nested thumbnails just visible (spatter from torch cutting also evident)	
Figure 35. Features of the origins for the rupture at corrosion defect #3	77
a) view of the rupture from the simulated corrosion defect	
b) fracture plane and OD cracking (thumbnail features circled)	
c) secondary cracking parallel and adjacent to the fracture plane	
d) secondary cracking along, in, and adjacent to the SSAW seam	

List of Tables

Table 1. Defect sizes and projected failure pressures	66
Table 2. Failure conditions versus projected failure response	70

Executive Summary

The appearance in the 1990s of corrosion severity assessment criteria derived consistent with plastic-collapse theory presented the industry with an alternative to the criteria empirically evolved beginning in the 1970s. While the industry now had a less conservative alternative to their empirical counterparts, there was no basis to identify which criterion was appropriate. This project has quantitatively evaluated these two sets of criteria to establish which is valid as a function of characteristic geometric features of the corrosion, as well as the vintage, grade and other metrics of the line pipe and the pipeline's service and loading. Consideration was given to the mathematical form of these criteria, their "validation" databases, the corrosion geometry, the line-pipe properties, and other factors through use of numerical and analytical techniques and demonstration full-scale testing.

Important observations and conclusions follow:

- all criteria had the form: $S_f = S_R \cdot \{f(\text{defect geometry})\}$ – which absent a defect requires S_R be empirically equal the defect-free failure stress, which was the ultimate tensile stress (UTS),
- specific minimum yield strength (SMYS) was uncorrelated with actual failure stress of pipes for early as well as modern vintage data, whereas the UTS correlates very well with the actual failure stress, and was free of bias with grade or vintage,
- a SMYS-based flow-stress rather than the UTS was the primary difference between 1970s criteria and 1990s plastic-collapse-based criteria, accounting for a conservative bias in excess of 25-percent on failure pressure, which unfortunately could cause non-conservative predictions in remaining defect size and in re-inspection interval,
- no practical difference exists in the way defect geometry is quantified by Modified B31G versus 1990s criteria when UTS is used as a reference stress, nor is there a significant difference in predicted failure pressure for the 1970s versus 1990s criteria,
- moderately conservative predictions are achieved by the 1970s and 1990s criteria when referenced to SMTS,
- there is no need to consider toughness limitations absent the effects of constraint, which are manifest primarily as deep smaller diameter pitting,
- constraint within naturally occurring corrosion can cause failure below predicted pressure for 1970s and 1990s criteria, as is evident in the full-scale vintage corrosion database,
- the divergence between collapse and the fracture analysis developed in this work can be used to identify combinations of high constraint and lower toughness that are a practical concern for failure at corrosion.

On the basis of this work, the 1970s and 1990s criteria are mutually compatible; the essential difference being excess conservatism that is not essential in applications where plastic collapse controls failure. A vintage value of SMTS could be used in lieu of the flow stress in such applications. However, where constraint is a consideration, as can develop for some forms of pitting corrosion in lower-toughness steels, caution should be exercised. Constraint does not appear to be an issue for defects shallower than 30-percent of the wall thickness, nor does there appear to be an issue in dealing with steels for which the full-size equivalent Charpy-vee notch energy is 20 ft-lb (27 J) or larger for operation above the brittle-to-ductile transition temperature.

This page intentionally blank.

Corrosion Assessment Criteria: **Rationalizing Their Use for Vintage vs Modern Pipelines**

Introduction

The possibility of metal-loss corrosion on buried steel pipelines could be anticipated from a theoretical perspective long before corrosion degradation progressed to the point that corrosion assessment criteria were needed, as corrosion of steel in contact with moist soil could be anticipated in view of work done by Pourbaix^{(1)*}. Similarly, while not practical or commercially available until the 1950s, now routine practices such as cathodic protection (CP) could be envisioned from the work of Faraday⁽²⁾ many decades before buried steel pipelines were considered to transport hydrocarbons or their corrosion became a concern. Thus, it was not surprising that corrosion was found on pipelines constructed of bare steel line pipe – the usual practice before early over-the-ditch coating schemes became practical.

Prior to the development of early above-ground tools to detect coating defects and corrosion that now form the basis for indirect inspection in external-corrosion direct assessment⁽⁴⁾, companies operating buried steel hydrocarbon pipelines evaluated the possible presence of corrosion using field-digs⁽³⁾ – that today are termed bell-holes. As degradation became progressively worse, and in some cases was found to be quite extensive as evident in Figure 1, it became clear that corrosion could lead to a leak, or rupture depending on the length of the through-wall defect and the properties of the transported product. Companies responded then to the threat of this metal loss the same way they have since the advent of in-line inspection, through rehabilitation. In extreme cases this involved uncovering areas of concern, followed by local reinforcement or replacement, and thereafter recoating and reburial of the pipeline, and site restoration^(e.g.,3,5). Without technical or empirical guidance, companies tended to err on the side of safety in reinforcement or replacement, which drove costs up and stretched the time on the spread where concern motivated additional bell-holes.

The natural gas industry began work to better understand the corrosion threat in the late 1960s and into 1971, with a view to quantify when reinforcement or replacement was needed rather than simply recoating. Archival data^(e.g.,6) indicate the Texas Eastern Transmission Corporation (then one of the large gas transmission companies), was among the first to evaluate the extent of corrosion, which had occurred on their system in spite of its being coated. Eventual degradation of this early over-the-ditch coating led to ingress of groundwater with metal-loss defects formed in those areas, promoting extensive rehabilitation for their long-line system. Early work in the late 1960s focused on the pressure capacity of corroded pipe as compared to the as-designed pipeline, in work done under contract with Battelle. This effort involved burst-testing corroded sections of line pipe, which was facilitated by the amount of corroded pipe available through rehabilitation. By mid 1971, the archives indicate concern for the effects of corrosion on pressure capacity broadened

* Numbers in superscript parenthesis refer to the list of references compiled after the conclusions to this report.



Figure 1. Metal-loss corrosion typical of the extremes found during rehabilitation underway in the 1970s

into the NG-18 Project¹ with the participation of two other gas transmission companies⁽⁷⁾. By mid 1971 almost 50 full-scale tests had been completed on corroded end-capped sections of line pipe⁽⁷⁾.

As time passed and the database grew, attention shifted to empirical trending to establish a corrosion assessment criterion, to help develop rehabilitation plans and to identify what areas needed reinforcement as opposed to cleaning and recoating. This empirical trending was first released in the early 1970s⁽⁸⁻¹⁰⁾ the format of which was largely unchanged in its release as ASME B31G⁽¹¹⁾ in the early 1980s. The empirical corrosion failure database continued to grow, and with time it was clear that the initial criterion was too conservative, a tendency evident in this growing database^(12,13) and in the published literature^(e.g.,14-16). Accordingly, the early 1970s criterion was updated, with “Modified” B31G introduced circa 1989⁽¹²⁾. This reporting also embedded a scheme to address exact area loss that could include adjacent patches of corrosion in the form of RSTRENG^(12,13).

Although Modified B31G was introduced to address excessive conservatism, independent studies continued to indicate growing conservatism for this “modified” criterion. A substantial body of empirical data⁽¹⁷⁻²⁰⁾ evolved that indicated Modified B31G remained quite conservative. Language associated with B31G and the related criteria restricted their use in line pipe whose toughness was “adequate” or “not significant” in the possible failure of the defect – apparently to ensure plastic-collapse controlled failure. Given their apparent roots in plastic-collapse, and

¹ Much of the early work on transmission pipelines was done under the auspices of the American Gas Association (AGA) as part of their project Number 18, which historically has been referred to as Project NG-18. This was the forerunner to the Pipeline Research Committee, which today is the Pipeline Research Council International.

motivated by the desire to understand sources for conservatism and reduce their significance, alternative criteria more formally derived in terms of plastic-collapse began to appear in the 1990s⁽²⁰⁻²⁶⁾. While different in format, predictions by these 1990s plastic-collapse criteria were similar – and clearly less conservative than the empirical family of criteria. This left the industry with two sets of corrosion assessment criteria that while apparently sharing their roots in plastic collapse led to much different results. The choice of which criterion was appropriate would be easy if only one was validated by full-scale testing. Unfortunately, the answer was not so simply determined, as each set of criteria had an extensive validation database.

This report presents results of a project that evaluates the 1970s and 1990s criteria to establish a technical rationale for the coexistence of two apparently conflicting full-scale databases involving metal-loss corrosion, and develop quantitative metrics that identify circumstances for which the above-noted two sets of corrosion assessment criteria are valid and appropriate.

Objectives and Scope

The objective of this project was to quantitatively determine when the two above-noted sets of corrosion assessment criteria are valid to assess corrosion defect severity, and to determine failure pressure. The work scope meets this objective as a function of characteristic geometric features and metrics, as well as the vintage, grade, and other metrics of the line pipe and the pipeline's service and loading.

Meeting this objective will help clarify current vague language like “adequate toughness” as it relates to ensuring plastic collapse controls failure. The benefit of this work for the Office of Pipeline Safety (OPS) and the industry is clarification and simplification of regulatory decisions made in regard to operation and maintenance of vintage pipelines. OPS also will have a clear determination of when true plastic collapse criteria are relevant in applications to so-called modern steels. The federally funded aspects presented in this report complement the Pipeline Research Council International (PRCI)-funded cost share that developed guidelines for corrosion when it lies close to or on longitudinal-seam welds and girth welds. This work is independently published and available from the PRCI⁽²⁷⁾.

Definitions

Terms used to describe aspects of pipeline integrity are defined in codes and specifications but often find inconsistent use in discussing failure behavior, design circumstances, or in describing abnormalities that may exist. The terms noted below and used herein include terms that are variously defined but herein are used consistent with ASME B31.8S⁽²⁸⁾, as are terms involving operation and design defined in 49CFR Parts 192 and Part 195⁽²⁸⁾, which regulate these aspects.

For the present, the design factor and the specified minimum yield stress² (SMYS) are as defined by 49CFR Parts 192 or 195 (e.g., see §105, §107, and §111 of Part 192) and ASME B31.4 and

² Regulations, codes, and specifications tend to use strength, which has units of force, in this usage, whereas this term defines a value with units of force per unit area, which is stress. To be consistent with its use and units, the term stress is used herein. Such is also done for UTS.

B31.8⁽³⁰⁾. The American Petroleum Institute (API) Specification 5L⁽³¹⁾ also includes definitions for SMYS and ultimate tensile stress (UTS), denoted specified minimum tensile stress (SMTS), the latter being adopted for present purposes. To ensure consistent understanding of terms beyond those defined in 49CFR, the ASME codes, and API Specification 5L, the following definitions are introduced:

- Anomaly – any deviation in the properties of the engineered product, typically found by nondestructive inspection. (The term indication is sometimes used in place of anomaly.)
- Flaw – a deviation in the properties or function of the engineered product that is outside of the engineering specifications for the type of service anticipated in design.
- Imperfection – a flaw that an analysis shows does not lower the failure pressure below the specified minimum yield pressure or limit functionality of the engineered product.
- Defect – a flaw that an analysis shows could reduce the failure pressure to below the minimum specified yield pressure or limit functionality of the engineered product.
- Leak – small-scale volume release of product through a typically short narrow breach in the pipe wall.
- Rupture – significant volume release of product through a long broad sometimes gaping breach or axial split in the pipe wall.
- Critical Length – the defect length at which the failure process transitions from leak to rupture.
- Critical Defect – a defect that an analysis predicts could fail below the pipeline’s maximum allowable operating pressure (MAOP), and limit in-service function.
- Transmission Pipeline – by 49 CFR 192.3, a pipeline operating at pressure causing a wall stress over 20-percent of the SMYS.

The language associated with B31G⁽¹¹⁾ as well as other similar criteria such as API 579⁽³²⁾ and related work dealing with locally thin areas⁽³³⁾ (often simply designated as LTAs) restricts their use to defects in areas free of “welds,” “sharp notches,” and “constraint,” in pipe with “adequate” toughness or where toughness is “not significant” in the possible failure of the defect. The limit on use for defects in areas free of welds, sharp notches, or constraint, is rational in that such criteria deal in terms of nominal stresses, with any stress concentration due to the corrosion embedded in the criterion. Apparently because engineers are familiar with these terms, and also toughness, they were not formally defined. However, reference to toughness as adequate or not significant in the possible failure of the defect is typically not familiar to engineers nor is it precise for this use. Recognizing this, these terms are defined subsequently in reference to plastic-collapse.

Approach

Technical Background and Issues

Engineering materials at low stresses exhibit linear-elastic deformation response, where the stretch is proportional to the load, but with sufficient load the limit of this proportional response is exceeded and the material deforms nonlinearly or fails. Because defining a proportional limit depends on the sensitivity of its detection, the concept of yielding was introduced, with the yield stress associated either with an easily detected offset strain or an easily measured strain. Early

structural materials, including some pipeline steels, showed occasionally inconsistent post-yield behavior, because early metals lacked great ductility or occasionally contained defects due to production or manufacturing.

For such reasons, early approaches for the design of civil and mechanical engineering structures used a working-stress design (WSD) philosophy. WSD precludes yielding, sizing components to limit the working stress to a level well below yield. Accordingly, the maximum allowable stress (MAS) is equal to SMYS reduced by a design factor (DF) whose value is less than one:

$$\text{MAS} = \text{SMYS} \times \text{DF} \quad (1)$$

The DF is the inverse of what is often termed a factor of safety (FoS). The DF offsets possible variability in materials and construction practices and in some cases also addresses uncertainty in service conditions and potential loadings. Where as-constructed components cannot be proven by proof-testing prior to service, the DF is logically larger than when it can be “proof-tested,” or where redundancy provides a secondary load path. Design codes for buildings, bridges, and ships, which cannot be proof-tested, often set the value of the DF from 0.6 to 0.66 for tension-loaded components. This is close to the value of 0.72, which has been used to limit the pressure in pipelines, which are proof-pressure tested by regulation, since the first consensus pipeline code emerged in the 1935⁽³⁴⁾.

Over time, the processing of structural materials improved their quality, fabrication processes such as welding were perfected, and inspection technologies were developed to assure quality. Safety inherent in such improvements was recognized and the structural codes evolved to keep pace with these developments. The first major change recognized that materials like steel possess significant and consistent post-yield deformation resistance, with strain-hardening increasing the stress well beyond the yield level, depending on the grade. Codes and standards based on plastic methods of structural analyses^(e.g.,35) and the resulting ultimate strength design (USD) or plastic-design philosophies evolved in regard to plastic-collapse or limit-state concepts that recognized this increased capacity. As time passed, these approaches were recognized as the appropriate practice, and have gradually transitioned into parallel use with WSD for many structural applications^(e.g.,36). Pipelines codes and regulations in selected countries have recently begun or made this transition. The next major change recognized that all loadings considered by codes and regulations do not act concurrently, nor can the structural performance and materials be simply represented by worst-case measures, but rather both were stochastic by nature. These stochastic aspects have been variously addressed by probabilistic design codes and related standards. As for USD, this began in the 1960s and since has gradually spread to various industries^(e.g.,37), recently impacting pipeline design for a few countries.

Until the advent of numerical schemes capable of analyzing the geometrically and physically nonlinear response of structures circa the 1980s, plastic-collapse analyses under USD were historically developed in regard to a “flow-stress.” This use of a flow-stress appears to be a stop-gap measure – introduced to simply account for the reserve strength and associated strain to failure due to strain-hardening beyond the yield stress. The benefit of the reserve strength and strain to failure led to definitions of flow-stress referenced to and marginally larger than the yield stress. For example, B31G defined the flow-stress, S_{fs} , as:

$$S_{fs} = 1.1 \times \text{SMYS} , \quad (2)$$

whereas Modified B31G used:

$$S_{mfs} = SMYS + 10 \text{ ksi (6.89 MPa) .} \quad (3)$$

Equation 3 is identical to the flow-stress used in the so-called NG-18 equations⁽³⁸⁾, which underlay B31G, and the prior trending done for Texas Eastern⁽⁶⁻¹⁰⁾, except that SMYS was used in place of the flattened-transverse-strap yield stress, which for subsequent use is denoted S_y . Other definitions of flow-stress used in structural design and defect assessment more commonly used a function of the yield stress and the UTS, with their average value being typical^(e.g.,39,40). The fact that flow stress typically was defined conservatively in reference to the UTS suggests concern remained that failure might occur before the structural “limit-load” associated with the UTS was achieved. Defining flow-stress conservatively in reference to the UTS might reflect concern that unanticipated fracture control failure, but equally could reflect limitations in technology used to develop plastic-collapse solutions. Of these, the latter is most likely as such conservative definitions of flow-stress underlie some nonlinear fracture-mechanics approaches^(e.g.,39,40).

The advent of numerical schemes capable of analyzing the complex nonlinear structural response circa the 1980s meant corrosion assessment criteria developed in the 1990s assumed that failure by plastic collapse in defect-free pipe occurred at the UTS^(e.g.,21-26). Accordingly it is plausible that differences between the 1970s criteria and those of the 1990s might simply lie in the choice of flow-stress. Unfortunately, it does not appear this simple; as significant full-scale databases exist that justify these apparently incompatible sets of corrosion assessment criteria.

Approach Adopted

The approach and related work plan for this project is conditioned by the two just-discussed observations. First, the possible contributory role of flow-stress to apparently conflict between 1970s and 1990s corrosion assessment criteria must be evaluated. Next, the extent to which databases actually support conflicting corrosion assessment criteria must be evaluated. Finally, technically based criteria must be developed to discriminate when failure at blunt defects assumed to occur by plastic-collapse can occur with fracture as a contributory mechanism. To meet the objective stated earlier, this understanding and the criteria discriminating the role of fracture must be developed and expressed as a function of characteristic geometric features and metrics, as well as the vintage, grade and other metrics of the line pipe and the pipeline’s service and loading.

As databases must be evaluated as must analytical and theoretical aspects, the approach involves a combination of empiricism and theoretical/analytical considerations. Once the role of flow-stress is understood, the databases are rationalized, and a criteria is developed to discriminate when fracture might be a consideration, the results will be expressed in terms of characteristic corrosion features presented as geometric metrics, with the role of vintage, grade and other metrics of the line pipe and the pipeline’s service and loading also evaluated. Finally, full-scale demonstration testing should be completed that while limited in scope confirms the results and defines a plan for broader validation.

Task Descriptions and Report Organization

Key tasks that derive from this approach as implemented range from an empirical focus and an analytical focus, through their integration, and into a task that used full-scale testing to

demonstrate the viability of the results developed. Five technical tasks were used to implement this approach, which culminated in reporting and technology transfer, as follows:

1. Quantify role of flow-stress based on literature database for defect-free pipe failure,
2. Rationalize disparities in validation databases for 1970s versus 1990s criteria,
3. Develop criteria to discriminate when blunt defect failure can be affected by fracture,
4. Develop guidelines for the use of 1970s versus 1990s criteria,
5. Complete demonstration testing, and
6. Reporting/technology transfer.

Task One considered the format of the various corrosion assessment criteria and evaluated the literature and archival data to determine the failure behavior of defect-free line pipe. This task evaluated results for vintage line pipe as well as modern production to determine the failure stress relative to the yield stress and the UTS. Empirical data were trended and contrasted with usual definitions of flow-stress as well as the definitions used in the failure criteria from the 1970s and the 1990s. This data coupled with the format of the criteria considered was used to identify the appropriate flow stress for vintage versus modern line pipe, which was contrasted with the flow stress adopted in the 1970s versus 1990s criteria. This result was used as input to Task Two.

Task Two evaluated the databases argued to support the 1970s versus 1990s criteria using the appropriate flow-stress as identified in Task One. These databases coupled with the appropriate flow-stress were trended to identify characteristic differences that remained between them as a function of the corrosion geometry, vintage, grade, toughness when available, and other metrics of the line pipe and the pipeline's service and loading. These results served as input to Task Four.

Task Three involved a range of numerical and related analyses that help discriminate conditions where blunt defect failure can be affected by fracture. As proposed, this task embedded three technical activities along with formatting the results for transfer to the fourth task. The three technical subtasks included:

1. evaluate the role of constraint as a function of defect geometry and pipeline loading,
2. evaluate the role of constraint as a function of line pipe properties, and
3. develop trends that determine the relevant corrosion assessment practice.

Literature and data on constraint, multiaxiality, yield-to-tensile ratio, and other factors potentially motivating failure by fracture rather than by plastic collapse were evaluated to guide analyses done as proposed for this project. This more comprehensive analytical database was then trended to identify causative factors for failure by plastic fracture versus collapse. Numerical results were developed in reference to corrosion geometry and line pipe flow and fracture properties characteristic by vintage, with other metrics considered including pipeline service and loading history. The results were analytically trended as input to Task Four.

Task Four combined the empirical evidence from Task Two with the numerical and analytical trends generated in Task Four to develop guidelines for the use of 1970s versus 1990s criteria in terms of corrosion geometry, vintage, grade, toughness when available, and other metrics of the line pipe and the pipeline's service and loading.

Task Five involved testing to evaluate the concepts identified and demonstrate their viability. Full-scale testing whose scope targeted these aspects was designed and completed.

The final task involved technology transfer with the deliverables developed, presented, and illustrated in a written report.

The above noted work scope was implemented according to the task order indicated above, and reported for each task in sequence, with the results presented and discussed by task.

Results – Task One: Flow-Stress and Format of the Criteria

Format of the 1970s Family of Criteria – NG-18 Equations

The family of criteria termed herein 1970s criteria has a format that traces to ASME B31G, whose format traces to work released as a proposal to the US Department of Transportation (DOT) in a form similar to that presented to the broader pipeline industry first in 1973⁽¹⁰⁾. The empirical structure for this was the part-through-wall (PTW) NG-18 equation alluded to earlier. The NG-18 PTW equation expressed the wall hoop stress at failure, S_f , as a function of the defect size for axially oriented defects in the form⁽³⁸⁾:

$$S_f = S_{fs} \left[\frac{(1 - A/A_o)}{(1 - A/A_o)(M^{-1})} \right], \quad (4)$$

where A is the actual area of the defect or crack on the longitudinal plane through the wall thickness, $A_o = L \cdot t$ where L is the axial extent or length (of the defect or crack), t is the wall thickness, and M is the bulging factor given as $((1 + 0.6275 L^2 / 2R t - 0.003375 L^4 / (4R^2 t^2))^{0.5})$, where R is the radius of the pipe. As the notation for A and A_o indicates, this form of equation could be applied to defects and cracks without regard for their being blunt or sharp.

Equation 4 shows that defect size was embedded as function of its actual area, and through its effect as bulging that developed locally where the defect or crack weakened the pipe. As indicated earlier, the NG-18 equation used a flow stress, denoted as done earlier as S_{fs} . Both the value of flow-stress and constants used to quantify defect area as a function of length and depth were empirically calibrated in reference to full-scale burst-pressure data that included the effects of geometry. This empirical calibration is as indicated in the flow-stress S_{fs} as defined in Equation 2.

Format of the 1970s Family of Criteria – B31G

The criterion that eventually became a supplement to ASME B31 known as B31G⁽¹¹⁾ circa 1984 developed from an initial proposal to the OPS, designated OPS 192.485, circa 1973. Except for changes viewed appropriate for an “acceptance criterion” developed for “code purposes”⁽⁷⁾, this proposal presented a residual strength criterion for metal-loss defects that was identical to the criterion developed initially for Texas Eastern^(6,9). Changes considered appropriate for code purposes were directed at simplicity and conservatism⁽⁷⁾, or necessity. The necessary change involved replacing the actual measured transverse flattened-strap yield stress, S_y , measured for each test pipe by SMYS, which was driven by the fact that actual yield would be unknown for service defects. Change for the sake of simplicity came by replacing the actual and exact defect

area by a parabolic representation that passed through the deepest point and the ends of the corrosion. On this basis the defect area was defined as $0.67 (dxL)$, where d denotes defect depth. Finally, because some results using the definition of flow-stress developed for Texas Eastern ($S_{fs} = S_y + 10$ ksi) led to values where the FoS was just unity, a slightly more conservative definition of S_{fs} was introduced in the form of Equation 2, apparently to provide safe predictions for short or shallow defects. The final change for simplicity replaced the three-term bulging factor by a simplified form.

The B31G equation has the form:

$$S_f = S_{fs} \left[\frac{1 - (2/3)(d/t)}{1 - (2/3)(d/t)(M^{-1})} \right], \quad (5)$$

where the symbols are as above except M is simplified to $(1 + 0.8 L^2 / D t)^{0.5}$, where D is the diameter of the pipe, and the flow stress is as noted in Equation 2. The proposal to the DOT also expressed this criterion in terms of an acceptable corrosion length in the form:

$$L \leq B (D t)^{0.5}, \quad (5a)$$

where the symbols again are as above with the symbol B embedding the influence of pressure and flow stress and the mathematical complexity of Equation 5 within a look-up chart. Equation 5a and this look-up chart remain in the Code supplement ASME B31G to this day.

Format of the 1970s Family of Criteria – API 579

The equation in API 579 (Level 1 approach) has the form:

$$S_f = \frac{SMYS}{0.9} \left[\frac{1 - (d/t)}{1 - (d/t)(M^{-1})} \right], \quad (5b)$$

where the symbols are as above and M has the form for B31G (i.e., $(1 + 0.8 L^2 / D t)^{0.5}$). In many ways this form is similar to B31G, as is evident for example in $SMYS/0.9 = 1.111 \cdot SMYS$. Thus, this form is not specifically evaluated aside from its implicit consideration in regard to comments on Equation 5.

Format of the 1970s Family of Criteria – Modified B31G and RSTRENG

Use of Equation 5 indicated overly conservative predictions of failure pressure as the full-scale test database grew. As was alluded to earlier, Modified B31G⁽¹²⁾ was introduced to address this conservatism. The functional form of Modified B31G is the same as that of Equations 4 and 5, which is logical as both Modified B31G and B31G have their roots in Equation 4. The essential difference in these equations lies in an alternative definition of flow-stress and recalibration of the function that accounts for the effects of defect geometry with a view to improve predictions and reduce the conservatism. As introduced earlier, the modified flow-stress, S_{mfs} was given as:

$$S_{mfs} = SMYS + 10 \text{ ksi (6.89 MPa)}. \quad (3)$$

This definition is identical to that used in the Texas Eastern criterion except that S_y is replaced by $SMYS$, which is necessary for field applications of such criteria because strap test results are not

available. Recalibration for the then available database led to use of 0.85 (dxL) to define the defect area in place of 0.67 (dxL) used in B31G.

Modified B31G has the form:

$$S_f = S_{fs} \left[\frac{1 - 0.85(d/t)}{1 - 0.85(d/t)(M^{-1})} \right], \quad (6)$$

where the symbols are as above and the flow stress is as noted in Equation 3. The value of M returns to its initial three-term expression as $((1 + 0.6275 L^2 / D t - 0.003375 L^4 / (D^2 t^2))^{0.5})$, when dealing with shorter defects where $L^2/Dt \leq 50$, but was replaced for longer defects with a two-term expression: $0.032(L^2/Dt) + 3.3$.

Along with the target of reducing conservatism in B31G, which led to Modified B31G, the RSTRENG concept grew out of “using Equation 4 repetitively”⁽¹²⁾ (where the correct equation number has been substituted). Thus, RSTRENG has the same functional form as that of Modified B31G.

Predictive Differences for B31G versus Modified B31G

Differences in predicted remaining strength due to the form of B31G versus Modified B31G are illustrated in Figure 2. Because the form of these equations is specific to pipe size and grade,

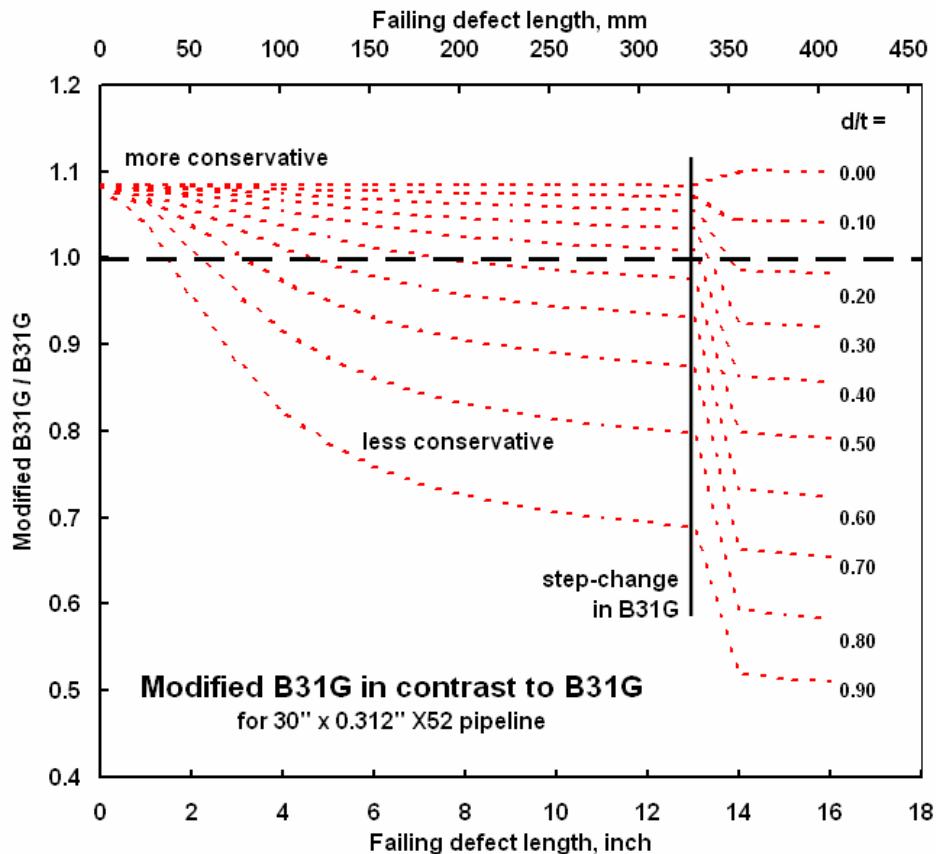


Figure 2. Comparison of Modified B31G with B31G illustrating relative conservatism

Figure 2 has been developed specific to a 30-inch (762-mm) diameter line pipe made of X52 steel with a wall thickness of 0.312 inch (7.93-mm). The y-axis in Figure 2 presents values of corresponding prediction for B31G as a function of the axial length of the corrosion defect, for contours of the maximum depth in the corrosion patch normalized by the wall thickness (i.e., constant values of d/t) shown as dashed lines. Perspective for the practical significance of the defect lengths and depths represented in Figure 2 can be gained in reference to sizes failing in service depending on the DF, or failing a high-pressure hydrotest. Analyses for this pipe geometry and grade according to B31G presented in Reference 26 indicate that all corrosion defects deeper than about 10-percent of the wall thickness and the order of an inch in length or longer would fail a high-pressure test to ~105-percent of SMYS. Likewise, such results show that virtually all defects deeper than 90-percent of the wall thickness, even for operation at the lowest design factor for gas-transmission applications. Similar analyses according to Modified B31G presented in Reference 27 indicate that all corrosion defects longer than several inches and deeper than about 30-percent of the wall thickness would fail a high-pressure test to ~105-percent of SMYS. Likewise, such results show that virtually all long defects deeper than 80-percent of the wall thickness fail by plastic collapse, even for operation at the lowest design factor. It follows that defect depths deeper than about 10-percent of the wall thickness are of practical relevance to discussion of the results in Figure 2.

If Modified B31G were equally conservative as compared to B31G, all depth contours would lie at a y-axis value of unity for all values of defect length. In contrast, because Modified B31G was developed as a less conservative alternative to B31G, all contours in Figure 2 would be expected to lie below a y-axis value of one. And if the recalibration of Modified B31G achieved more or less uniform reduction in this conservatism, such trends would cluster close to each other at a more or less constant value of the y-axis less than one. However, as can be seen from the trends in Figure 2, Modified B31G is anything but consistently less conservative than B31G. Indeed, for defects shorter than 8 inches (~203 mm) with depths less than 50-percent of the wall thickness, Modified B31G is more conservative than B31G, and increasingly so as the defects become shorter and shallower. In contrast, for long defects deeper than 50-percent of the wall thickness the recalibration as Modified B31G does achieve more conservative predictions as compared to B31G. Somewhat surprisingly, Figure 2 shows that the amount of conservatism embedded in Modified B31G is strongly dependent on defect depth and length, rather than constant. Curiously, this depth dependence shows the conservatism is decreasing as defect depth and length increase – which is opposite to what would be logically desired.

While Figure 2 is specific to a 30-inch (762-mm) diameter line pipe made of X52 steel with a wall thickness of 0.312 inch (7.93 mm), the trends evident there apply across all combinations of pipe properties. Of these trends, the clear and strong effects of the step change in the definition of B31G on conservatism will shift somewhat as it depends on the pipe diameter and wall thickness, and will shift to shorter and shallower defects as these parameters diminish. A final point to note is that both of these corrosion criteria simulate the response of such defects only in terms of the defect length and depth, which means any effect of defect width is ignored.

Finally, while the introduction of Modified B31G was directed at a reduction in conservatism as compared to B31G, this recalibration appears to broaden the spread between the failure trends for these criteria as a function of defect length and depth, and a conservative shift to higher failure pressure for shorter and shallower defects. The concurrent empirical recalibration of the effect of corrosion geometry and the definition of flow stress between Equations 5 and 6 thus

appears more a consideration of an expanded database than it does consideration of the perceived need to reduce conservatism in Equation 5. This observation is supported by the work-scope presented in developing Equation 6, and in reporting its recalibration⁽¹²⁾. Archived reports of burst-testing done at Battelle in the 1980s^(e.g.,41) in support of remediation projects for pipeline companies suggest the evolution of Equation 6 more repeated the process that led to Equation 5 (but with a broader database) rather than assess why Equation 5 was conservative.

Use of an expanded database in evolving Equation 6 is significant to meeting the objective of this project, as it reflects co-mingling of burst pressure data for pipelines with differing vintages, as one can reasonably anticipate remediation driven by degradation due to corrosion that progresses with time. Thus, burst-testing started in the mid to late 1960s is likely to involve much earlier vintage pipelines than would burst-testing done in the mid to late 1980s. This possibility that B31G began to appear conservative because its roots lay in empirical trending of early vintage pipelines that as time passed involved increasingly recent construction will be evaluated subsequently. Suffice it here to note the recalibration as Modified B31G involved the order of 100 full-scale tests in contrast to the ~50 burst-test results that are embedded in the Texas Eastern calibration that underlies B31G. This database had expanded still further by the time the continued validation of RSTRENG appeared – although much of that targeted effects such as complex corrosion shapes^(12,13).

Evolution of the 1990s Criteria

The advent of numerical methods capable of dealing with nonlinear structural response allowed more general understanding of the failure process at patches of corrosion. It also facilitated numerical simulation of a burst test. As this understanding developed and a simulated burst-test database developed, the results were trended analytically much the same as had been done decades earlier for physical testing. This trending of numerical experiments gave rise to alternatives to the mathematically simple criteria that have evolved since the 1970s. Several alternative criteria were developed in this manner⁽²⁰⁻²⁶⁾, while another had its roots in a less complex applied-mechanics approach⁽¹⁸⁾.

Each numerically-based trending made use of a database that reflected comparable numerical practices that involved nominally similar assumptions, with all considering collapse at a stress equal to the UTS or a value related to it³. Accordingly, the resulting criteria developed by trending these numerical databases could be anticipated to produce similar failure pressure as a function of the size⁴ of the corrosion patch. The only essential came in the trending of their numerical results. In this phase, some chose to retain the format of the NG-18 PTW equation (i.e., Equation 4), while others chose to abandon the form of Equation 4 for various reasons, as follows.

³ Practical adaptation of such numerical solutions where the UTS is known must default to the SMTS, as the UTS is never known in blind field applications. Thus, practical forms of this equation and its contemporaries would replace the UTS by SMTS. Where equations have been empirically calibrated to SMTS, they are so presented. When calibrated to UTS, one can anticipate a constant designed to shift from UTS to SMTS would exist as a pre-multiplier to any term used to account for the effect of geometry.

⁴ Such analyses generally considered length and depth, with width explored to a lesser extent.

Format of the 1990s Set of Criteria – PCORRC

In trending their numerical database, Battelle⁽²²⁾ chose to abandon the form of Equation 4 for several reasons. First, in reviewing archived burst-test results from the 1960s it was apparent that several burst tests of corroded pipe removed from service failed at hoop stress very close to the measured UTS specific to the pipe tested^(e.g.,8). Second, analysis considering issues such as end-cap loads in burst tests, local multiaxial stress effects and multiaxial load-induced constraint, yield-to-tensile ratio, and the UTS as a reference stress concluded failure at corrosion should occur locally at the UTS unless fracture intervened prior to reaching the UTS⁽²¹⁾. Reference 21 also evaluated failure in defect-free line pipe as a reference against which to compare historical definitions of flow-stress. This analysis done in regard to vintage line pipe showed that failure in defect-free pipe occurred at a hoop stress almost coincident with the UTS, suggesting that the empirical value of flow-stress is equal to the UTS. Finally, Battelle chose to abandon the form of Equation 4 because it coupled *concurrent* empirical trending of both flow-stress and defect geometry and did so in regard to a database that ignored the results of defect-free failure testing.

The resulting format chosen was:

$$S_f = S_R \left(1 - \frac{d}{t} \left(1 - \exp \left(C_1 \frac{L}{\sqrt{Rt^*}} \right) \right) \right) \quad (7)$$

where t^* is the (minimum) remaining wall thickness below the defect, the defect-free reference stress, S_R , is the UTS, and the curve-fitting constant C_1 determined by trending the then available numerical results was found to be -0.157 in the initial reporting of this criterion, with values as small as -0.222 considered subsequently as additional numerical work became available. Note that PCORRC does not explicitly consider “bulging” or any stress concentration due to it, as such effects are implicit in C_1 .

This equation was labeled PCORRC as it was introduced, which followed in reference to *Pipeline CORROsion Criterion*. Battelle has compared predictions of this collapse-based model with their historical database, which includes data from the early vintages and lower-strength grades used in calibrating B31G⁽¹¹⁾ through that for Modified B31G⁽¹²⁾, and the continuing validation of RSTRENG⁽¹³⁾, as well as that developed and reported for modern grades by BG⁽²⁶⁾. Good predictions that scattered uniformly and tightly around a one-to-one trend were found for all results when the value of S_R was taken as UTS, except for selected early-vintage pipe data, as will be discussed shortly. When the SMTS was used in lieu of the UTS, as must occur in practice, the data fall close to a one-to-one, except with a slightly conservative bias.

No consideration was given to statistically optimizing this criterion in reference to the full-scale empirical database used to calibrate B31G or Modified B31G. This choice was motivated by the observation that selected portions of this data appear inconsistent with a collapse criterion and might involve some role for fracture^(21,23,25). This situation was specific to selected burst tests involving the early vintage Gr A and Gr B pipe. Selected tests with these grades involved reuse of corroded test sections after patching or cutouts, and other aspects considered to limit their consistency with plastic-collapse-criteria. Using data where fracture has a possible role is inappropriate for empirical trending in criterion like B31G as well as for optimization of analytically trended criteria like PCORRC. It is inappropriate for empirical curve-fitting because data possibly involving fracture do not satisfy the requirement of “adequate” toughness or that

toughness is “not significant” in the possible failure of the defect. It is clearly inappropriate for analytically trended criteria that reflect plastic-collapse, as fracture can occur prior to locally achieving the UTS.

Format of the 1990s Set of Criteria – British Gas (BG) LPC-1

Unlike PCORRC, the BG trending of their numerical formulation used a format comparable to Equation 4^(20,42). The related early literature does not indicate empirical or other consideration of failure in defect free pipe, and indeed predictions were not made in the early reporting for cases where tests were done on such pipe. The BG criterion expressed as a simple curve-fit is referred to as LPC-1, as BG chose to present their work in technology levels comparable to the three tiers adopted by API 579, and elsewhere.

The LPC-1 has the form:

$$S_f = C_2 S_R \left[\frac{1 - (d/t)}{1 - (d/t)(M^{-1})} \right], \quad (8)$$

where the symbols are as above, with the constant $C_2 = 2 / (D/t-1)$, and S_R taken as SMTS or 90-percent of the standard tensile UTS. For all defect lengths the value of $M = 1 + 0.31 L^2 / D t$ – with $d/t \leq 0.85$.

While there was discussion of the generic functional form of this criterion, no rationale was indicated for retaining the basic form of Equation 4. The BG criterion was statistically tested and optimized in reference to an empirical burst-test database comprising a mix of modern steels for which plastic collapse is certain to control failure, and the historical Battelle database that included a mix of earlier vintages and lower-strength grades. Recognizing that the B31G criterion began to be considered conservative as the empirical database grew increasingly modern, as alluded to earlier, the decision to optimize a numerically trended criterion using a mixed empirical database is somewhat curious. But, as the constants were so determined, good predictions for this database are anticipated and were indeed reported for newer as well as many vintage line pipes.

Format of the 1990s Set of Criteria – Det Norske Veritas (DNV) RP-F101

As with the BG formulation, DNV trended results of numerical analysis (apparently available via their membership in a group program and likely also some DNV-developed full scale burst-test data^(43,44)) in a format comparable to Equation 4⁽²⁴⁾. The DNV criterion in this format is simply referred to as DNV-RP-F101 – Corroded Pipelines in reference to their document presenting this formulation⁽⁴⁵⁾. Like BG, DNV chose to present their work in a format comparable to the NG-18 PTW equation, which thus has the form:

$$S_f = C_3 S_R \left[\frac{1 - (d/t)}{1 - (d/t)(Q^{-1})} \right], \quad (9)$$

where the symbols are as above, $C_3 = (D - t)^{-1}$, and S_R is taken as the UTS. As for the BG criterion, the value of Q that symbolically replaces M was taken as $1 + 0.31 L^2 / D t$.

Discussion of the functional form of this failure criterion⁽⁴⁶⁾ indicated the decision to retain this form involved the current acceptance of this form in the Code literature as B31G. As with BG, the DNV criterion involves some optimization in reference to an empirical burst-test database. While not clear, the DNV database likely complements the BG database with empirical DNV results, which as with LPC-1 opens to question the practice of optimizing an analytical criterion by fitting to empirical trends. Again, because the constants were determined through a mix of analysis tempered by empiricism, good predictions for the underlying database are anticipated and indeed are reported.

Contrasting Predictions for the 1990s Criteria

The mathematical form of the 1990s criteria whose roots lie in collapse-based numerical analysis is comparable for Equations 8 and 9, whereas Equation 7 is quite different. Prior work⁽²⁶⁾ has compared Equations 7 and 8 extensively, while more recently they have been statistically evaluated along with the 1970s criteria and others by comparison to the full-scale database for corroded pipe burst tests⁽⁴⁷⁾.

Reference 26 found predictions by Equations 7 and 8 to “give similar failure predictions.” Like PCORRC, the BG LPC-1 equation gave non-conservative failure predictions for several Gr B tests, even though the BG equation included some optimization in regard to the full-scale test database. This conclusion regarding prediction problems with a collapse-based formulation was cited previously in Reference 23, and repeated again in broader forum in Reference 25. Even RSTRENG was found in Reference 26 to make non-conservative failure predictions for some Gr B pipe tests, albeit only a few. Finally, it was noted that the Gr B pipe material apparently had a high brittle-ductile transition temperature that is above the normal design temperature for buried transmission pipelines.

Reference 47 compared Equations 7-9 along with six other such formulas in terms of a full-scale database for corroded-pipe burst tests. Of the 215 test results tabulated during the continued validation of RSTRENG, a total of 48 results were culled from the database. While this culling generally reflects results that were inappropriate, two defect-free burst tests were removed without apparent reason – possibly implying such criteria are not perceived appropriate for shallow defects nor should they be accurate as defect size tends to zero. In spite of established difficulties in reference to the early vintage data, which underlay the conservatism in B31G to be addressed by Modified B31G, all data was pooled without regard to vintage, nor was analysis done to assess their effect on the results.

Statistical comparisons of predictions made in comparison to full-scale data by definition favor the empirical curve-fits to the database – as the database being “predicted” is the basis for their functional form and “tuning” in terms of curve-fit constants. Accordingly, criteria like Modified B31G should fit exactly or be most accurate, aside from scatter inherent in the database. In contrast, models derived analytically will be more challenged. That said, the quality of the tuning for the empirical criteria that accordingly are expected to do well was evident throughout the range of statistical metrics considered although B31G was least successful of these based on the “average” statistic. The analytically-based equations noted here as Equations 7 and 9 did equally good as compared to Modified B31G in terms of the “average” statistic reported. However, these analytically-based criteria were slightly less successful in some statistical metrics, which is not a surprise as such models were not “tuned” to match this database. Curiously, Equation 8 was excluded from this evaluation.

Generic Format of the 1970s and 1990s Criteria

Whether based on an empirical trending or theoretical plastic-collapse analysis for blunt defects or fracture-mechanics analysis for sharp defects, failing defect sizes depend on two parameters. One is the wall stress in defect-free pipe while the second is the defect orientation, size, and shape. Equations 4 to 9 express these two parameters in the same simple generic mathematical form:

$$S_f = C \cdot S_R \cdot \{f(\text{defect geometry})\}. \quad (10)$$

As before, S_f is the hoop stress at failure, C is a constant that can involve pipe geometry or FoS, S_R is a reference stress, and $f(\text{defect geometry})$ embeds the effects of the defect geometry. In this form, the value of $f(\text{defect geometry})$ tends to unity as the size of the defect decreases to zero. Mathematically, when the defect has no effect (as occurs for defect-free pipe) the term $f(\text{defect geometry})$ is by definition one. In turn, this means that the product of C and S_R must be equal to the UTS, or empirically equal to the hoop-stress in a burst-test of defect-free line pipe.

It follows that Equation 10 should not be empirically trended without explicit consideration of results for defect-free pipe, and that the product of $(C \cdot S_R)$ should not be independently selected nor mutually determined empirically with the term $f(\text{defect geometry})$. However, past empirical practice has involved the independent selection of the product of $(C \cdot S_R)$, which has been done without regard for trending defect-free burst-testing. Moreover, the effects of defect geometry in the function, $f(\text{defect geometry})$, have been empirically trended subject to a flow-stress whose value does not necessarily reflect the failure of defect-free pipe.

It is possible that the decision to embed the effects of a flow-stress whose value does not match the failure of defect-free pipe in $f(\text{defect geometry})$ as has been historical practice contributes to the apparent difference in the 1990s criteria as compared to the 1970s criteria, and the uncertainty as to which criteria is appropriate and when. This aspect is evaluated next relative to the hoop stress at failure for defect-free line pipe.

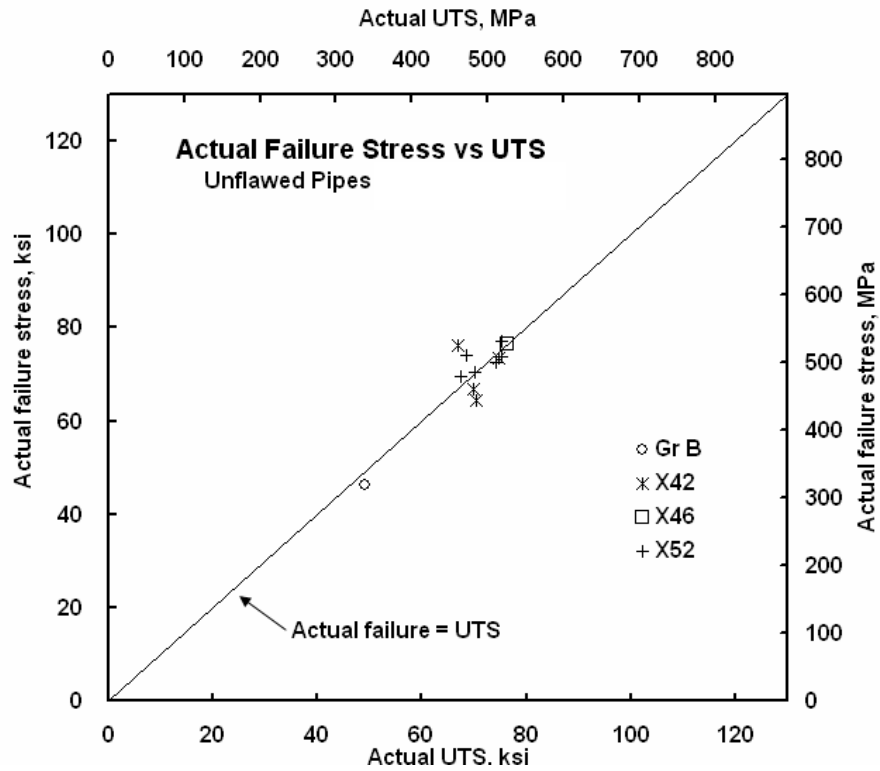
Failure Stress of Defect-Free Line Pipe

The mathematical form of Equation 10 generic to Equations 4-6 (empirical models of the 1970s), and Equations 7-9 (1990s numerically-based approaches) requires the product of C and S_R be equal to the UTS for cases trended to collapse analyses, or the hoop-stress in burst-tests of defect-free line pipe for empirically calibrated models. This section presents empirical results for burst-testing of defect-free line pipe as the basis to evaluate a functionally appropriate flow-stress, and by inference the value of the product of C and S_R . Battelle archival data for vintage line pipe and for modern line pipe provide the basis for this comparison.

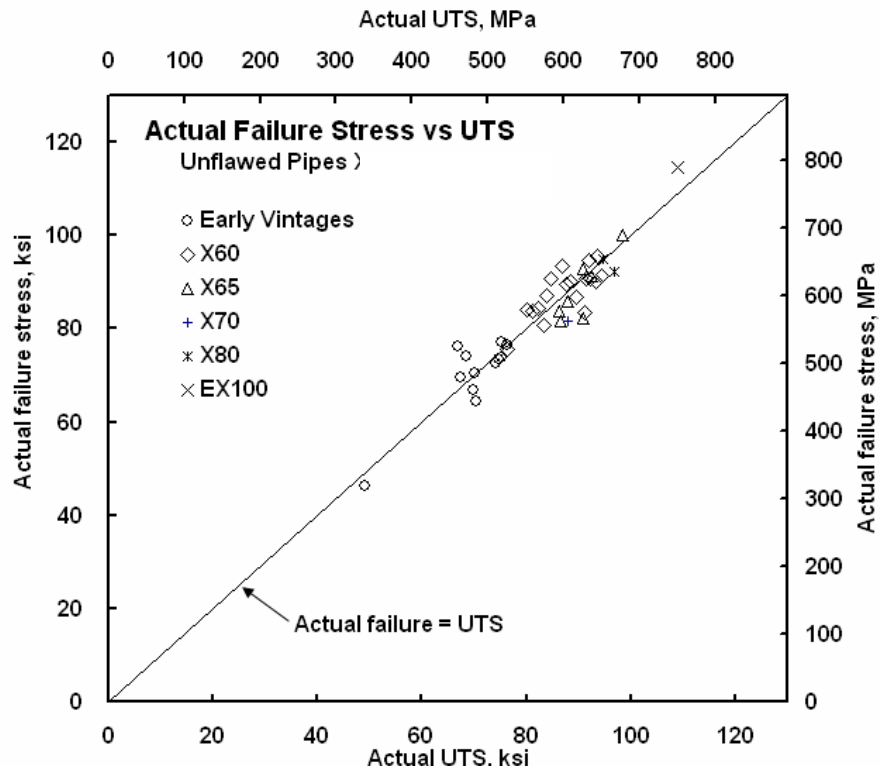
Figure 3 trends the failure stress in burst-testing defect-free line pipe presented on the y-axis as a function of the corresponding value of the UTS⁵ shown on the x-axis, covering Gr B through a 1960s 100 ksi yield quenched and tempered (Q&T) steel identified herein as EX100⁶. Figure 3a

⁵ Round-bar results were found in the archives in many cases, and are the common basis for the UTS in this figure.

⁶ The Q&T EX100 would experience additional tempering of the plate next to the longitudinal seam and the end-cap welds due to the thermal cycle of the weld, this pipe burst at a hoop stress approaching the UTS for this case.

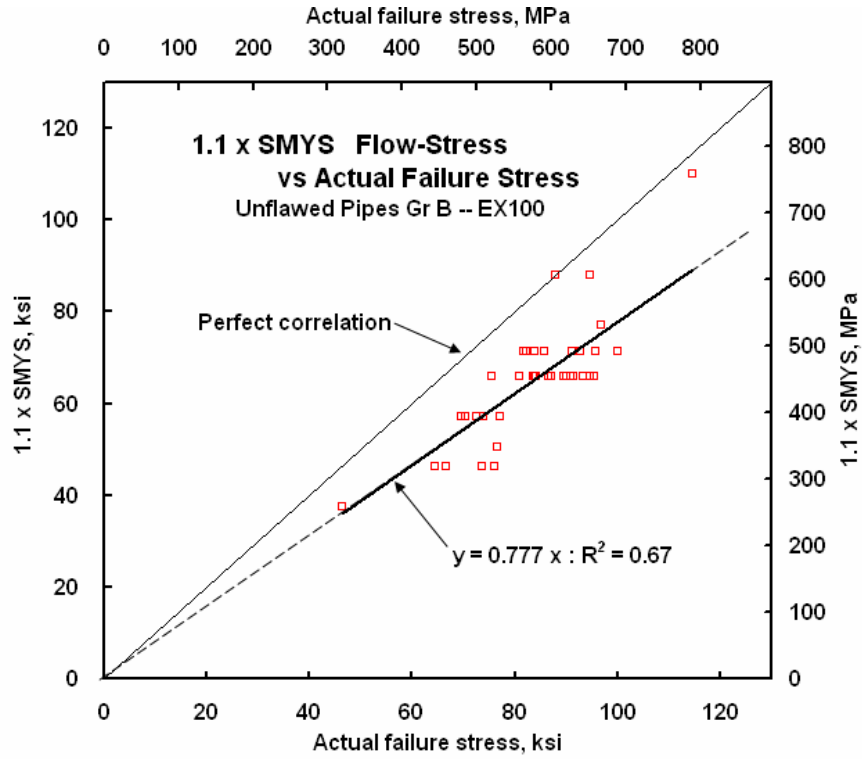


a) early vintage Gr B through X52

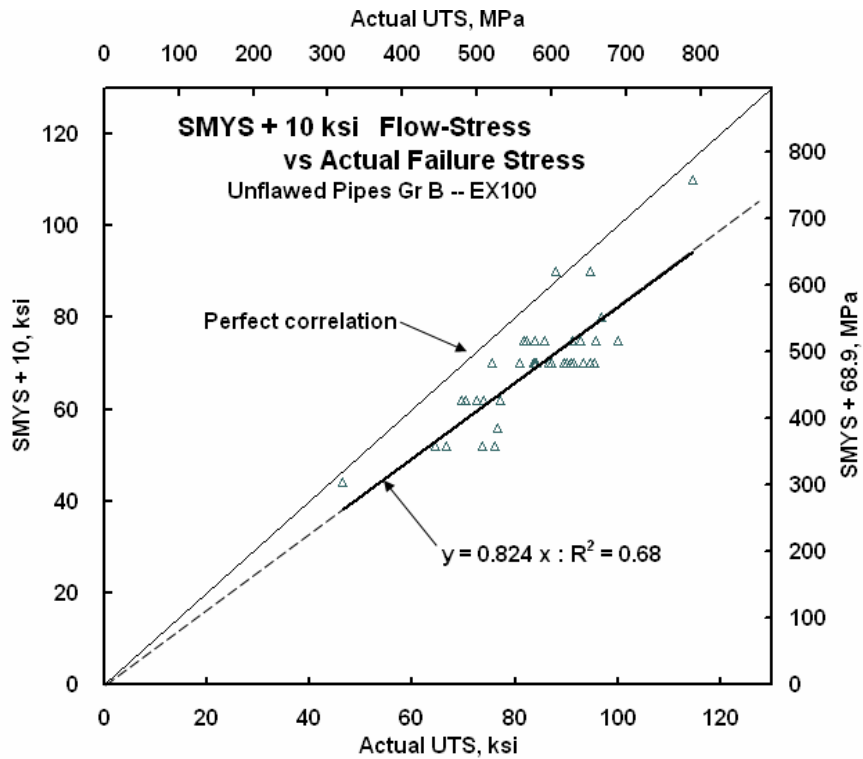


b) 1960s and 1970s line pipe along with recent vintage pipe

Figure 3. Actual failure stress compared to the actual UTS



a) 1.1 x SMYS definition



b) SMYS + 10 ksi definition

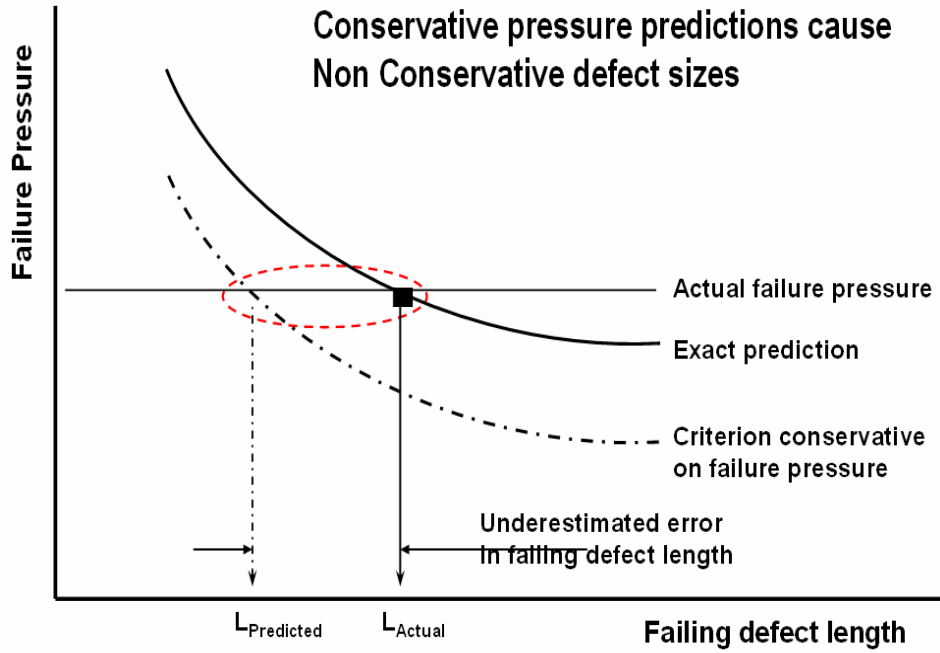
Figure 4. Definitions of flow-stress compared to actual failure stress

covers results from Gr B through X52 with 12 results that are specific to early vintage line pipe, as these data reflect archives for testing on line pipe removed from service for pipelines being rehabilitated prior to 1975. Such steels could be considered typical of the early-vintage steels evaluated in calibrating B31G. Figure 3b adds 29 additional results to the vintage line pipe that are included for reference in this figure being shown as open circular symbols. The additional data represents 1960s and 1970s vintage X60 and X65, along with results for higher-strength steels produced from circa 1985 through 1997.

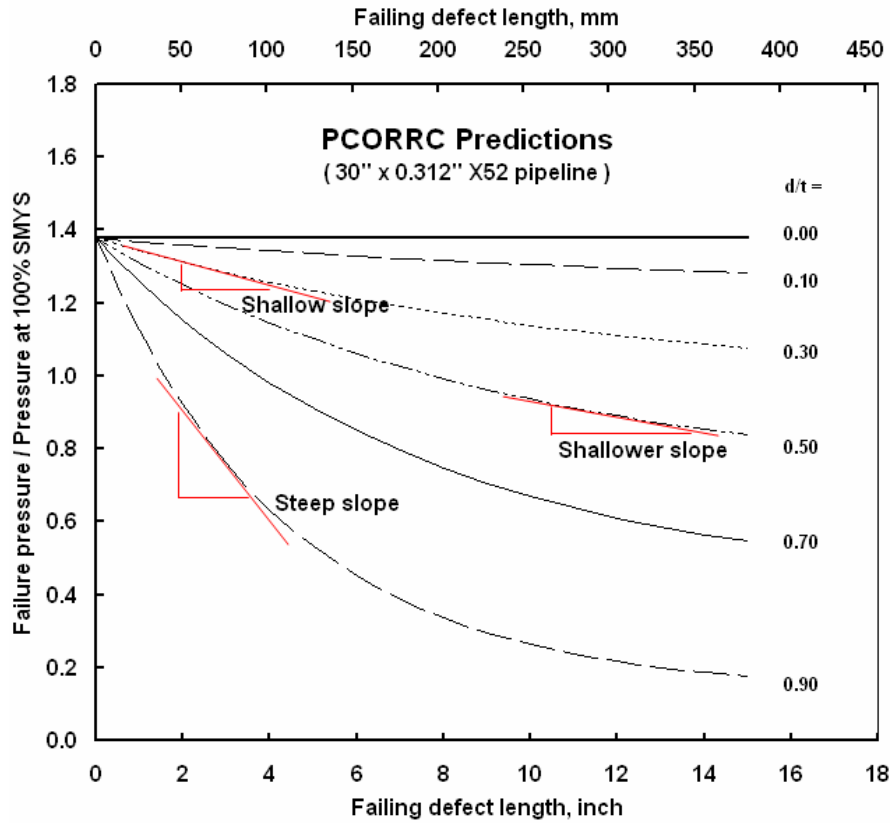
The results in Figure 3a indicate that early vintage line pipes fail at hoop stress levels the order of the UTS. The mean-trend for these data for vintage line pipe was fit by an equation $y = 1.0039x$ with an R^2 statistic of 0.76. Thus, on average the failure stress is very close to the UTS for these burst-test results. Consideration of the trend for the results covering the higher strength grades represented in Figure 3b by symbols other than the open circles leads to a similar outcome. The mean-trend for data representing higher-strength grades produced subsequent to the vintage line pipe was best-fit by an equation $y = 0.9957x$ with an R^2 statistic of 0.72. Again, on average the failure stress is very close to the UTS for these burst-test results. It is not a surprise that this group of results is fit by a line whose slope lies between those just listed, which is still closer to one, indicating the UTS and the actual failure stress shows no vintage dependence in its trend to match the actual wall hoop stress at failure in burst-testing of line pipe. BG results support this observation, as they have variously reported that the burst pressure of modern pipe can be determined in reference to failure at the UTS⁽⁴⁸⁾.

The results in Figure 3a bring into question the empirical use of a flow-stress whose value was other than close to the UTS when the vintage burst-test results were being trended for Texas Eastern. Likewise, the results in Figure 3b bring into question the continued use of a flow-stress whose value was other than close to the UTS when more recent steels were added to the database used to recalibrate and develop Modified B31G. The extent to which the definitions of flow-stress used historically lead to missed predictions absent any concern for the effects of geometry is apparent in Figure 4, with results for the B31G flow-stress presented in Figure 4a and that for Modified B31G presented in Figure 4b. It is evident in Figure 4a that use of $1.1 \times \text{SMYS}$ in B31G leads to an error in predicted failure stress that is conservative by 23-percent on average. Figure 4b indicates that use of $\text{SMYS} + 10 \text{ ksi}$ (68.9 MPa) as the flow-stress in Modified B31G leads to an error in predicted failure stress that is slightly less conservative, with the error being 28-percent on average. The standard deviation on these errors is about 70-percent larger than occurs if the UTS is used as the defect-free reference stress. The largest error for use of flow-stress defined as $1.1 \times \text{SMYS}$ is conservative by 39 percent, while that for $\text{SMYS} + 10 \text{ ksi}$ (68.9 MPa) is conservative by 32 percent, and that for UTS is conservative by 12 percent. It follows from Figures 3 and 4 that both flow-stress definitions lead to a significant bias in predicted defect-free failure stress, whereas that for the UTS leads to a nominally accurate prediction on average.

The presence of bias in predicted failure stress is significant when such criteria are used to assess remaining safe life when serviceability is evaluated, as is illustrated in Figure 5a. This figure schematically presents the failure pressure shown on the y-axis as a function of failing defect length on the x-axis, with results for constant depth defect typically represented by a line drawn through predictions for the same depth. Failing defect lengths are plotted on contours of constant defect depth for PCORRC predictions of failure pressure in Figure 5b, which serves to indicate typical trends, as will be discussed shortly.



a) impact of conservative pressure predictions



b) sensitivity of predicted pressure with defect depth and length

Figure 5. Trends in predicted failure pressure and defect shape and size

The upper contour shown in Figure 5a depicts actual failure pressure, as would be predicted if the failure criterion adopted were exact. For the sake of this discussion a defect of a given length and depth associated with this contour is shown in this schematic as the solid square symbol. The corresponding failure pressure for this defect is indicated in Figure 5a by the horizontal line through this data point, directed to the y-axis. The corresponding length of this defect is indicated by the vertical line dropped to the x-axis, while as noted its depth corresponds to that associated with the contour shown. A conservative prediction for this situation is also included in Figure 5a, shown as the dashed contour. By definition, predicted failure pressures that are conservative for this same defect depth involve pressures less than those indicated by the “exact” trend. Thus, this dashed line schematically representing results of a conservative prediction lie on a contour that falls below the exact trend in this figure. The failing defect length associated with this conservative prediction is by definition the length indicated by dropping a vertical line from the intersection of this conservative contour and the actual failure pressure. As can be seen from the figure, the defect length associated with the conservative (dashed) contour falls well below the actual length indicated by the exact prediction (the solid contour). The disparity between the predicted and actual lengths at failure is highlighted in the figure by the dashed ellipse set below the x-axis in reference to the actual and predicted lengths. Clearly, this shorter predicted crack length is non-conservative – as it implies a greater distance for crack growth until crack instability and an axial split (or possibly a rupture).

It is apparent from the illustration in Figure 5a that a conservative prediction of failure pressure leads to a non-conservative error in predicted defect length, the error for which increases as the predicted failure pressure becomes more conservative. Significantly, this error increases as the slope of these predicted trends diminishes, as occurs for longer defects and for pressures more typical of service as compared to hydrostatic testing. This is evident in Figure 5b where the slope of typical failure bounds is shown to decrease with both longer cracks, and shallower cracks. In contrast, there is less effect on defect size due to inherently conservative predictions as the defects become shorter and deeper. But, regardless of defect size, the best predictor of failure pressure is an accurate one that is free of any bias. This implies criteria that embed a FoS on failure pressure, either directly through a constant imposed for this purpose, or indirectly through a conservative flow-stress, have limited utility in life assessment.

Summary for Task One

Task One has considered the format of the various corrosion assessment criteria in reference to the literature and archival data to determine the failure behavior of defect-free line pipe. This task evaluated results for vintage line pipe as well as modern production to determine the failure stress relative to the yield stress and the UTS. Empirical data were trended and contrasted with the definitions of flow-stress used in failure criteria formulated in the 1970s and the 1990s. This data was coupled with the format of the criteria and used to identify the appropriate flow stress for vintage versus modern line pipe, and determine if vintage warranted use of a different flow-stress. Some key observations and conclusions follow:

- all corrosion assessment criteria – whether empirically developed in the 1970s or formulated by trending numerical results in the 1990s had the same form: $S_f = C \cdot S_R \cdot \{f(\text{defect geometry})\}$,

- with this mathematical form, when there is no defect present the term f (defect geometry) is by definition one, which means the product of C and S_R in this function must be equal to the UTS, or empirically equal to the hoop-stress in a burst-test of defect-free line pipe,
- failure pressure data for defect-free pipe evaluated to identify the appropriate value of the product of C and S_R indicate the appropriate value of their product is the UTS,
- the historical definitions of flow-stress adopted for the 70s criteria were inappropriate and with a heavy bias to conservatism – in excess of 25-percent on failure pressure, and
- analysis indicated a bias in predicted failure pressure as might be achieved by use of a conservative reference stress was inappropriate for general use in corrosion assessment because conservative pressure predictions indicated non-conservative life assessment.

Results from Task One suggest that databases argued to support the 1970s versus 1990s criteria should be evaluated in reference to the appropriate flow-stress identified in Task One as the UTS. Thereafter, once recast relative to the appropriate flow-stress these databases should be trended to determine if characteristic differences remain between them as a function of the corrosion geometry, vintage, grade, toughness when available, and other metrics of the line pipe and the pipeline's service and loading.

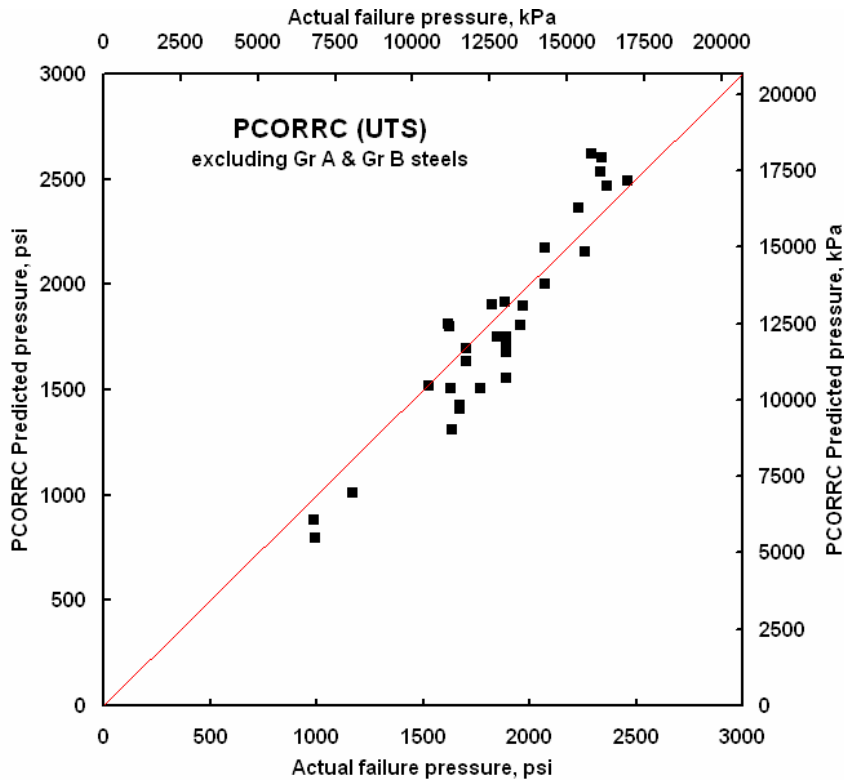
Results – Task Two: Empirical Aspects

Implications of Prior Work and Task One

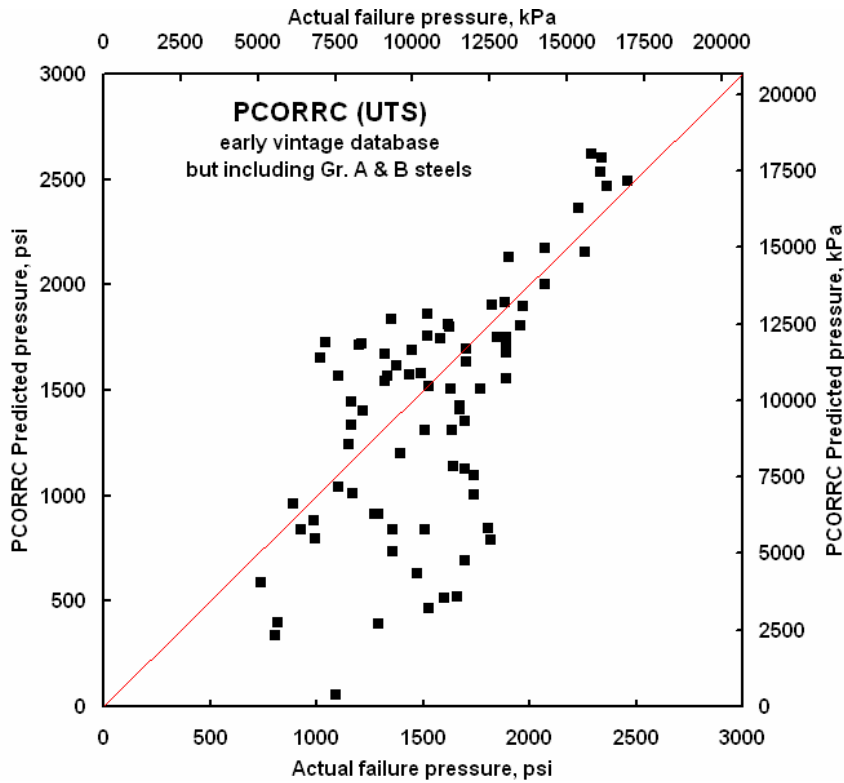
As noted in developing the approach for this project, extensive full-scale databases exist that apparently support the early metal-loss assessment criteria B31G and Modified B31G (equally RSTRENG), which appear conservative in contrast to the recently developed plastic-collapse-based corrosion criteria. PRCI Project PR-3-9509 initiated at Battelle in 1995 concluded a select group of burst-tests involving early vintage Gr B line pipe in the database supporting the 1970s criteria significantly drove this conservatism^(23,25).

As the Battelle project was concluding, PRCI initiated a multi-contractor Project PR-273-9803 in 1998, which was centered at BG. This work challenged BG and their subcontractors at Battelle and Shell Global Solutions to rationalize apparently disparate predictions of metal-loss failure for the 1970s versus the 1990s criteria, and to harmonize their validation databases. This work was centered at BG, because concurrent to the work started at Battelle in 1995, BG ran a major multi-client project the results for which remain confidential their clients. While such results remained confidential, synergy between these projects and their conclusions was anticipated, and with appropriate confidentiality concurrence details covering the numerical analysis and full-scale testing were shared selectively to the multi-contractor project reported as Reference 26.

In assessing the results developed for the BG multi-client project, the PRCI multi-contractor report concluded⁽²⁶⁾ that full-scale testing provided broad validation for the 1990s criteria. This conclusion was drawn without concern for the line pipe properties, as the project focused on higher-toughness modern-vintage line-pipe steels. With that conclusion, the objective of this project can be met by identifying criteria for which collapse-based criteria correctly predict failure across the database developed as the empirical basis first for B31G⁽¹¹⁾ and later for Modified B31G⁽¹²⁾ and the continued validation of RSTRENG⁽¹³⁾.



a) database but excluding Gr A and Gr B steels



b) early vintage database including Gr A and Gr B steels

Figure 6. PCORRC predictions of burst-test failure pressure referenced to the UTS

The PRCI multi-contractor project considered this vintage database and concluded⁽²⁶⁾ that failure in several grade B pipe tests fell well below that anticipated by plastic-collapse-based criteria, as was previously found by Battelle^(22,23). Likewise, as concluded previously by Battelle, this multi-contractor project concluded⁽²⁶⁾ that, apart from the grade B pipe tests, collapse-based predictions were generally consistent with the historical database for other pipe grades. Support for this conclusion follows from Figure 6a⁽²³⁾, which shows plastic-collapse-based predicted failure via PCORRC for the vintage pipe burst-test database culled to specifically exclude results for Gr A and Gr B. In contrast, the results in Figure 6b, which includes the data culled from Figure 6a, shows plastic-collapse-based predictions can be in clear with the full burst-test database.

As just implied, Figure 6 selectively presents PCORRC collapse-based predictions for the vintage single-defect burst-test database, where the UTS is used as the reference stress. Figure 6a culls results for early vintage GR A and Gr B steels, while Figure 6b includes these results. The results in Figure 6a show that PCORRC referenced to the UTS, which is one of several similar analytically trended plastic-collapse criteria, provides viable predictions for the failure pressure for the database for vintage line pipe. As expected, when the actual value of UTS is used, the predicted trend scatters more or less uniformly about a one-to-one trend indicating exact predictions. In contrast, when the full early vintage database is considered as done in Figure 6b, the predictions show a strong non-conservative bias, and also show significant scatter. It is this bias and scatter that is cited to support the view that collapse-based criteria are inappropriate for early-vintage line pipe. Such results also are cited to support the suggestion that 1970s empirical criteria based on a curve fit of such data are inherently different from the 1990s collapse-based approaches.

The multi-contractor project centered at BG that began in 1998 also concluded⁽²⁶⁾ that several burst-tests in the early vintage database are problematic for collapse-based criteria possibly because they involved repeated pressurization, or possibly overly conservative defect shape approximations for quite deep (beyond 70-percent of the wall) and long corrosion patches in Gr B and Gr A25 pipes. Finally, that work identified⁽²⁶⁾ that the Gr B pipe material involved a high brittle-ductile transition temperature (DBTT) that lies above the normal design temperature for buried transmission pipeline. However, as for the prior Battelle work, criteria to distinguish when to use the “early 1970s criteria” versus “the modern 1990s criteria” were not quantified. Thus, one focus for the evaluation of the empirical data in Task Two is quantitative analysis of factors such as repeated pressurization. Thus, this prior work points to analysis of that data to rationalize whether defect geometry, or unusual properties for the vintage Gr A and Gr B data account for problems evident when collapse-based predictions are used.

The trends in Figures 3 and 4 from Task One also provide direction for evaluation of the empirical database involving the early vintage Gr A and Gr B line pipes. These figures point to artificially embedded conservatism that enters the 1970s criteria through the use of an SMYS-based flow stress rather than the UTS. This conservatism contributes to the apparent differences between 1970s criteria and 1990s plastic-collapse-based criteria. And because the 1970s criteria co-mingle the effects of flow-stress and geometry on failure stress (equally pressure), it is logical that the effects of geometry are not represented appropriately. With this insight, Task Two also evaluates the early vintage Gr A and Gr B line pipes targeting primarily trends in grade, vintage, and defect geometry.

Early Vintage Database and the Effect of Repeat-Testing

The potential significance of repeated pressurization leading to non-conservative predictions in testing involving the early vintage line pipe was evaluated through archival records for this burst testing. This analysis indicated that 26 of the 129 results that comprise the database used for the recalibration as Modified B31G involved repeated testing of the same corroded pipe segment. These 26 results represent an even larger fraction of the database circa calibration of B31G, which comprised roughly 56 results depending on the date for which the file information is evaluated. The repeat-testing involved pipe segments that contained multiple patches of corrosion. After one patch failed and the segment was blown-down, a cut-out or repair was made and the segment retested. One such pipe segment experienced a total of 32 repeat-test pressure cycles, although no results from this testing were included in the database. Evaluation of the files indicates this repeat-test practice involved segments of vintage Gr A, Gr B, and what was designated as X52.

The observation that about half of these results that comprise the B31G calibration database include the effects of large pressure cycles is significant, as follows. The repeat-testing involves a recurrent pressure-time history, which for typical burst-testing involves gradual pressurization. High gradually increasing pressures, some the order of SMYS, induce stable tearing / cracking that can cause pressure reversals when failure does not follow immediately due to that cracking. Both cracking and pressure reversals can cause a significant reduction in failure pressure on the next pressure-up cycle. As pressure reversals were not uncommon in such pipes⁽⁴⁹⁾, such recurrent pressure cycles could easily promote cracking and pressure reversals that promote failure at pressure less than expected for predictions referenced to the UTS, such as PCORRC.

Pressure cycling also leads to a phenomenon known as cyclic hardening⁽⁵⁰⁾, which is common in lower-strength steels. A few cycles of even moderate local strain could, through cycle-dependent hardening, elevate the flow-resistance to levels that exceed the UTS in such steels⁽⁵⁰⁾. Accordingly, cyclic hardening due to repeat-testing could cause plastic-collapse-controlled failure at pressures above that predicted for criteria referenced to the UTS, such as PCORRC. As such, the actual failure pressure for repeat-tests could be underestimated by PCORRC or other criteria referenced to the UTS, which opens the door to repeat-test failures above predictions by PCORRC.

It follows that when predicted failure pressure referenced to the UTS is compared to the actual behavior, as in the format of Figure 6, such predictions could fall above as well as below the one-to-one line. Of interest is the observation that the cyclic hardening will tend to reduce creep-induced stable tearing, such that the mechanism of stable tearing and pressure reversals could compete with cyclic hardening. The extent to which phenomenon like stable tearing, pressure reversals, and cyclic hardening and their mutual competition accounts for the scatter and non-conservative predictions in Figure 6b is evaluated in Figure 7. Figure 7 presents results on coordinates where the y-axis is predicted failure pressure via PCORRC referenced to the UTS and the x-axis the actual failure pressure. On these coordinates, non-conservative predictions fall above the one-to-one line, while conservative results fall below the line.

Figure 7 differs from Figure 6 in that only the early vintage database circa calibration of B31G, with Figure 7a isolating the early vintage database that includes the early vintage Gr A and Gr B line pipes. When the repeat-testing is included as in Figure 7a, the PCORRC plastic-collapse predictions seem to follow more of a vertical trend, as opposed to tracking the one-to-one line

indicated in the figure, and also show significant scatter. This creates the impression these results are not correlated in regard to plastic-collapse. A large number of data points that fall well above the line comprising very non-conservative predictions. Likewise, a large number of data points fall well below the one-to-one line, suggesting very conservative predictions.

The situation evident in Figure 7a is greatly changed when the repeat-testing results are excised, as is apparent in Figure 7b. Whereas the trend in Figure 7a appears uncorrelated in regard to collapse-based predicted failure pressure, at least the bounds on the predictions now have a slope consistent with correlation. As can be seen in contrasting Figure 7b with Figure 7a, many of the more non-conservative predictions disappear when repeat-test data are excised, and the number of points well below the line also has been diminished. This balanced outcome suggests little real competition between the underlying mechanisms, which was alluded to above. It follows from the difference apparent between Figures 7a and 7b that many of non-conservative predictions previously associated with DBTT and other aspects of the early vintage Gr A and Gr B line pipe are largely due to the effects of repeat-testing.

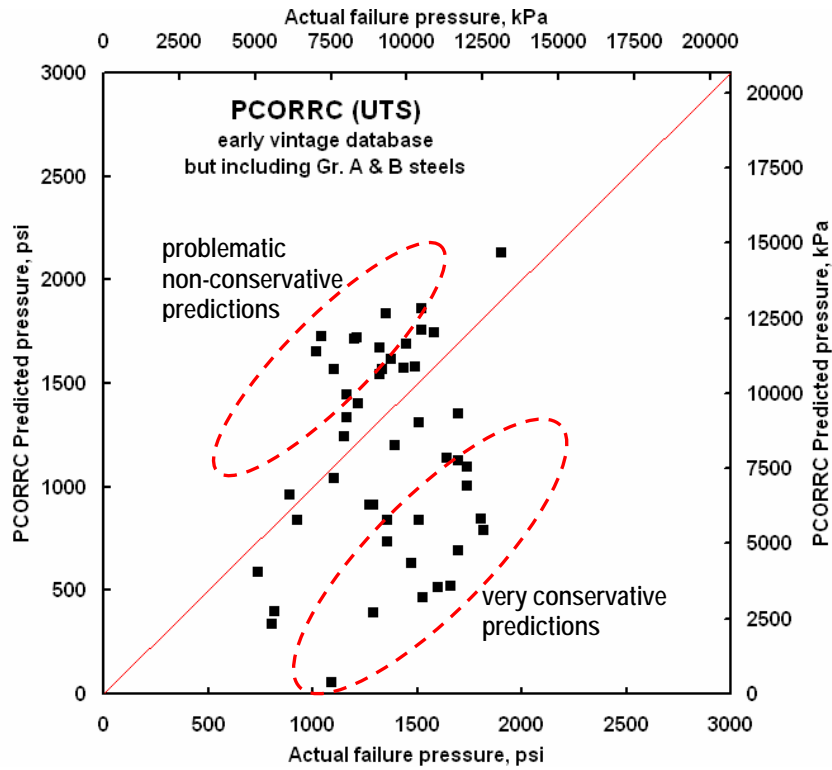
As evident in Figure 7b, only two points remain to be rationalized above the line, while many more are of concern in the scattered conservative results below the line. These aspects are considered next.

Trends in Line Pipe Mechanical Properties

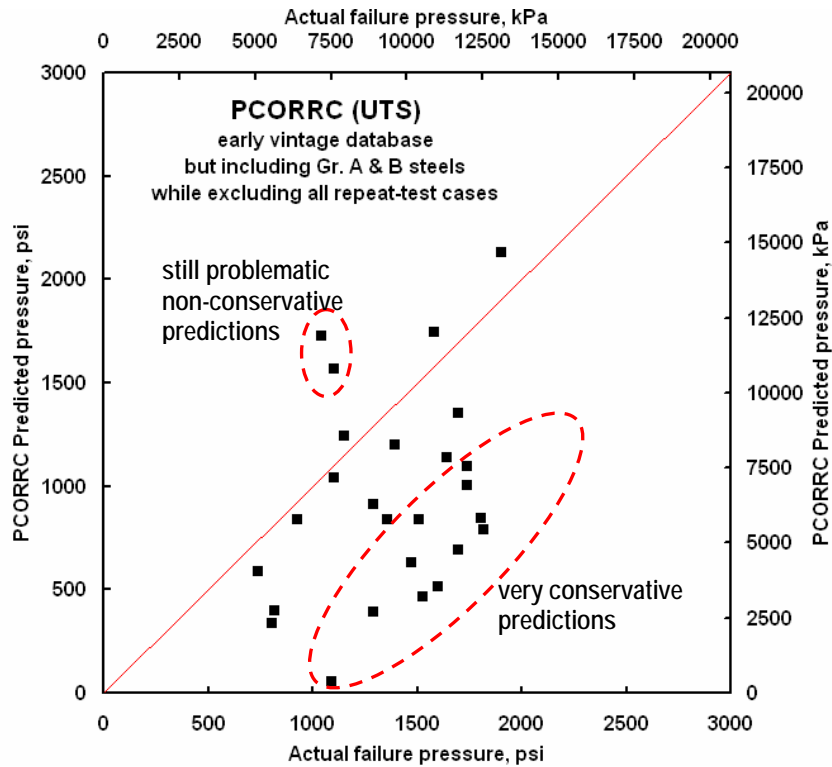
With the effect of repeat pressurization removed, and flow-stress not a factor for predictions referenced to the UTS, only defect shape and size remain along with the possible role of DBTT or uncertainty in UTS. While defect shape and size are much better documented in the files than is DBTT or statistical trending of UTS for these specific early-vintage steels, certain trends in the data suggest consideration of the properties before evaluating the role of defect geometry.

The mechanical property relevant to plastic collapse is the UTS, along with consideration of sufficient fracture resistance to ensure that fracture does not occur prior to collapse. In contrast, when the database now used to represent vintage line-pipe steels was being developed, and even into the early 1990s, there was little interest in these properties for many pipeline applications aside from adequately characterizing the steel. For this reason, there are many tests documented in the database for which no UTS is reported, and even less information regarding fracture behavior. Surprisingly, apparent “gaps” in actual yield stress (AYS) also exist, in spite of this variable being much more fundamental to this database. Such gaps are evident where a constant value of yield stress is reported for a range of pipes of the same grade, evidently because limited tensile properties were developed for one pipe segment and considered the same for the rest. It follows that the most fundamental element of the empirical criteria of the 1970s – the yield stress – and the key to the collapse-based criteria of the 1990s – the UTS – are in some ways uncertain for portions of this database. This uncertainty exists for AYS only for a few cases, whereas many results appear in question for the UTS. This section evaluates aspects related to these properties, and the implications for results that remain “problematic” after the repeat-testing data was culled, with the data of concern shown in Figure 7b.

Where actual properties are reported, variability in that value can be an issue due to scatter from the testing practice as well as inherent material variability. Uncertainty in the AYS and the UTS was evaluated in regard to archived data as the first step to rationalize the several data points that remain problematic in reference to Figure 7b. File data documenting mechanical properties were

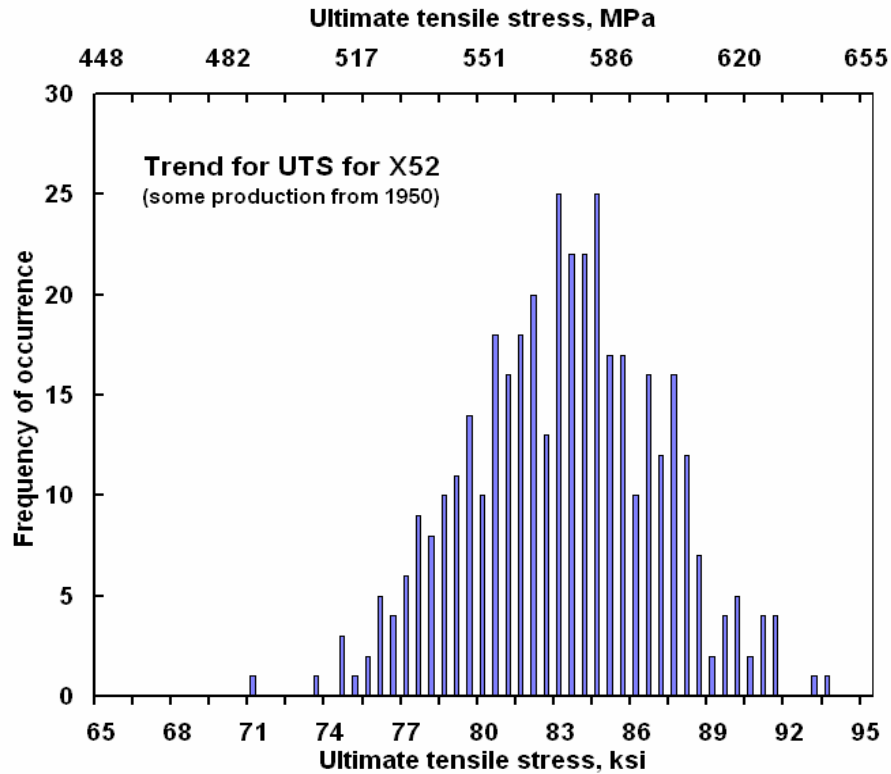


a) vintage database including early Gr A and Gr B line pipes

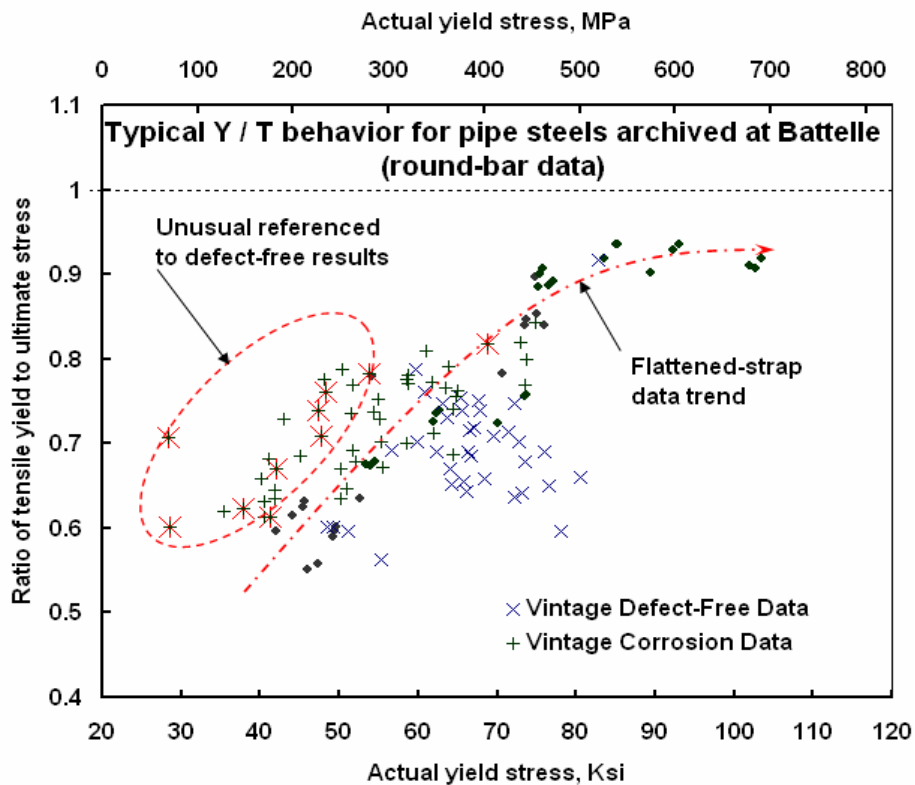


b) vintage database including early Gr A and Gr B line pipes – but excluding repeat-test cases

Figure 7. Analysis of the vintage database in terms of PCORRC referenced to the UTS



a) distribution of UTS for some 1950s production



b) Y/T for the vintage database, excluding repeat-test cases, and archived results

Figure 8. Trends in mechanical properties for vintage large-diameter line pipe

located that covered a range of large-diameter line pipe produced in the 1940s through 1950 for grades X42 and X52. Values of the AYS and UTS were digitized and statistically characterized, a typical result for which is shown in Figure 8a in regard to the UTS. These results are specific to 30-inch-diameter X52 line pipe produced in 1950. As can be seen from these data that are typical for both the AYS and the UTS, the statistical analysis showed their variance ranged from ~ 0.045 through ~ 0.05 . Such variability in actual properties is simply too small to be a first-order factor in rationalizing the significant bias and scatter evident in Figure 7b, although it could contribute to small-scale random scatter, like that in Figure 6a.

Because the UTS was not a primary concern when the database for corrosion of vintage line pipe was developed, the possibility that occasional entries in this database were other than actual measured results was evaluated. Cases where different values of the AYS were reported with a constant value of UTS appear open to question as do cases where the UTS corresponded to SMTS (in current versus historical standards). To better identify potential entries that did not reflect measured data, the ratio of yield stress to (ultimate) tensile stress, Y/T, was determined for the vintage line pipe portion of the database and plotted as a function of AYS. Equally, Y/T was developed for the defect free-data base for which the mechanical properties were a major focus, and so more complete and certain. Finally, Y/T was determined for a wide variety of data in Battelle's archives as a reference against which to compare the vintage database. These results are summarized in Figure 8b, where Y/T is plotted as a function of the corresponding value of the AYS. AYS was used in lieu of grade to develop continuity in Y/T as a function of the yield stress, and to provide for inherent variability in AYS as a function of grade.

Figure 8b presents results for Y/T for a range of grades from X42 through X80, which for the solid symbols in this figure represent round-bar testing of line-pipe steels. The lower-strength results from about X60 and below represent production from the 1940s through the 1960s, while the results for the higher-strengths reflect production through circa 2000. Figure 8b also includes a trend representing the central tendency of data for a similar period representing flattened strap testing, which is included for the sake of completeness. This reference database is contrasted with Y/T determined for the corrosion database, which are shown as the + symbols. Also shown are values for Y/T data for the defect-free testing that underlies Figure 3, which is shown as the X symbols. The trend for Y/T for the defect-free database logically encompasses the scope of Y/T for the corrosion database developed from many of these same steels, and steels of the same vintage. Consequently, results for the corrosion database that lie at values of Y/T well above that for either the general trend or more specifically the defect-free database could be considered questionable.

It is clear from Figure 8b that a portion of the Y/T results for the corrosion database lie at relatively high values of Y/T as a function of AYS, which implies the values of UTS reported for these pipes are suspect. While this cluster lies well above the typical trend, they are even further above the data for defect-free burst testing of vintage pipe. Accordingly, this cluster has been circled and labeled "unusual" in Figure 8b. Significantly, a higher value of Y/T means a lower value of its inverse, which translates to values of UTS used to predict plastic-collapse being smaller than likely for some pipes. For such cases, the predicted failure pressure could fall well below the actual result. Cases for which this apparently has caused predictions to fall well below actual failure pressure in Figure 7b are shown by asterisk symbols in Figure 8b.

Trends in Line Pipe Fracture Properties

The role of DBTT and toughness in terms of Charpy vee-notch (CVN) energy also were considered in regard to archived file data, and the significant bias evident in the data points that remain problematic in reference to Figure 7b. Relevant file data for DBTT and toughness of large-diameter line pipe produced since the 1940s were located – all based on CVN testing. While relevant data were selectively identified, lower toughness and the effects of DBTT cited in Reference 26 as a potential source of concern are largely irrelevant in light of the trends in Figure 7b. This is because these factors promote failures at pressures below that associated with the UTS. Review of Figure 7b shows the opposite situation dominates – as most of the problematic results in Figure 7b involve an actual failure above that predicted by plastic-collapse. As such, fracture due to low toughness or high DBTT causing premature fracture is not a dominant concern for the results in Figure 7b. Indeed, only two data points marked problematic that lie above the line could be rationalized by such considerations.

Trends in Defect Geometry and Measurement Accuracy

Previous sections have shown that neither statistical uncertainty in the UTS nor premature fracture are major factors for under-predicted failure pressure in Figure 7b, whereas for a portion of these data Y/T indicated the reported UTS could rationalize this trend. In addition to the apparently significant role of Y/T, the conservatism collapse-based failure pressure in Figure 7b could be rationalized through problems in the reported defect geometry.

As for evaluation of the role of line pipe properties, archived files were gathered that characterize defect geometry. Some useful information detailing defect geometry was located in files created during recalibrating B31G as Modified B31G and its continued validation as RSTRENG. But as is the case with most projects, such files targeted tabulations and sketches directly relevant to that recalibration. In addition to those files, surprisingly detailed archives were located that pertained to burst testing back to the early vintage line pipe, which were apparently salvaged from office archives as staff retired. Binders containing close-up photographs and other notes were found in more detail than was anticipated or could be dealt with within this work scope. Subsequent labor-intensive examination could prove useful as only a cursory review was possible as compared to the detail available.

The records indicate that the two non-conservative data points that remain well above the one-to-one line in Figure 7b involve shorter, but relatively deep defects. While fracture properties are sparse for this early testing, both of these data points had reported values of DBTT that were above or comparable to the ambient test temperature. Accordingly, some tendency to fracture also could underlie these tests failing at pressures non-conservative to predictions based on UTS. Another aspect that could underlie these tests failing at pressures non-conservative to predictions based on UTS involves their being short, deep defects. Figure 5b illustrates that predicted failure pressure becomes increasingly sensitive to both defect length and depth as defects become shorter and shallower. In contrast, failure pressure predicted is only sensitive to defect depth for longer defects. It follows that these two predictions also could reflect uncertainty in their measured length and depth.

Measured length and depth are simply defined and typically well controlled for machined defects. In contrast, naturally occurring corrosion involves significant variation in defect shapes and sizes. As discussed above, consideration of trends in failure pressure as a function of defect

length and depth shows that predicted pressure can be very sensitive to small changes in either defect length or depth for certain combinations of length and depth. Accordingly, small errors in measurement accuracy can be an important factor. A related but equally important factor involves the approach adopted to report defect size and shape. For example, quantifying defect length and depth for corrosion with the complexity evident in Figure 1 during the late 1960s, prior to the current understanding of defect interaction, involved decisions of whether adjacent defects behaved as a single defect. In addition, quantifying that corrosion involved the use of a maximum depth and a defect length. Again, predicted failure pressure could vary significantly – depending on that actual depth profile over defect’s length.

Consideration of the data points below the one-to-one line in Figure 7b indicated two trends that, within this work scope, could not be evaluated quantitatively. First, several of the features reported involved very long defects (many feet), some of which also were very deep in places. It is unusual to find large patches of areal corrosion wherein such lengths with the corresponding depths would be considered non-interacting defects. Second, this group of data points comprised some shorter, but also quite deep defects. To date, such defects have received only limited numerical consideration.

As just outlined, problems in characterizing corrosion geometry can develop either by errors in measurement, the need to represent complex features by two linear dimensions, or as a result of categorizing interacting defects as a single defect. Of these, measurement errors tend to be random, and except for shorter, deeper defects, too small in contrast to the disparity in predicted versus observed pressure evident in Figure 7b. Because measurement error is considered to be random, but the results in Figure 7b show some significant bias, one might conclude that errors in measured shape and size are unlikely a factor in rationalizing these trends. In contrast, reporting the length of two or more interacting adjacent defects as a single defect could easily double the absolute reported length for a given defect. Such misinterpretation could easily account for the disparities present in this figure – and seems plausible for the era considered as “rules” for interaction had yet to be developed. It remains for some future project to evaluate this conclusively.

While not conclusively demonstrated, it appears many of the data points indicated to be “problematic” below the one-to-one line in Figure 7b likely are misrepresented as single defects, with a shape and size that is poorly characterized by the historic reporting practices. In addition, short and deep single defects are poorly characterized analytically, with little work available for this combination of shape and size. Interacting defects likewise are poorly characterized analytically, with criteria to assess interaction widely varied. While a less than satisfying picture because the role of geometry is not quantify conclusively, it appears that sufficient archival data exist to address this aspect and support numerical analysis needed to quantify this issue as part of some future project.

Accounting for Defect Geometry and Implications of Y/T

It is apparent from consideration of properties in Figure 8 that some of the trends in Figure 7b can be rationalized in regard to misreported values of the UTS. In reference to Equation 10, one aspects associated with defect geometry should be as important as the mechanical properties. Comparing the equations proposed to assess corrosion severity, many of the 1990s criteria adopted the same approach as used in the 1970s criteria, while PCORRC chose to abandon that format. This section uses the empirical database to assess the extent to which the form of

equation used to account for the effects of geometry leads to fundamentally different predictions of failure pressure. To this end, predictions made by Modified B31G (equally RSTRENG) are compared to PCORRC in Figure 9. Possible complication due to use of flow-stress versus UTS as the reference stress is eliminated from this comparison by using the UTS as the reference stress for both criteria. This choice should not cause bias in the empirical data used in this comparison, as the UTS was previously shown via Figure 3 to be the appropriate defect-free failure stress, being without bias for either grade or vintage.

Figure 9 presents predicted failure stress for UTS-based Modified B31G on the x-axis with the corresponding results for PCORRC shown on the y-axis. It is apparent from this comparison that PCORRC is nominally identical to Modified B31G when both are referenced to the UTS at moderate to higher pressures. However, at lower pressures there is a shift in this trend for a few cases – with PCORRC appearing conservative in comparison to Modified B31G. This cluster of results lies curiously parallel to the one-to-one trend, although shifted to lower pressures, as indicated by the short trend-line drawn through these several points. Evaluation of the underlying data indicates this cluster of results reflects cases where the reported value of UTS falls within the cluster labeled “unusual” in Figure 8b. Several such results involve values of UTS reported as SMTS for Gr B or Gr A (per current and past editions of API 5L), or has a value well below the usual trend for yield to tensile ratio, Y/T, of line pipe steels. As noted earlier, analysis of data underlying Figure 7b also indicated that results labeled “problematic” that involved conservative PCORRC predictions have values of UTS involved with these “unusual” Y/T results, which are identified by asterisk symbols in Figure 8b. Significantly, all of the collapse-based failure pressure predictions in Figure 9 that do not show geometry correlated between PCORRC and Modified B31G lie within this cluster of “unusual” properties. It follows that unusually low values of the reported UTS are responsible for the break from correlation

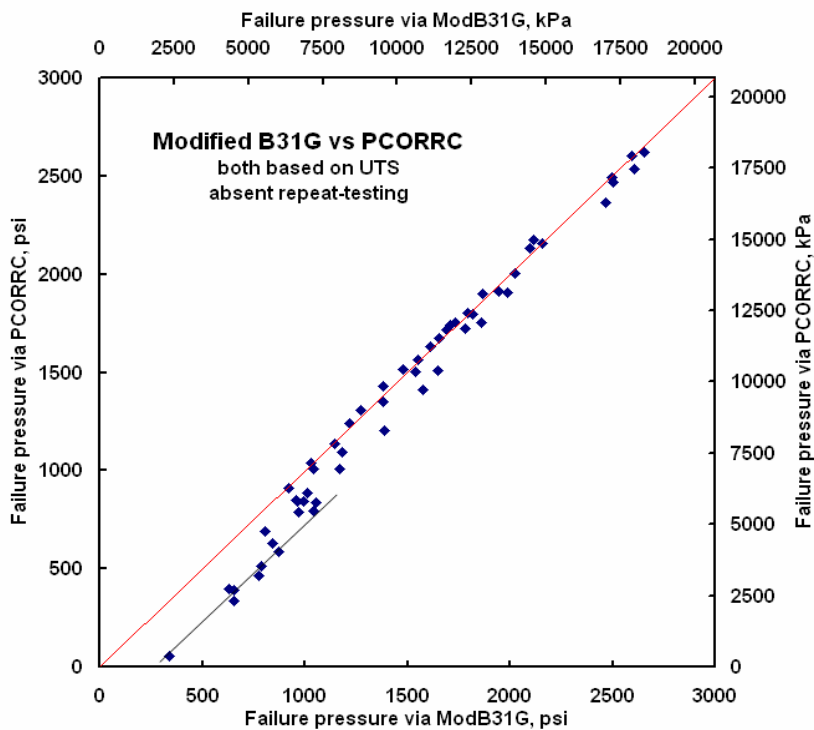


Figure 9. UTS-based comparison of geometry effects for Modified B31G and PCORRC

between these 1990s and 1970s criteria.

On this basis, Figure 9 indicates that Modified B31G and PCORRC assess the effects of blunt defect geometry on failure response more or less comparably. As each is typical of the 1970s and 1990s criteria, respectively, these results indicate there is no essential difference in the manner defect geometry is quantified in these decades-different criteria. It follows that defect geometry has little role in the perception that the early vintage data or related empirical criteria are unique or conservative in comparison to the data and criteria of the 1990s. Moreover, no evidence was found suggesting that the 1970s database involves geometric features that would not develop in modern line pipe as it experiences corrosion. However, there are defect features that can form regardless of vintage, such as pits within pits developed with microbiologically induced corrosion^(e.g.,51) (MIC), and other forms of corrosion, for which local constraint could promote failure at pressures less than predicted by the currently available criteria. This and other aspects involving the geometry of the corrosion defect will be addressed analytically in Task Three.

Role of Flow-Stress in Lieu of UTS

Figures 3 and 4 discussed in Task One indicated that the flow-stress embedded in B31G and Modified B31G as well as RSTRENG introduced significant conservatism to these criteria as compared to the actual failure behavior of defect-free line-pipe steels, without bias for vintage or grade. Figure 9, interpreted together with Figure 8b, indicate that Modified B31G and PCORRC address the effects of blunt defect geometry more or less comparably. As Equation 10 indicates failure pressure predictions involve a reference stress and a term that accounts for defect geometry, and geometry does not appear to be a factor, any differences in predictions between Modified B31G and PCORRC must be due to the choice of a flow-stress in lieu of the UTS.

On this basis, the use of an empirical flow-stress chosen without regard to the actual defect-free empirical trends underlies apparent differences evident in the empirical data are analyzed by a 1970s versus a 1990s criterion. As Figures 3 and 4 indicate the UTS is the appropriate reference stress free of bias for grade of vintage, the use of flow-stress as the reference stress artificially embeds conservatism in related failure predictions.

Summary for Task Two

Task Two evaluated the databases developed historically to support the 1970s versus 1990s criteria, from properties testing to full-scale burst testing of defect-free and corroded line pipe. Coupled with the appropriate reference stress identified in Task One as the UTS, these data were trended to identify characteristic differences that remained between Modified B31G taken to represent the 1970s criteria and PCORRC taken to represent the 1990s plastic-collapse-based criteria. This trending considered corrosion geometry, and the line-pipe's vintage, as well as mechanical properties and toughness when available, which were sufficient to directly relate the 1970s criteria and database to the 1990s Criteria. These results will serve as input to Task Four. Some key observations include:

- many data points labeled “problematic” in Figure 7b reflect use of a reported value of UTS that is “unusual” in regard to trends for line-pipe steels in general, as well as the defect-free database specific to the corroded-pipe testing,

- many of the data points labeled “problematic” in Figure 7b likely involve compound corrosion features, which absent criteria to identify interacting defects in the late 1960s and early 1970s were categorized as single defects – problems in characterizing the complexity of real corrosion features circa the late 1960s also could be a factor, as could historic reporting practices that relied on length and depth alone in contrast to the process used today in regard to RSTRENG,
- from an analytic perspective, some combinations of defect shape and size, including short and deep single defects, are not well characterized, which is also true for interacting defects – while a less than satisfying picture because the detailed role of geometry remains ill-quantified today, sufficient archival data exist to address this aspect within some future work scope directed at the details of shape and size, and measurement practices, and the numerical analysis needed to support these aspects – such might be considered in some future project,
- use of an SMYS-based flow stress rather than the UTS was indicated to be the source of conservatism and differences between 1970s criteria and 1990s plastic-collapse-based criteria.

No essential difference was identified in the way defect geometry was quantified by the 1970s versus 1990s criteria, nor was there clear evidence that the 1970s database involves geometric features not found in modern line pipe as it experiences corrosion. However, there are features that can form regardless of vintage, such as pits within pits developed with MIC for which local constraint could promote failure at pressures less than predicted by the currently available criteria. This and other aspects involving the geometry of the corrosion defect will be addressed in Task Three.

Results – Task Three: Analytical Aspects

Task Three was directed at analyses to discriminate conditions where blunt defect failure can be affected by fracture. Such analyses were directed by what was found in the prior tasks as well as trends reported in prior or parallel projects.

Implications of Prior Work and Task Two

Following completion of the PRCI work initiated in 1998 which fell short of criteria to identify the applicability of the 1970s criteria versus the 1990s criteria, working in conjunction with the GRI the PRCI initiated GRI 8521 at Battelle to develop guidelines for assessing corrosion at welds⁽²⁷⁾. In contrast to the pipe body, certain types of weld can be much more fracture brittle. Thus, one focus of this project was discriminating conditions where blunt defects overlying welds could be affected by fracture. That work determined⁽²⁷⁾ that constraint due for example to the loading, the local state of stress, or possibly microstructural gradients could lead to fracture at an otherwise blunt defect at a nominal stress less than when constraint was absent. The role of constraint was illustrated through fractography that revealed cracking in corrosion defects where constraint was a factor. That work also illustrated fracture-controlled failure in axially oriented corrosion where the corrosion tended to form as a necklace of adjacent pitting; where pits within these pits formed, as occurs for some forms of MIC. In both cases, constraint could facilitate fracture in steels where the toughness was not adequate to ensure plastic collapse and failure at

the UTS. And, as Y/T can cause strains to localize in stress raisers like pits, the post-yield mechanical properties also could be a factor.

To provide operators and regulators with a technically sound approach to corrosion assessment, the role of constraint must be understood, and criteria that determine when failure occurs at the UTS or some lower flow-stress must be developed. Also, criteria must establish when reduced toughness or ductility is a factor, and determine what toughness is “adequate” to preclude the possibility of fracture-controlled failure at otherwise blunt defects.

This task, as proposed, included three technical analysis subtasks evaluating constraint, and a task formatting the results for transfer to the fourth task directed at guidelines for the use of 1970s versus 1990s criteria. The three analytical subtasks included:

1. evaluate constraint and its role in promoting fracture as a function of defect geometry and pipeline loading,
2. evaluate the role of line pipe properties in promoting constraint leading to fracture, and
3. develop trends for input to Task 4 to determine the appropriate corrosion assessment practice.

Results were developed addressing geometry and line pipe flow and fracture properties in a generic fashion to facilitate consideration of issues like line pipe vintage, with other practical metrics such as pipeline service and loading history. The results were analytically trended as input to Task Four.

Background to Numerical Analyses to Characterize the Role of Constraint

For the present analyses, constraint effects are evaluated in reference to the stress-strain field at the root of a defect, which subject to the flow and fracture properties of the line-pipe steel have nucleated a crack. The role of constraint in the continued growth or fracture at this initiated crack is broadly developed in the published literature. The role of constraint became evident following experimental work^(e.g.,52-54) showing the fracture resistance at initiated cracks can not be simply characterized by single-parameter fracture mechanics. Consistent with the historical evolution of fracture mechanics, early formulations developed constraint analyses in regard to linear-elastic fracture mechanics (LEFM), which were more broadly characterized in terms of nonlinear fracture mechanics^(e.g.,55-60) (NLFM).

As for the work by BG in their multi-client project started in 1998, the present formulation uses modern higher-toughness line pipe as its starting point. Where NLFM results are required, use is made of published experiments for a modern X80 line pipe steel⁽⁶¹⁾. Such NLFM properties are available for a set of single-edge-notched bend (SENB) specimens and a set of single-edge-notched tension (SENT) specimens, where shallow through deep cracks have been used to develop a range of crack-tip constraint levels. The test data show that the J-R curves for X80 pipeline steel are strongly constraint dependent. To facilitate transfer of the experimental J-R curves to those for actual cracked components, like flawed pipeline, “constraint-corrected” J-R curves are developed.

The nonlinearity typical of even some early-vintage line pipe steels is addressed through use of the NLFM parameter $J^{(e.g.,62,63)}$. Constraint is addressed in reference to the two-parameter $J-A_2$ formulation of Chao and Zhu⁽⁶⁴⁾, which is adapted to quantify the constraint effect on the crack-

tip fields and the J-R curves. The constraint parameter A_2 is extracted by matching the J- A_2 solution developed by numerical analysis via finite element analysis (FEA) for specific cracking configurations. A constraint corrected J-R curve is formulated next as a function of the constraint parameter, A_2 , and crack extension, Δa , which is then validated in reference to laboratory specimen results. Using the test data of J-R curves for the SENB specimens, a mathematical expression representing a family of the J-R curves is constructed for X80.

A general method and procedure to transfer the experimental J-R curves from laboratory to actual cracked components is proposed next. This adaptation is demonstrated by its application in assessing flaw instability, a pipeline with an axial surface crack. This adaptation for pipelines is validated by comparison to the usual collapse-based predictions. In this adaptation, the predicted J-R curve is found to be higher than that for the SENB specimen with the same crack length to width ratio. Using this predicted J-R curve and crack driving force obtained by FEA, the failure pressures of the pipeline at the crack initiation and instability are predicted and discussed specific to a crack depth of 50-percent of the wall thickness.

Evidence of Constraint for Line-Pipe Steels and Pipeline Applications

Constraint effects on fracture resistances for pipeline steels have been studied for decades^(e.g.,65). More recently, in 2002, crack-tip opening displacement (CTOD) fracture resistance curves indicated a constraint effect for X52 line-pipe steel⁽⁶⁶⁾, whereas constraint effects were shown in terms of J-R curves for X70 line-pipe steel⁽⁶⁷⁾. Likewise, in 2002 constraint effects were evident in full-scale fracture testing through J-R curves for cracked pipes with different circumferential through wall cracks under four point bending load, in results that also showed a geometry-dependence⁽⁶⁸⁾. Subsequently, significant constraint effects were shown in the J-R curves of SENB and SENT specimens made of X80 and X100 pipeline steels⁽⁶¹⁾. It follows that constraint effects are not new in line-pipe steels or pipelines.

For sustained ductile tearing at a crack as is possible in tough steels, a large increase in the loading-carrying capacity of pipeline steels as characterized by constraint-dependent J-R curves can occur beyond the limits by conventional analysis^(e.g.,67). Thus, it also follows that the constraint dependence of J-R curves and its effect on fracture behavior must be accounted for, and viable methods developed to characterize and assess its effects.

Mechanical Properties of the X80

As indicated above, modern X80 line-pipe steel was considered whose mechanical properties were determined from N550 line pipe supplied by TransCanada Pipelines Ltd. (TCPL), as noted in Reference 61. As outline therein, all specimens were cut and machined from pipe with an outside diameter (OD) of 1219 mm (48 inches) and wall thickness of 12.7 mm (0.5 inch). Tensile properties were measured using full-thickness (25 mm x 11.5 mm) samples oriented in the longitudinal direction. The true stress-strain curve is illustrated in Figure 10. The tensile test results show that the 0.2-percent offset yield stress of X80 is 570 MPa, the 0.5-percent total yield stress is 576 MPa, the UTS is 675 MPa, the elongation for the two inch gage length is 42.2 percent and the final reduction of area is 68.3 percent. In elastic-plastic fracture analysis, it is usual to fit the true stress-strain curve in the form of Ramberg-Osgood power-law relation:

$$\frac{\varepsilon}{\varepsilon_0} = \frac{\sigma}{\sigma_0} + \alpha \left(\frac{\sigma}{\sigma_0} \right)^n \quad (11)$$

where the reference stress σ_0 is taken as the 0.2-percent offset yield stress, the reference strain ϵ_0 is taken as σ_0/E with E being Young's (elastic) modulus taken as 207 GPa. Figure 10 indicates a good fit is achieved in comparison to the actual response of this steel through use of a hardening parameter $\alpha = 1.07$ and a strain-hardening exponent, $n = 13$.

Fracture Specimen Geometries and Fracture Resistance

SENB and SENT specimens were used to determine J-R curves⁽⁶¹⁾. For the present work, results for the SENB specimen are used to benchmark the fracture resistance, while results for the SENT specimen are used to evaluate the validity of the present analysis formulation for the effects of constraint.

Reference 61 notes that the SENB specimens were sized as recommended by ASTM E 1820⁽⁶⁹⁾, except for the initial crack length was varied to develop different levels of crack-tip constraint. Specimens were side grooved using a tool shaped to a CVN for a total thickness reduction of 20 percent, in an attempt to develop plane strain conditions along the crack front. The specimen width, W , was 23 mm with initial crack length a varied producing ratios of a/W between 0.24 and 0.64, which reflects shallow to deep cracks and develops different fracture constraint levels at the crack tip. The un-cracked ligament length, b , is by definition $W-a$, while the specimen thickness $B = W/2$ was 11.5 mm.

J-R curves were determined for the SENB specimens following ASTM E 1820. After fatigue pre-cracking according to the procedure in ASTM E 1820, all SENB specimens were loaded at ambient temperature (about 20°C) in three-point bending with a span of 92 mm. After testing, the specimens were heat tinted and then broken in liquid nitrogen. The initial and final crack lengths were measured on the fracture surface by the 9-point technique described in ASTM E 1820. The criterion for uniform crack extension given in ASTM E 1820, which requires that none of the nine physical measurements differ by more than 5-percent from the average physical crack size, was not met for the final crack length, primarily because splitting occurred during the tests. (For some specimens with severe splitting, the difference among the nine physical measurements for the final crack length was as high as 40-percent.) However, lateral splitting was not observed for crack extension $\Delta a \leq 0.2$ mm. Figure 11 presents the fracture resistance as characterized experimentally by the J-R curves for the X80 SENB specimens.

The initiation toughness (J_i) used to characterize fracture resistance at the onset of stable ductile crack growth can be defined using the J-R curve at the critical stretch zone width (Δa), which can be measured on the fracture surface using a scanning electron microscope (SEM). It has been shown that J_i is not dependent on stress triaxiality or crack-tip constraint and can be treated as a material property⁽⁶⁸⁾. As it has been reported $\Delta a_i \approx 0.2$ mm for SA333 Gr6 pressure vessel steel⁽⁶⁸⁾ as well as for XCrNi1811 structural steel⁽⁷⁰⁾, crack extension at $\Delta a = 0.2$ mm is used to define fracture initiation herein. From Figure 11, values of the fracture initiation toughness for X80 pipeline steel at the crack extension of $\Delta a = 0.2$ mm are obtained as 420, 407, 290, 370, 250, and 287 kJ/m² for $a/W = 0.24, 0.25, 0.42, 0.43, 0.63,$ and 0.64 , respectively. On the other hand, as specified in ASTM E 1820, the fracture initiation toughness is defined as the intersection of the measured J-R curve and the 0.2-mm offset line, which is parallel to the construction or blunting line. For X80, the 0.2-mm offset line is $1868(\Delta a - 0.2)$ mm, which is included in Figure 11. From this figure it is apparent that the 0.2-mm offset-fracture-toughness varies from 400 to 1010 kJ/m², which leads to much larger values of initiation toughness as compared to that defined at a crack extension of 0.2 mm.

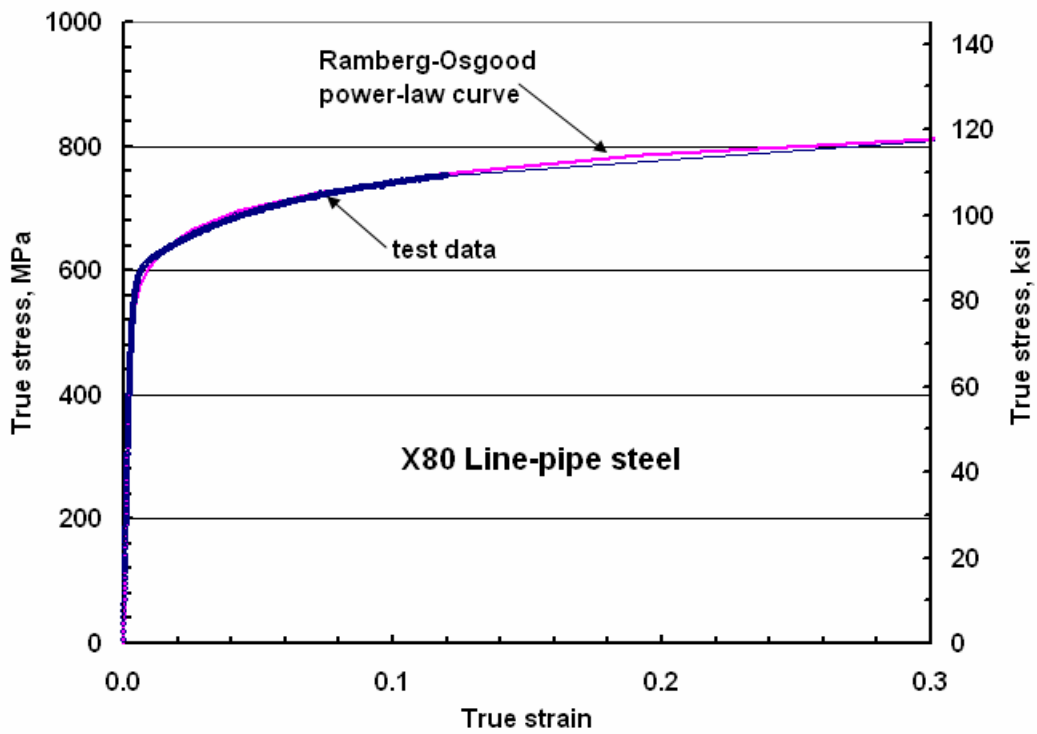


Figure 10. True stress-strain curve of X80 line-pipe steel

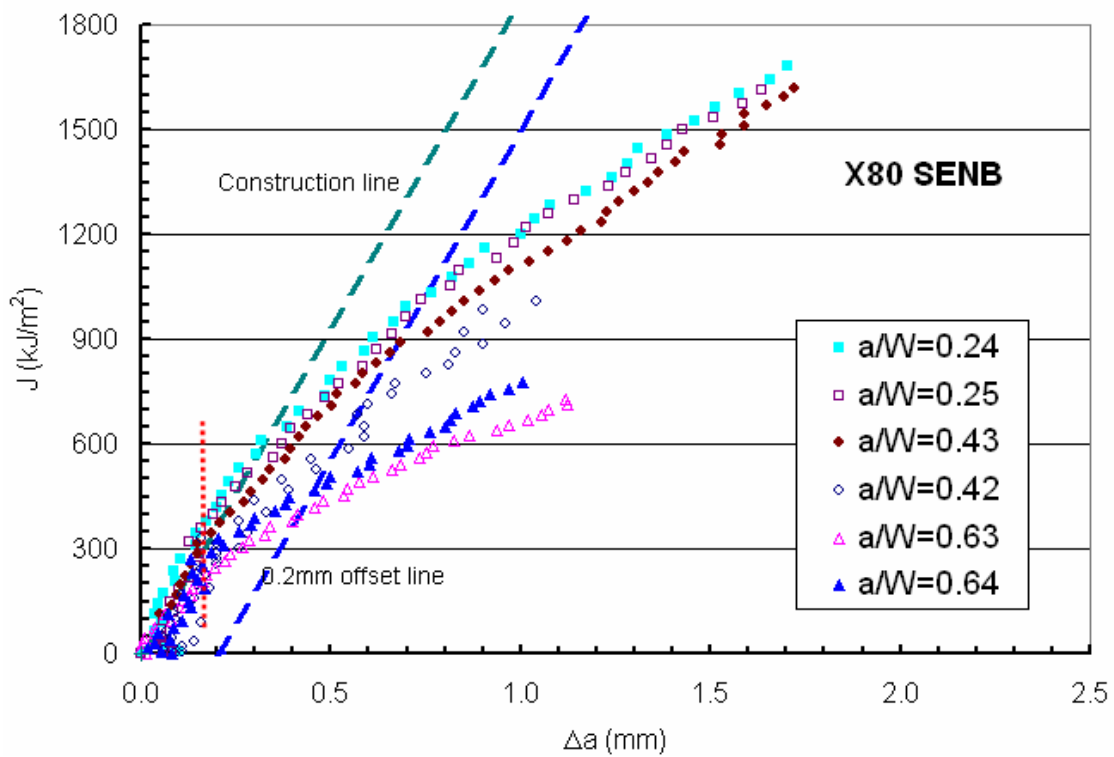


Figure 11. Experimental J-R curves for SENB specimens

In contrast to SENB specimens, a standard procedure to calculate the J-resistance is not available for SENT specimens. Using an estimation scheme, Shen et al⁽⁶¹⁾ obtained the J-R curves for SENT specimens the results for which are shown in Figure 12. As noted earlier, these J-R curves will be used to validate the predicted J-R curves later, which will be formulated using the test data for the SENB specimens.

Numerical Calculations and Constraint Analyses

Finite Element Analysis

Plane strain elastic-plastic FEA using the commercial software package ABAQUS⁽⁷¹⁾ was done to calculate the crack-tip stress and strain fields and determine fracture parameters for the test specimens. The constraint parameter A_2 is extracted from the crack-opening stress distribution at the crack tip when the specimen loading reaches the initiation toughness, where the deformation involves the large scale yielding (LSY) and so A_2 attains a nearly constant value.

Because of symmetry, only one half of each specimen was modeled with two-dimensional FEA using the typical FEA mesh illustrated in Figure 13. A fine mesh was used with the smallest element size of 0.002 mm focused on the crack tip, and an increasingly coarse mesh was generated elsewhere. The FEA mesh consisted of 1925 nodes and 604 eight-node plane strain isoparametric elements with reduced integration. The local mesh encircling the crack tip contained 23 rings of elements with each ring having 18 elements. The same number of elements and nodes were used for all test specimens. For the SENB specimens, a concentrated load was applied on the top of ligament. For the SENT specimens, a uniform distributed load was applied on the end.

In the FEA, the stress-strain relation follows the usual nonlinear elastic constitutive equation in the three dimensional form:

$$\frac{\varepsilon_{ij}}{\varepsilon_0} = (1 + \nu) \frac{\sigma_{ij}}{\sigma_0} - \nu \frac{\sigma_{kk}}{\sigma_0} \delta_{ij} + \frac{3}{2} \alpha \left(\frac{\sigma_e}{\sigma_0} \right)^{n-1} \frac{s_{ij}}{\sigma_0} \quad (12)$$

where σ_0 and ε_0 and α and n are as defined earlier, ν is the Poisson ratio, and $s_{ij} = \sigma_{ij} - \sigma_{kk} \delta_{ij}$ is the deviatoric stress, δ_{ij} is the Kronecker delta, and $\sigma_e = (3s_{ij} \cdot s_{ij}/2)$ is the von Mises effective stress. For the stress-strain curve for X80 pipeline steel shown in Figure 10, the material constants are $\sigma_0 = 570$ MPa, $E = 207$ GPa, $\alpha = 1.07$, $n = 13$, and $\nu = 0.3$.

Figure 14 shows distributions of the crack opening stress, $\sigma_{\theta\theta}$, obtained from the FEA at different deformation levels as a function of distance from the crack tip for the SENB specimens with $a/W = 0.24$ and 0.42 , respectively. The results in this figure indicate that the opening stress near the crack tip decreases as loading increases for normalized distance r . Under LSY, the linear distribution of $\sigma_{\theta\theta}$ for large r shows the influence of global bending on the crack-tip stress fields.

The J- A_2 Solution

The J- A_2 three-term solution proposed by Yang et al^(57,58) is used to characterize the crack-tip fields and quantify constraint levels for all specimens considered. Under plane strain conditions, the asymptotic stress field near the crack tip for a power-law material can be expressed as:

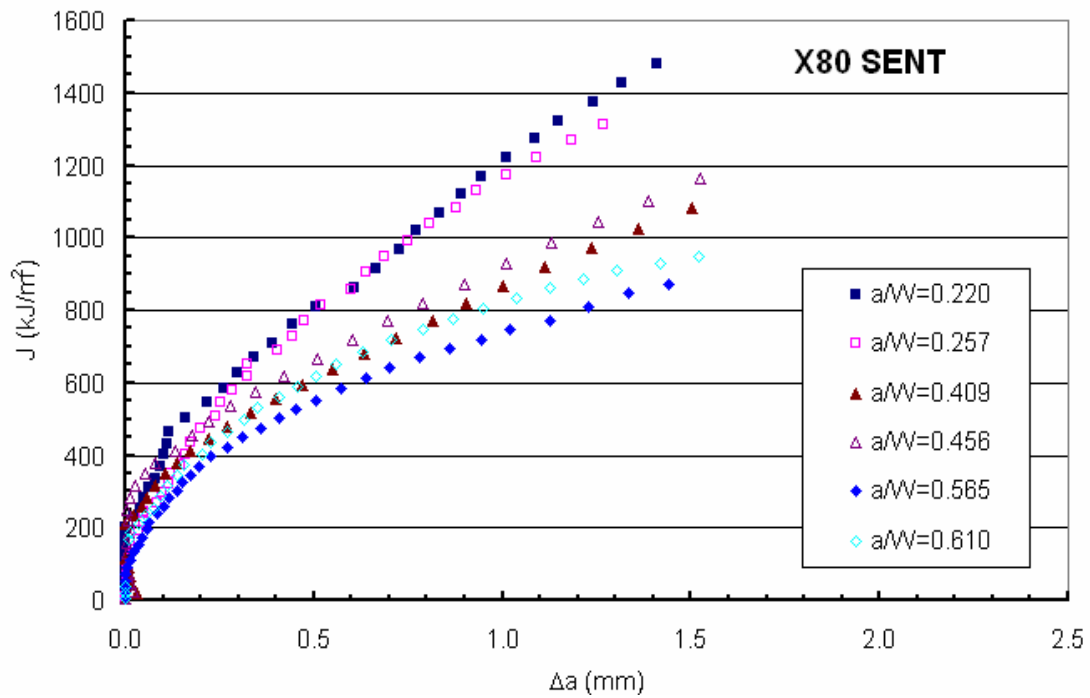


Figure 12. Experimental J-R curves for SENT specimens

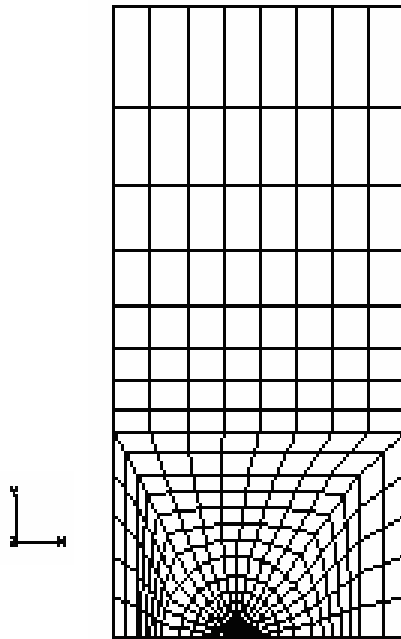
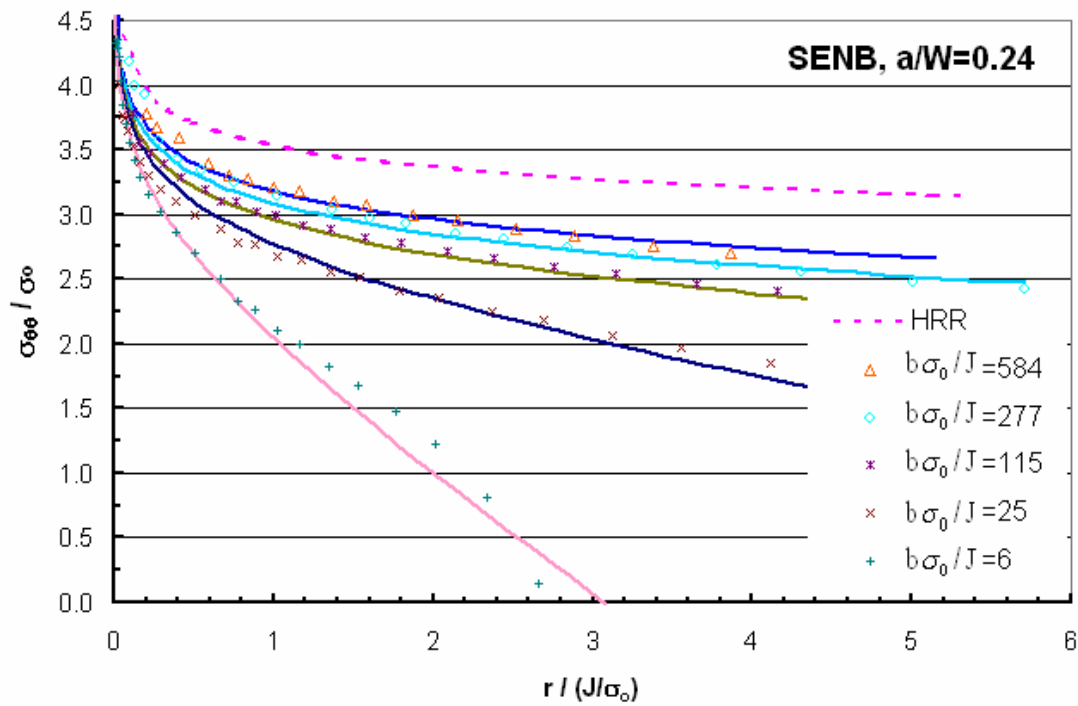
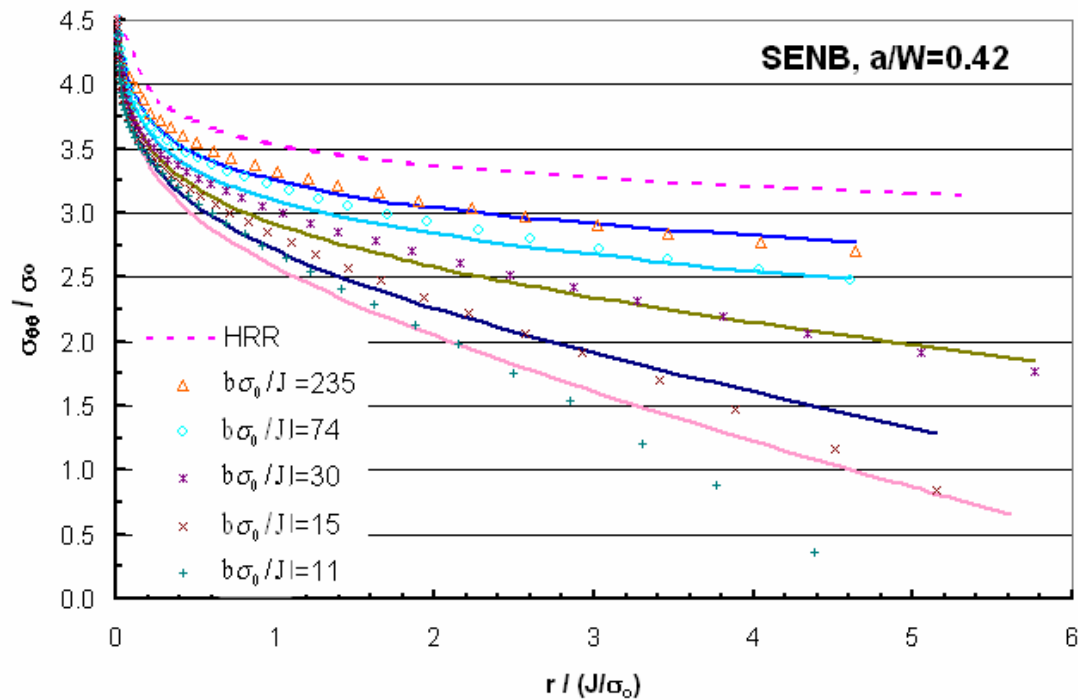


Figure 13. Typical finite element mesh for test specimens



a) a/W = 0.24



b) a/W = 0.42

Figure 14. Distribution of opening stress σ_{00} along the distance from the crack tip (symbols are FEA results, the lines reflect asymptotic solutions)

$$\frac{\sigma_{ij}}{\sigma_0} = A_1 \left[\left(\frac{r}{L} \right)^{s_1} \tilde{\sigma}_{ij}^{(1)}(\theta) + A_2 \left(\frac{r}{L} \right)^{s_2} \tilde{\sigma}_{ij}^{(2)}(\theta) + A_2^2 \left(\frac{r}{L} \right)^{s_3} \tilde{\sigma}_{ij}^{(3)}(\theta) \right] \quad (13)$$

where the stress angular functions $\tilde{\sigma}_{ij}^{(k)}(\theta)$ ($k=1, 2, 3$) and the stress power exponents, s_k , ($s_1 < s_2 < s_3$) depend only on the strain hardening exponent n , and are independent of the other material constants (i.e. α , σ_0 , and ϵ_0) or the parameter A_2 . The values of $\tilde{\sigma}_{ij}^{(k)}(\theta)$ and s_k are tabulated in Reference 72. In Equation 13, L is a characteristic length parameter, with $L = 1$ mm being adopted in this work. The parameters A_1 and s_1 are related to the HRR^(62,63) singularity field by:

$$A_1 = \left(\frac{J}{\alpha \epsilon_0 \sigma_0 I_n L} \right)^{-s_1}, \quad s_1 = -\frac{1}{n+1} \quad (14)$$

and $s_3 = 2s_2 - s_1$ for $n \geq 3$. The constraint parameter A_2 is an unknown constant to be determined using the point matching method, by matching the opening stress from the J- A_2 solution with the FEA result at $r/(J/\sigma_0) \approx 1$ to 2, for example.

The Modified J- A_2 Solution

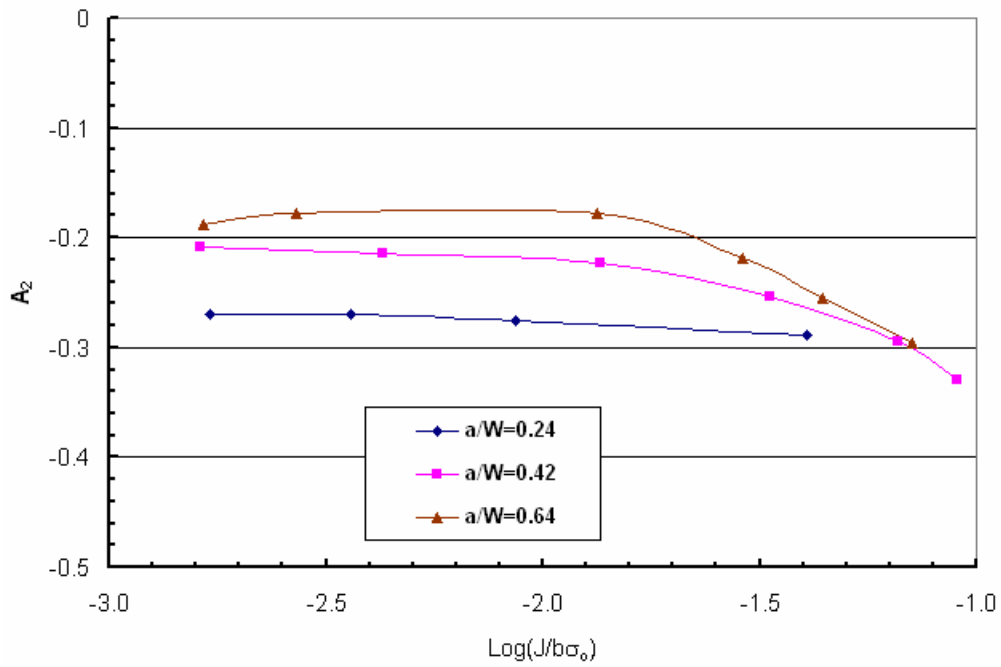
For deep crack bending specimens under LSY or fully plastic deformation, it has been shown that the global bending stress significantly affects the crack-tip field. As a result, the J- A_2 three term solution (i.e. Equation 13), fails to correctly describe the crack-tip field. To eliminate the influence of the global bending stress on the asymptotic crack-tip stress field, Chao et al⁽⁶⁰⁾ recently proposed a modification of the J- A_2 solution for the crack opening stress ahead of the crack tip, i.e. at $\theta = 0^\circ$, in bending specimens as:

$$\frac{\sigma_{\theta\theta}(0)}{\sigma_0} = A_1 \left[\left(\frac{r}{L} \right)^{s_1} \tilde{\sigma}_{\theta\theta}^{(1)}(0) + A_2 \left(\frac{r}{L} \right)^{s_2} \tilde{\sigma}_{\theta\theta}^{(2)}(0) + A_2^2 \left(\frac{r}{L} \right)^{s_3} \tilde{\sigma}_{\theta\theta}^{(3)}(0) \right] - \frac{6Mr}{\sigma_0 b^3} \quad (15)$$

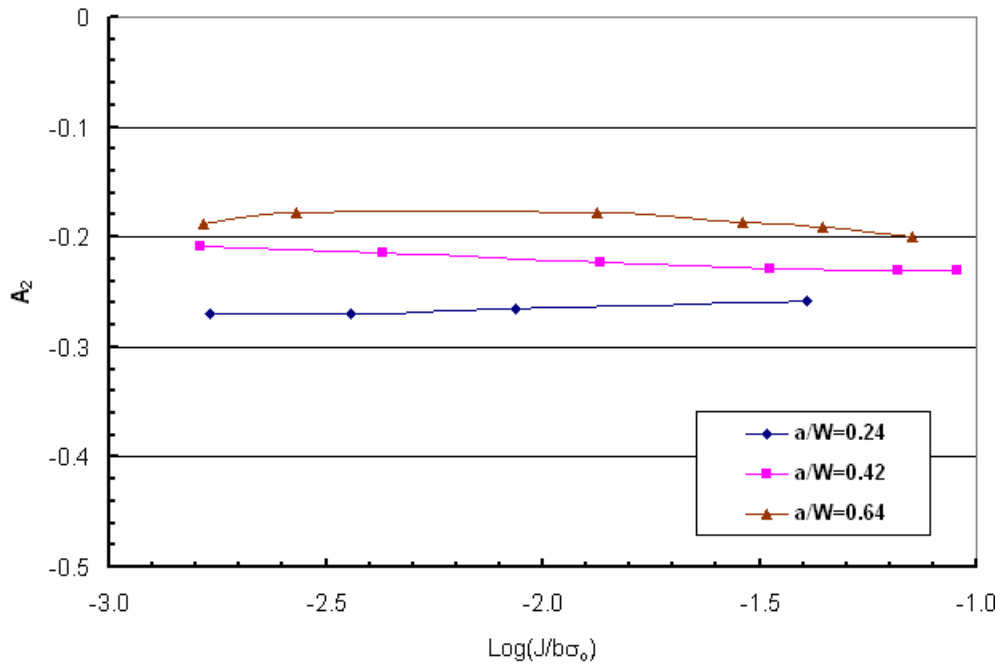
where M is the global bending moment. The modified J- A_2 solution still only involves the two parameters, namely the applied load (J and M) and constraint parameter (A_2).

Determination of the Constraint Parameter A_2

The constraint parameter A_2 is usually determined by matching the opening stress, $\sigma_{\theta\theta}$, from the J- A_2 solution with the FEA result at $\theta = 0^\circ$ and $r/(J/\sigma_0) \approx 2$. Figure 15 depicts the variations of the constraint parameter A_2 with the applied loading J for the SENB specimens with $a/W = 0.24$, 0.42, and 0.64. The parameter A_2 in Figure 15a is determined by the J- A_2 solution via Equation 13, while the parameter A_2 in Figure 15b for the modified solution is determined by the modified J- A_2 solution or Equation 15. Comparison shows that the A_2 values determined using Equations 13 and 15 are almost the same and constant for all loading for the shallow crack ($a/W = 0.24$), but are different for the two deeper cracks under LSY. Without the global bending influence, A_2 is theoretically a constant independent of loading at LSY⁽⁶⁴⁾. This implies that the global bending stress has significant influence on the crack tip fields for the deep cracks under LSY, but has no significant effect for the shallow cracks or deep cracks under small scale yielding (SSY). After having considered the global bending influence, Figure 15b indicates that A_2 determined by Equation 15 is a nearly load-independent constant for the three specimens. Specifically, $A_2 \approx -0.27$, -0.23 , and -0.18 , respectively for $a/W = 0.24$, 0.42, and 0.64. These



a) the J-A₂ solution without global bending



b) the modified J-A₂ solution with global bending

Figure 15. Variation of A₂ with J for SENB specimens considering global bending

results indicate that it is reasonable to use the load-independent parameter A_2 to quantify the constraint level of a J-R curve for a specific geometry.

With the value of A_2 determined as just discussed, the crack-tip stress field can be determined from the (modified) J- A_2 solution for a given loading of J (and M). Figure 14a presents distributions of the opening stress determined from the J- A_2 solution at five deformation levels from SSY to LSY for the SENB specimen with shallow crack of $a/W = 0.24$. (Note that for the fully plastic deformation of $b \cdot \sigma_0/J = 6$ in Figure 14a, the modified J- A_2 solution is used.) Figure 14b shows the opening stress determined from the modified J- A_2 solution at five deformation levels for the SENB specimen with deep crack of $a/W = 0.42$. Both figures include the HRR solution. These results indicate that the modified J- A_2 solution matches well with the FEA results at all deformation levels. Accordingly, the modified J- A_2 solution should be used to characterize the crack-tip field and quantify the constraint level at the crack tip for X80 pipeline steel.

Constraint Correction of J-R Curves for Ductile Crack Growth

General Methodology

Following the concept of J-controlled crack growth, Chao et. al.^(59,64) proposed the concept of J- A_2 controlled crack growth by extending the J- A_2 two-parameter description for stationary cracks to growing cracks with small crack extension. The J- A_2 description was used to analyze ductile crack growth, and an engineering method developed to quantify the effects of constraint on J-R curves.

As demonstrated above for X80, the constraint parameter A_2 is nearly load-independent, and thus the A_2 determined at the crack initiation load remains constant for subsequent stable crack growth. Therefore, when small crack extension occurs within the J- A_2 dominant region, A_2 can be considered to be constant. Under J- A_2 controlled crack growth, the curve of J-integral resistance versus crack extension Δa , can be expressed by a power-law relationship, as suggested in ASTM E 1820:

$$J(\Delta a, A_2) = C_1(A_2) \left(\frac{\Delta a}{k} \right)^{C_2(A_2)} \quad (16)$$

where $k = 1$ mm, and the coefficients $C_1 A_2$ and $C_2 A_2$ are undetermined functions of A_2 . (Note that C_1 and C_2 are constant in the original ASTM E 1820 formulation.) Equation 16 extends the current ASTM J-R curve concept, $J(\Delta a)$, to a constraint corrected J-R concept, $J(\Delta a, A_2)$. This requires determining the functional dependencies of C_1 and C_2 on the constraint parameter A_2 . Once the functional forms of $C_1 A_2$ and $C_2 A_2$ are obtained, a family of constraint-corrected J-R curves is fully determined. As indicated above, Equation 16 contains two unknown variables, C_1 and C_2 for a given A_2 , which requires two independent equations to solve for these values.

Whereas Chao and Zhu⁽⁶⁴⁾ proposed a procedure to determine the functions C_1 and C_2 in reference to the initiation toughness and the ductile tearing modulus defined in ASTM E 1820, a more general approach is developed here. Basically, the two necessary independent equations can be established at any two points of crack extension for the experimental J-R curves. The first point can be chosen at crack extension, Δa_1 , where the crack initiates, and the other point can be chosen at crack extension, where the crack has extended beyond initiation, Δa_2 . The J-integrals corresponding to these two points are denoted by:

$$\begin{aligned} J|_{\Delta a_1} &= J_{\Delta a_1}(A_2) \\ J|_{\Delta a_2} &= J_{\Delta a_2}(A_2) \end{aligned} \quad (17)$$

where $J_{\Delta a_1}(A_2)$ and $J_{\Delta a_2}(A_2)$ are two known functions of A_2 determined by best-fitting test data extracted from at least three experimental J-R curves. In principle, if Δa_i ($i = 1-2$) is chosen between 0.2 and 2 mm, it automatically satisfies the ASTM E 1820 criterion for acceptable data. However, if a specimen exhibits much longer crack extension ($\Delta a \geq 2$ mm), choosing Δa_i outside of that range may yield a better overall fit for the J-R curves⁽⁷³⁾.

Substituting Equations 17 into 16, one obtains the following set of simultaneous equations:

$$\begin{aligned} C_1(A_2)(\Delta a_1 / k)^{C_2(A_2)} &= J_{\Delta a_1}(A_2) \\ C_1(A_2)(\Delta a_2 / k)^{C_2(A_2)} &= J_{\Delta a_2}(A_2) \end{aligned} \quad (18)$$

Equation 18 can be used to determine the functions C_1 and C_2 of A_2 . The valid range of A_2 , based on past studies, is between -1 and 0, as the crack-tip constraint increases from low to high. Solving C_1 and C_2 for a series of A_2 values within this range ($-1 < A_2 < 0$) provides the functional dependencies of C_1 and C_2 with respect to A_2 . Finally, least-square regression analysis provides the desired functional forms of C_1 and C_2 in terms of the constraint parameter A_2 .

For a given material, once the expression for the constraint-corrected J-R curve, or Equation 16, is obtained, the J-R curve can be accurately predicted for any specific cracked geometry (e.g., non-standard specimens or actual structural components), provided that the constraint parameter A_2 is known for that cracked geometry, or would be determined numerically as outlined herein.

Construction of Constraint-Corrected J-R Curve

Using the SENB test data shown in Figure 11 and the method described above, a constraint corrected J-R curve in terms of A_2 can be constructed for X80 pipeline steel. Two equations are set up to solve for C_1 and C_2 at $J = J_{0.2\text{mm}}$ and $J = J_{1.0\text{mm}}$. Using the (modified) J- A_2 solution at $J_{0.2\text{mm}}$, the value of A_2 for each SENB specimen is determined.

Figure 16 plots the $J_{0.2\text{mm}}$ versus A_2 and $J_{1.0\text{mm}}$ versus A_2 relations. It appears that $J_{0.2\text{mm}}$ is not very sensitive to the specimen geometry, and a linear relationship can be easily fitted between $J_{1.0\text{mm}}$ and A_2 . As such, one has:

$$\begin{aligned} J_{0.2\text{mm}} &= 337.3 \\ J_{1.0\text{mm}} &= -4417.1A_2 \end{aligned} \quad (19)$$

where the J-integral has unit in kJ/m^2 . Substitution of Equation 19 into Equation 18 leads to:

$$\begin{aligned} C_1 0.2^{C_2} &= 337.3 \\ C_1 1.0^{C_2} &= -4417.1A_2 \end{aligned} \quad (20)$$

From Equation 20, the functions of $C_1(A_2)$ and $C_2(A_2)$ can be approximated as:

$$\begin{aligned} C_1(A_2) &= -4417.1A_2 \\ C_2(A_2) &= -1.61A_2^2 - 3.14A_2 \end{aligned} \quad (21)$$

Finally, substituting Equation 21 to Equation 16, the constraint-corrected J-R curve for X80 pipeline steel is found as:

$$J(\Delta a, A_2) = -4417.1 A_2 \left(\frac{\Delta a}{1 \text{ mm}} \right)^{(-1.61 A_2^2 - 3.14 A_2)} \quad (22)$$

where the J-integral has units of kJ/m^2 . Equation 22 indicates that the constraint corrected J-R curve is a function of A_2 and Δa . If A_2 is known for a specific geometry, the J-R curve can be easily predicted from Equation 22.

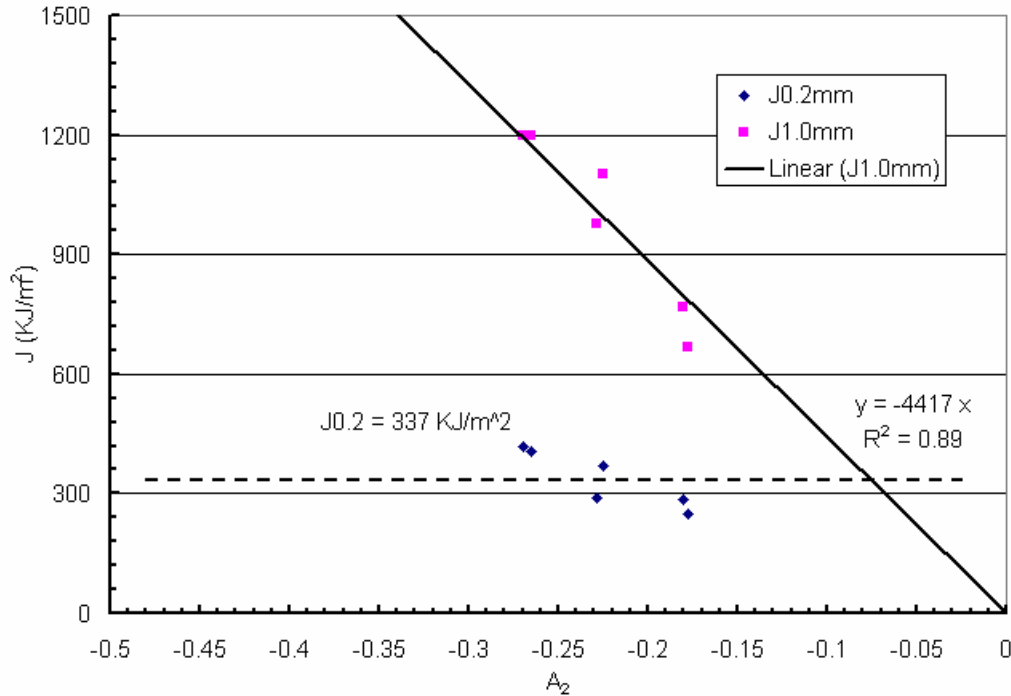


Figure 16. Variation of $J_{0.2\text{mm}}$ and $J_{1.0\text{mm}}$ with constraint parameter for SENB specimens

Validation of Predicted J-R curves

For the SENB specimens with $a/W = 0.24, 0.42, \text{ and } 0.64$, the values of A_2 evaluated for $J_{0.2\text{mm}} = 337.3 \text{ kJ/m}^2$ are $-0.27, -0.23, \text{ and } -0.18$, respectively. Thereafter, the J-R curve can be predicted from Equation 22. Figure 17 compares the predicted J-R curves with the experimental J-R curves for these three SENB specimens. Likewise, Figure 18 compares the predicted J-R curves with the experimental J-R curves for the SENT specimens with $a/W = 0.25, 0.41, \text{ and } 0.57$, respectively. These comparisons show that the predicted J-R curves from Equation 22 match well with the experimental data for both SENB and SENT specimens. Therefore, the constraint-corrected J-R curve or Equation 22 can be effectively used to predict the J-R curve for any specimen or actual component, provided that the constraint parameter A_2 is known a priori.

Application to Prediction Failure Pressure of a Cracked Pipeline

FEA Simulation and Constraint Analysis

For purposes of this illustration a pipeline with an OD of 762 mm and a wall thickness of 23 mm is considered subjected to internal pressure. For the sake of simplicity in this illustration, this pipeline is found to contain a very long axial surface crack on its exterior, with a crack depth of

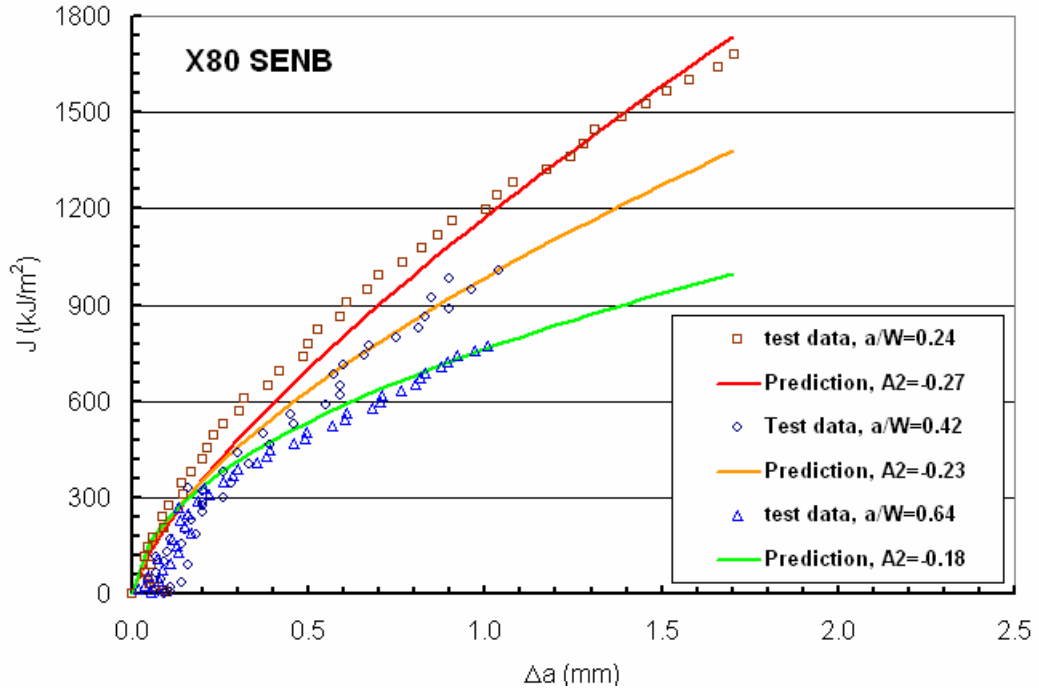


Figure 17. Comparison of predicted and experimental J - R curves for SENB specimens

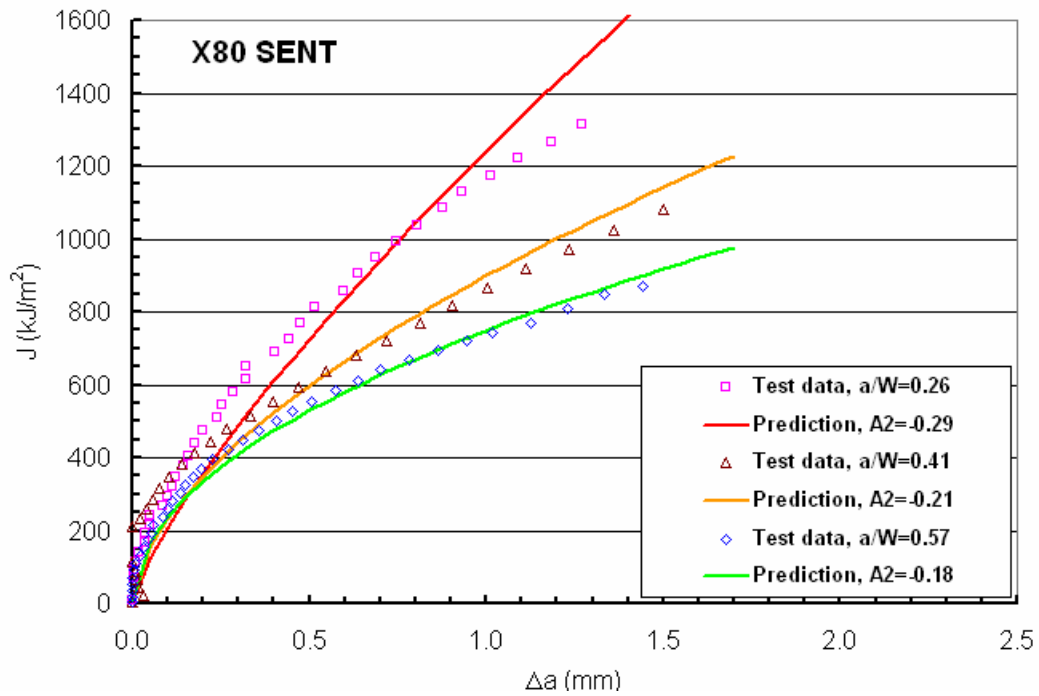


Figure 18. Comparison of predicted and experimental J - R curves for SENT specimens

50-percent of the wall thickness. Because the crack is very long, plane strain deformation can be reasonably assumed for the cracked pipe. As a result and in light of symmetry, one half of the circular cross-section is modeled using the FEA mesh shown in Figure 19. In this FEA model, a very fine mesh is generated near the crack tip with the smallest element size of 0.003 mm, with a coarser mesh used elsewhere. The mesh involves 3107 nodes and 944 eight-node plane strain isoparametric elements with reduced integration. The boundary conditions reflect symmetry and the only applied load is internal pressure.

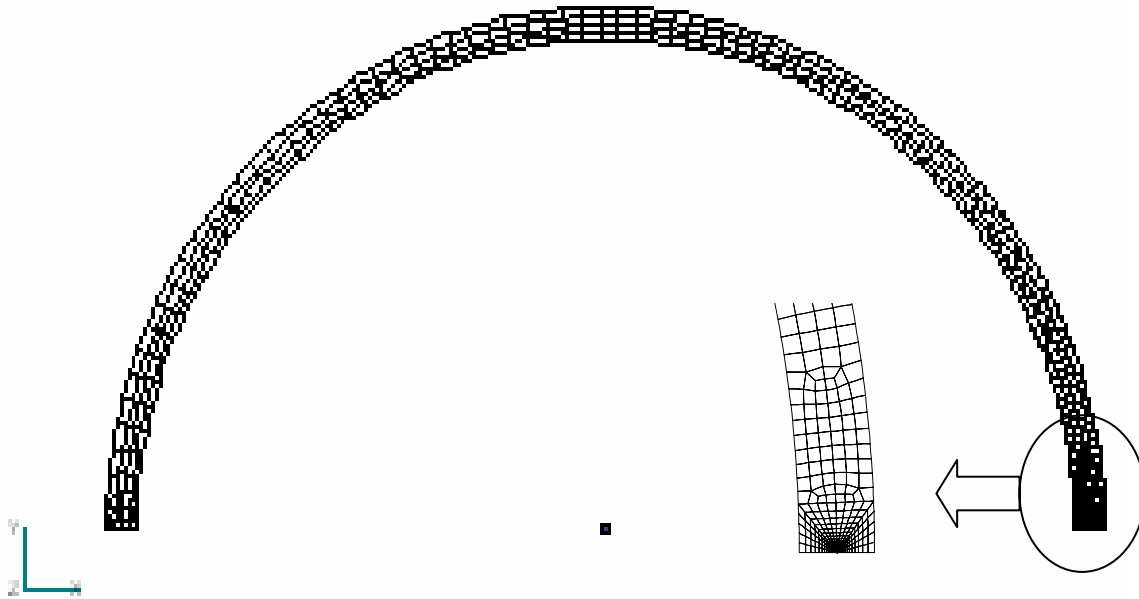


Figure 19. 10Finite element mesh for pipe with an axial surface crack of $a/t = 0.5$

Figure 20 shows the distribution of crack opening stress determined by FEA calculations and the $J-A_2$ solution (Equation 13) along the distance from the crack-tip, at different deformation levels from SSY to LSY for the X80 pipe with a surface crack of $a/t = 0.5$. The constraint parameter A_2 is taken as -0.25 for all cases. Note that the HRR solution is also included in Figure 20. It is apparent that the global bending stress has insignificant influence on the crack-tip, and the $J-A_2$ three-term solution is well matched with the FEA results at all deformation levels, whereas the HRR field does not fit the FEA results even under SSY. This indicates that the $J-A_2$ solution can be used to characterize the crack-tip field for this surface crack in this X80 pipeline.

Predicted J-R Curve for the Cracked Pipeline

Replacing the value of -0.25 for A_2 in Equation 22 of the constraint-corrected J-R curve yields the predicted J-R curve for the X80 pipe with a long axial surface crack of $a/t = 0.5$ as follows:

$$J(\Delta a) = 1104.25 \left(\frac{\Delta a}{1 \text{ mm}} \right)^{0.886} \quad (23)$$

where the J-integral is in kJ/m^2 . This J-R curve is plotted in Figure 21 and compared with those for the SENB specimens.

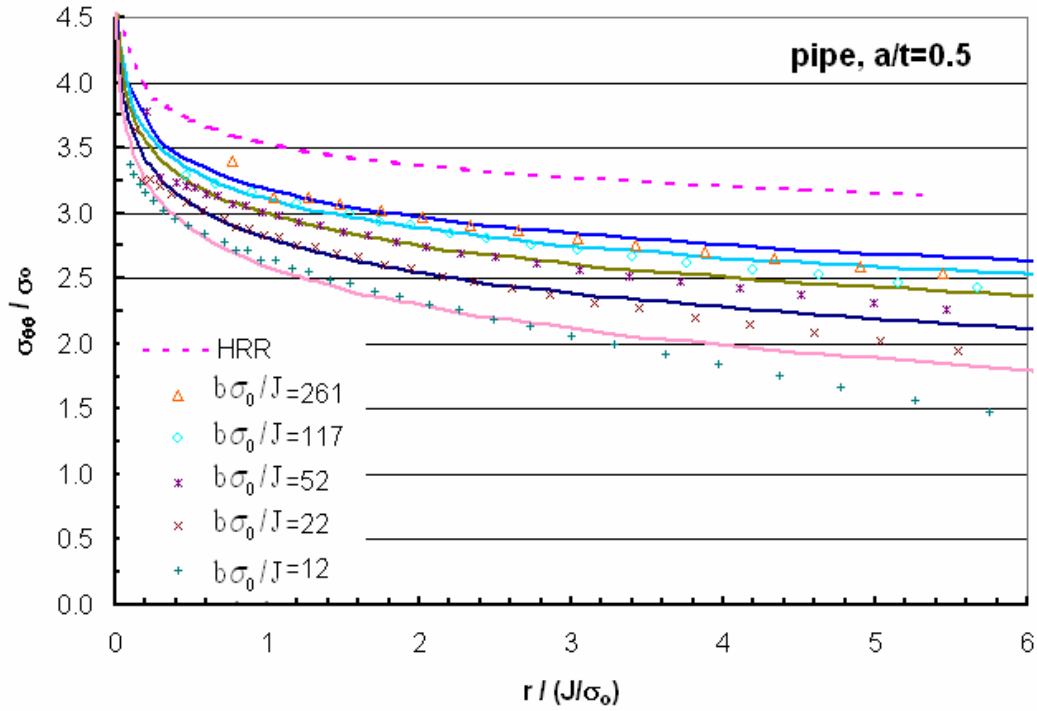


Figure 20. Distribution of the opening stress determined from the FEA and J-A₂ solution along the distance from the crack tip

It indicates that the J-R curve for the cracked pipe is much higher than that for the ASTM standard SENB specimen with $a/W = 0.64$ or 0.5 , and may coincide with that for the SENB specimen with $a/W = 0.35$. Therefore, using the J-R curve from the ASTM standard specimen could overly underestimate the fracture resistance and so the limit load-carrying capability of the X80 pipe.

Predicted Failure Pressure via Plastic Collapse

For a pipe containing a longitudinal surface defect under internal pressure, the burst pressure p_d at the plastic collapse can be predicted by the PCORRC criterion⁽²³⁾ for blunt defects using the following equation:

$$p_d = \sigma_{uts} \frac{2t}{D} \left(1 - \frac{d}{t} \left(1 - \exp \left(-0.157 \frac{L}{\sqrt{R(t-d)}} \right) \right) \right) \quad (24)$$

where σ_{uts} is the ultimate tensile stress, $D = 2R$ is the average diameter of the pipe, t is the wall thickness, d is the defect depth and L is the defect length. PCORRC is as defined earlier – a UTS-based plastic-collapse criterion for blunt defects derived independent of fracture mechanics analysis. Thus, the limit pressure determined by Equation 24 is a plastic collapse failure load.

For very long defects Equation 24 simplifies to:

$$p_d = \sigma_{uts} \frac{2t}{D} \left(1 - \frac{d}{t} \right) \quad (25)$$

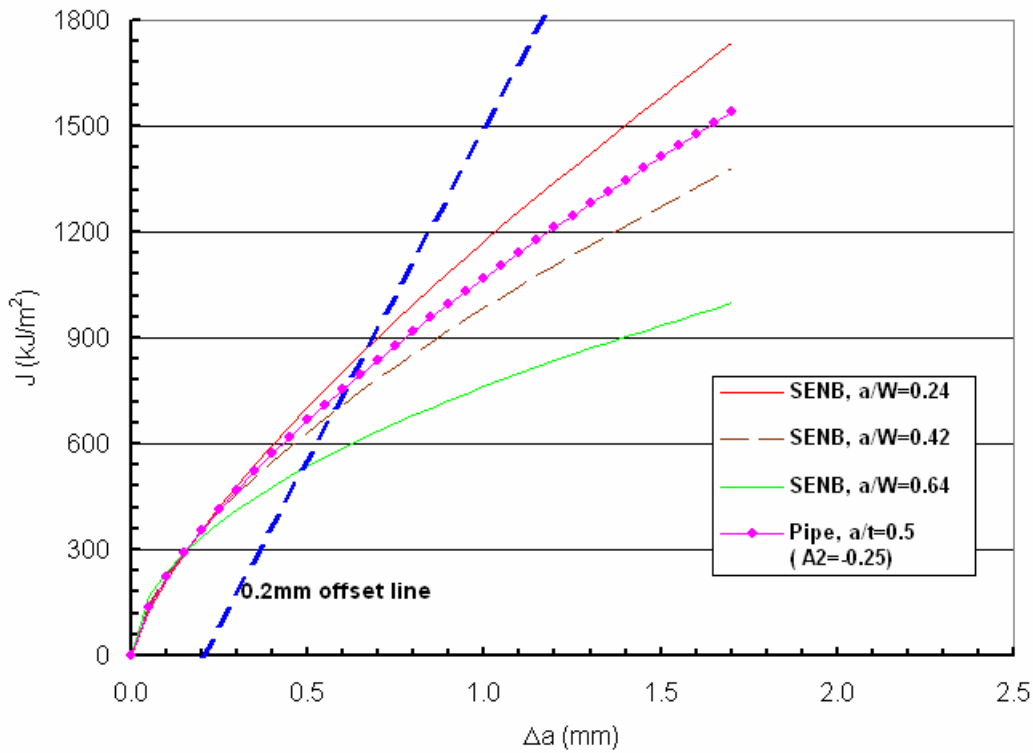


Figure 21. Predicted J-R curve for X80 pipe with a surface crack and compared with those for SENB specimens

For the cracked X80 pipe, $\sigma_{uts} = 675$ MPa, $D = 739$ mm, $t = 23$ mm with $d/t = 0.5$ for the example considered. For these conditions, Equation 25 predicts the burst pressure as $P_d = 21$ MPa at plastic collapse. Under LSY conditions in ductile steels, initially crack tips blunt, so Equation 25 should provide a reasonable estimate of the limit pressure at plastic collapse for the X80 pipeline under consideration. The next paragraphs assess the consistency between this “macro” model and the behavior characterized by fracture mechanics.

Predicted Failure Pressure via Elastic-Plastic Fracture and Assessment of the J-A₂ Concept

For NLFM, failure for a crack occurs when the crack driving force J reaches the fracture resistance, J_R , such that:

$$J = J_R \quad (26)$$

From the J-R curve as shown in Figure 21 for the cracked pipeline, the crack initiation toughness at crack extension of 0.2 mm and the 0.2 offset-toughness are determined as 337 kJ/m² and 796 kJ/m², respectively. For the cracked X80 pipe, the crack driving force, i.e., variation of the J-integral with the internal pressure is obtained in the FEA simulation, and shown in Figure 22. From Equation 26 and this figure, the failure pressures corresponding to the 0.2-mm toughness and the 0.2 offset-toughness are approximately determined as 19.1 MPa and 22.5 MPa. These values are very close to and bound the plastic collapse pressure of 21 MPa, indicating that ductile crack initiation and instability are close to plastic collapse for such a thin wall pipe. The crack

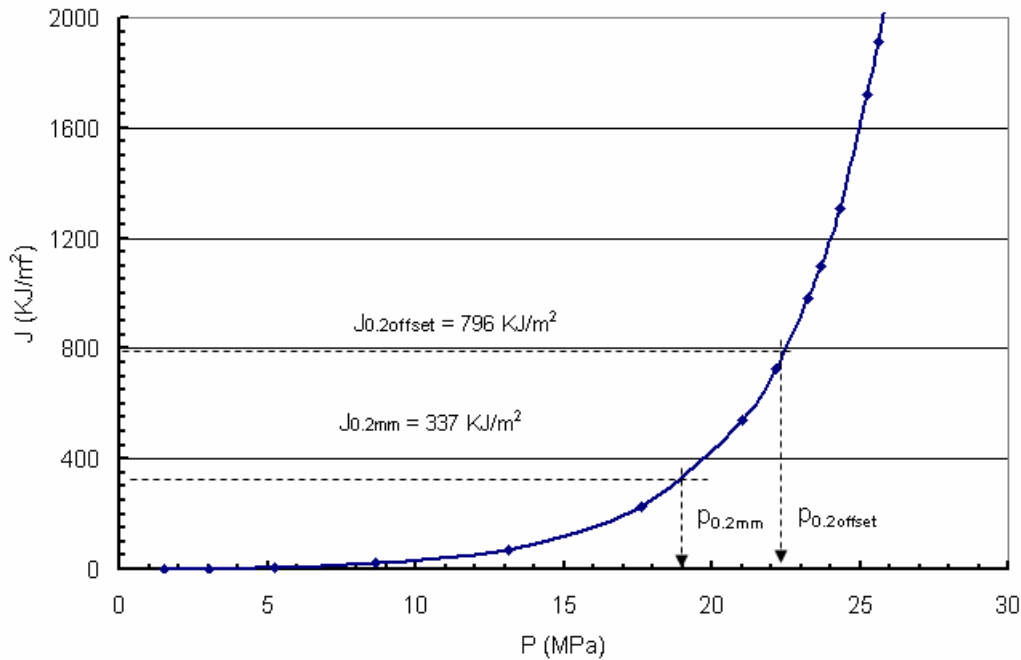


Figure 22. Variation of J-integral with internal pressure for the cracked pipe

depth for this case is 50-percent through wall, consistent with the case considered in the above plastic collapse analysis.

Therefore, at least for this case, the fracture failure pressure of deeply cracked pipelines at the crack initiation and instability can be bounded by pressures corresponding to the 0.2-mm toughness and 0.2-mm offset toughness, respectively. Such is not surprising, as the mechanism of failure for plastic-collapse through the net-section ligament is void nucleation, growth, and coalescence – which is identical to the process that underlies stable tearing as characterized by NLFM.

Implications for High-Constraint Scenarios

In higher-toughness steels there is sufficient resistance to stable tearing to support LSY leading to the redistribution of stresses and strains. Even where high constraint develops that reduces the relative fracture resistance as evident in Figures 11 and 12, there is sufficient fracture resistance to ensure the plastic collapse limit pressure (e.g., Equation 24) is achieved. However, where the relative toughness is low because of inherently low fracture resistance or the effects of DBTT for service below the DBTT, constraint can affect significant reduction in the apparent fracture resistance. This is evident from the present formulation in two interrelated ways, as follows.

The effects of constraint evident in Figures 11 and 12 is developed by differences in crack depth, loading conditions, and specimen geometry, whereas it also could be developed for shallow cracking in regard to differences in local stress field. These figures indicate that the J-R curve corresponding to high constraint has the lowest value of initiation resistance, and also the lowest resistance to continued cracking. The implication is that cracking can develop and continue under conditions of high constraint well before it occurs for low constraint, all else being equal.

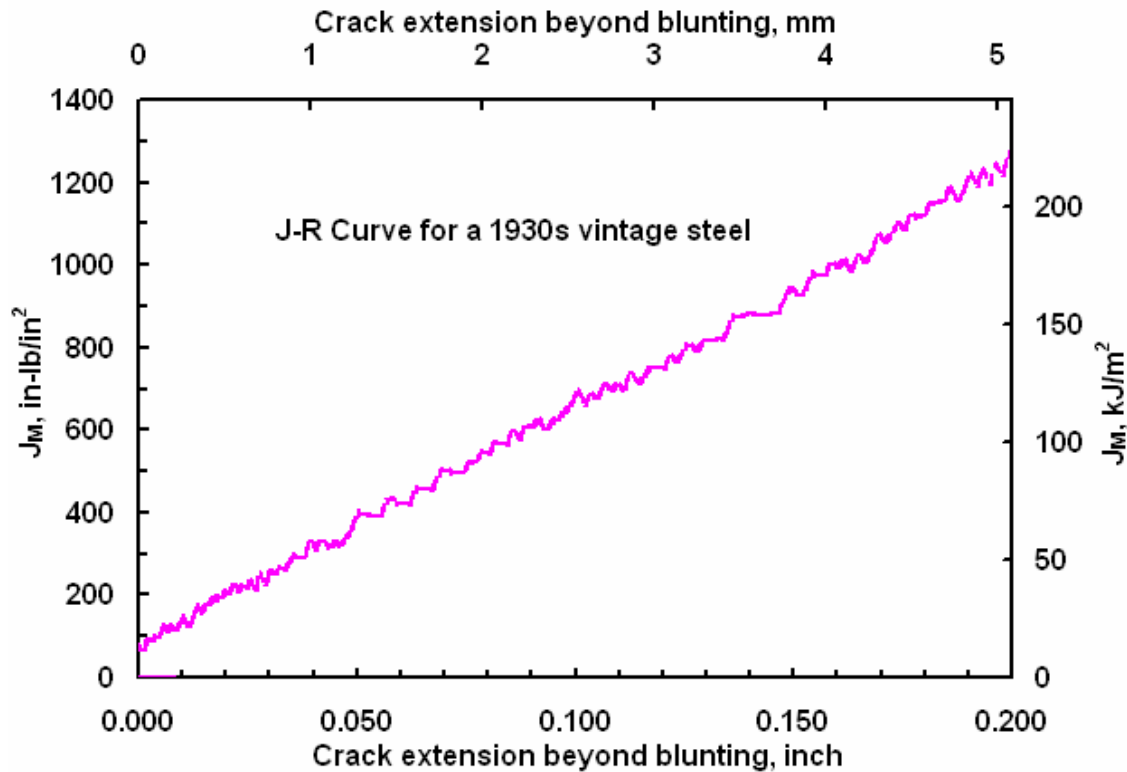


Figure 23. J-R curve for early-vintage line pipe

That is, because of reduced apparent cracking resistance, the effect of high constraint is to facilitate both the initiation of cracking, as well as to promote continued cracking, all else being equal. The key issue in this context is the relative significance of this effect. Figure 22 shows that the value of J as a driving force for cracking is nonlinearly proportional to pressure, being very strongly proportional to pressure for LEFM conditions and SSY.

It follows that the effects of constraint in reducing fracture resistance is manifest in pipelines as a decrease in pressure-carrying capacity that is most significant in or near LEFM conditions. For such situations, the decrease in failure pressure is nominally linear with the constraint-induced decrease in J_R . Lower-toughness steels admit only SSY and tend toward LEFM behavior. Accordingly, lower-toughness steels or steels where DBTT leads to lower toughness in service will be sensitive to the influence of constraint whereas scenarios where the toughness is higher will be relatively less sensitive. For the present concern involving constraint in otherwise blunt corrosion features, this formulation indicates that lower toughness facilitates the effects of constraint and related cracking. In turn, this means that testing lower-toughness steels or steels with limited ductility at the service temperature will fail prematurely where corrosion-induced metal-loss occurs. Rather, it means that where constraint develops because of the shape of the corrosion features and its loading, relatively lower toughness could facilitate failure at lower pressure. That is, evidence or significant effects due to constraint is situation specific, depending on the level of constraint in combination with the relative toughness.

Unfortunately, it is difficult to transform the level of constraint in combination with the relative toughness and its role in facilitating failure into specific ranges of toughness wherein constraint

is a factor. Clearly both lower toughness and higher constraint together can be problematic – but on their own neither constraint nor lower toughness is a concern in promoting fracture in lieu of plastic collapse. It is possibly for this reason that the historical toughness limitation for use of B31G is stated non-quantitatively in reference to cases where “toughness was not a factor in the failure.”

Until further analyses are done to better quantify “high constraint”, corrosion features involving spherical pits within somewhat larger pits, spherical pits whose in-plane size is the order of the wall thickness, and near conical pits should be viewed with concern. For example, the feature in the vintage database that fails non-conservatively in regard to RSTRENG and the 1990s criteria is a single pit with a near circular in-plane shape whose diameter is a few times the wall-thickness, with a near conical bottom at a depth of about three-quarters of the wall. Of course, any crack-like feature or local stress concentration other than due to the metal loss must be avoided.

Some quantitative guidance also can be derived from the above analysis, by comparing initiation toughness levels at which collapse predictions of the failure pressure (e.g., Equation 24) begin to diverge from the present fracture-based approach as a function of decreasing relative toughness. Not surprisingly, trial-and-error analyses indicate this divergence develops when the crack driving force shown in Figure 22 tends toward the LEFM and SSY response that develops over the near-linear portion of this trend. Interpolation between Figure 22 and Figure 21 leads to values of constraint-corrected J for the pipeline that shift the upper-end of the toughness range shown in Figure 22 down to the pressure predicted by Equation 25, which was 21 MPa. Such order-of-magnitude analysis indicates the divergence between collapse and fracture develops at toughness levels less than that for this X80 by the order of 30-percent or more. Comparing the fracture resistance expressed as by J-R curve for SENB specimens of 1950s vintage line pipe steel shown in Figure 23 with that in Figure 11 for the SENB response for the X80 clearly indicates such a decrease. On this basis constraint can be a factor for this vintage line-pipe steel. Because its fracture resistance is comparable for most other vintage line-pipe steels, one could conclude constraint has broad practical significance.

The key for the future is to couple analysis such as the generic formulation developed here with other mechanics analysis to characterize practical combinations of geometry and loading induced constraint as a function of toughness. Only then can the historical toughness prohibition limiting use where “toughness was not a factor in the failure” be translated into quantitative metrics. But, as this outcome will involve corrosion geometry, use of such criteria will not be simply expressed in terms of line-pipe vintage or grade, and could require more refined definition of corrosion geometry than provided by most current second-generation ILI tools. Absent this, pit-like features could simply be reinforced where they are encountered in rehabilitation projects.

Summary for Task Three

Task Three involved a range of numerical and related analyses that help to identify conditions where blunt defect failure can be affected by fracture. Guided by literature, data, and trends evident for constraint, multiaxiality, yield-to-tensile ratio, and other factors potentially driving failure by fracture rather than by plastic collapse, a generic NLFM analysis of constraint was formulated and calibrated with the assistance of FEA and laboratory experiments specific to X80 line pipe steel. Use was made of J-R curves for X80 pipeline steel that with FEA calculations, and the $J-A_2$ fracture theory led to a generic approach to determine constraint-corrected J-R

curves. With this generic formulation, parametric analysis could be done relative to corrosion geometry and line pipe flow and fracture properties characteristic by vintage. For the present study, the results were analytically trended and validated in reference to predictions of a deeply cracked pipeline, for use as guidance for Task Four.

In regard to constraint effects and X80 line-pipe steel several trends can be identified, as follows:

- the J-R curves for X80 are strongly geometry or constraint dependent, consistent with a wide range of similar results of line pipe and pipelines,
- the J-A₂ three term solution can be used to correctly quantify the constraint effect on the crack-tip fields and J-R curves, but for deep cracked bending specimens under LSY, the modified J-A₂ four term solution is necessary to account for the global bending stress,
- a generic expression for constraint corrected J-R curves was formulated in reference to SENB specimens, and validated by comparison to J-R curves for SENT specimens,
- the approach was validated by comparison to plastic-collapse predictions via PCORRC, with fully-ductile fracture failure pressure predictions matching the collapse result.
- trends based on the divergence of collapse and fracture analysis as a function of toughness and constraint are consistent with results from Tasks One and Two, and indicate that without high constraint lower toughness is not an issue for failure at blunt corrosion, and
- the results indicate that constraint can be a factor leading to practical problems with collapse-based corrosion predictions at full-size equivalent (FSE)-CVP levels that might be as high as 30 to 40 ft-lb – but again, low toughness simply facilitates the onset and growth of cracking. Such toughness levels appear high in comparison to the reported toughness that underlies the vintage corrosion database, for which FSE CVN values as low as 20 ft-lb have been reported.

Until further analyses are done to better quantify “high constraint”, corrosion features involving spherical pits within pits, spherical pits whose in-plane size is the order of the wall thickness, and near conical pits should be viewed with concern. Of course, crack-like feature or local stress concentration other than due to the metal loss are not addressed by such criteria.

While not considered, the present analysis coupled with parametric FEA could quantify combinations of geometry and toughness for which constraint could be a factor.

Results – Task Four: Guidelines for Using the 1970s versus the 1990s Criteria

In Task One it was observed that the empirical results for defect-free pipe indicated the UTS correlated with the hoop-stress at failure, which was consistent with plastic-collapse theory. Further analysis contrasting the 1970s criteria with the 1990s criteria using UTS as a flow-stress showed there was little difference in the relative effects of the corrosion geometry between these criteria. On this basis, the first task concluded there was little inherent difference in the criteria of the 1970s versus the 1990s except for use of a flow stress in the 1970s criteria whose value was not supported by the empirical evidence or by theoretical considerations. When idiosyncrasies in the 1970s empirical database, such as use of repeat-testing or problems in characterizing corrosion geometry were excised from that database, apparent empirical

differences between these decades-different criteria vanished. Task Three indicated constraint coupled with lower toughness could lead to non-conservative predictions by UTS-based criteria. However, without further quantitative analysis based on the approach formulated it was not possible to quantify specific toughness levels at which related problems would become a practical concern.

This task develops guidelines for the use of 1970s versus 1990s criteria based on the results of the prior tasks and the related literature, which is considered next.

Implications of Prior Work

The implications of most prior work have been considered in the prior tasks with the exception of the cost-share project for this study.⁽²⁷⁾ That project included analysis of the role of toughness and defect geometry in the transition from fracture-controlled failure to collapse-controlled failure for sharp defects, which represent a worst-case as compared to blunt corrosion defects. It also addressed the role of constraint in terms of empirical analysis of field failures where this aspect apparently was a factor. Finally, that project considered the implications of residual stresses that might be a factor for fracture, but not for plastic collapse.

Toughness limitations to ensure plastic collapse were noted in reference to B31G⁽¹¹⁾ where use is limited to line pipe whose toughness was “adequate” or “not significant” in the possible failure of the defect. Section Four of API 579 precludes use of its criterion in applications areas where toughness might be inadequate, and provides separate sections to deal with cracking or possibly brittle response. As indicated in Task One, such language is directed at ensuring plastic-collapse controls failure but there is no guidance indication of a minimum toughness.

Because B31G has been considered applicable to vintage and lower toughness steels, a measure of the minimum toughness for its use was considered in regard to the lower-bound toughness for the early database. FSECVP energies as low as ~20 ft-lb (27 J) can be found reported in full-scale burst test databases for that era^(e.g., 38).

Regarding PCORRC (and by inference PCORR) the notation with its development indicated it should be applied only to moderate to high toughness steels, with an initial and conservative FSECVP limit indicated at 45 ft-lb (61 J)^(e.g., 22). Subsequent quantitative analysis for sharp defects based on the PRCI ductile flaw-growth model (DFGM)⁽⁷⁴⁾ indicated⁽⁷⁵⁾ that plastic collapse can be ensured for all combinations of line pipe geometry and properties for FSECVP values greater than 100 ft-lb (135 J). As such work has been directed at ensuring plastic collapse controls failure; such values reflect upper-bound scenarios. Other more recent work indicates that plastic collapse can control the failure of shallow sharp defects geometries at much lower values of FSECVP⁽⁷⁶⁾, with similar trends also occurring for very deep defects⁽⁷⁶⁾. More recent extensive parametric analysis detailed in Appendix C of Reference 27 indicates the transition to **widespread** fracture control at sharp defects can occur at toughness levels the order of 20 ft-lb (27 J) for a range of line pipe geometries and grades. Consideration of the trends in Appendix C indicates that this transition to collapse-control occurs first for defects with depths from 30 to 70-percent of the wall thickness. These trends also indicate that shallow defects the order of 20-percent of the wall thickness and less are typically collapse controlled, as are very deep defects.

Regarding constraint, one field failure was evaluated in Reference 27 where deep spherical pitting corrosion produced failure at rather low failure pressures in otherwise rather tough steel in comparison to the lower FSECVP energies found reported for vintage full-scale burst tests as

noted above. As such pits reflect high constraint features; concern also was noted for the effects of constraint, which appears justified in light of the analytical trends presented in Task Three. But, as for toughness, the absolute role or significance of constraint was not yet quantified.

Finally, prior work has shown that where plastic collapse controls failure, residual stresses are diminished by the extensive plastic flow prior to failure. In contrast, tensile residual stresses can be an issue where fracture might control failure.

Guidelines for Using 1970s versus 1990s Criteria

Flow-Stress Considerations

The 1970s versus 1990s criteria clearly differ in regard to the defect-free reference stress used. The 1970s criteria make use of a flow-stress whose use and definition do not reflect the empirical trends of the database these criteria were developed for. Figures 3 and 4 clearly indicate the use of a flow-stress other than the UTS is not justified. Moreover, Figure 3 implies SMYS has little correlation with the actual failure stress, as functions of SMYS scatter significantly with actual failure stress and do not track a one-to-one trend. This implication is clear from Figure 24, which shows SMYS is uncorrelated with the actual failure stress for early as well as modern vintage data. Note in this figure that the data represent the same results considered earlier in terms of Figures 3 and 4. The essential difference here is SMYS is considered directly as the independent variable, with the actual failure stress taken as the dependent variable. Also shown in this figure are $SMYS + 10 \text{ ksi}$ (68.9 MPa) and $1.1 \times SMYS$. As with Figure 3, these parameters do not correlate well with the actual failure stress, although $SMYS + 10 \text{ ksi}$ (68.9 MPa) can be seen as a lower-bound to the actual failure stress, but is badly scattered in this role. In contrast to SMYS and the functions of SMYS considered, the value of the UTS correlates very well with the actual failure stress, and is free of bias in either grade or vintage, as is evident in Figure 4.

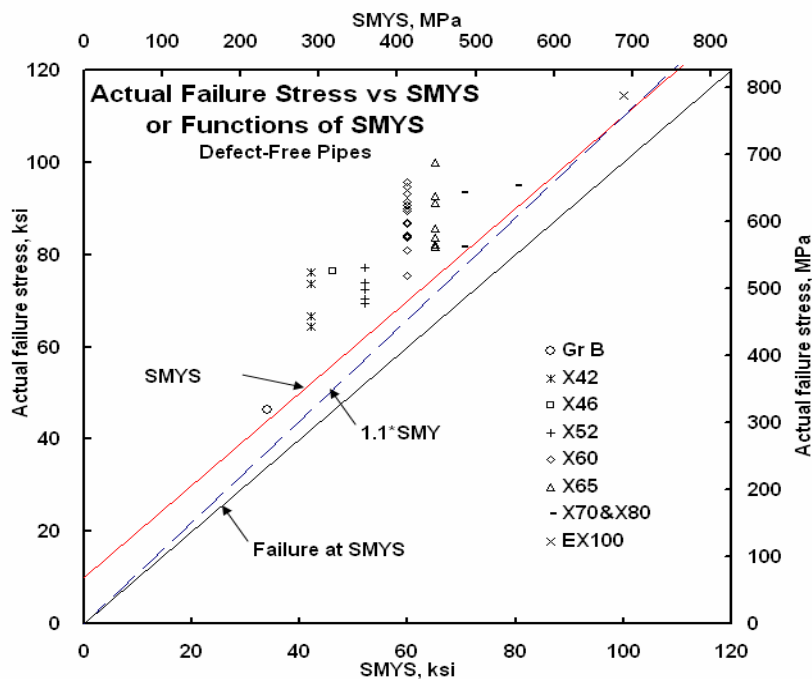


Figure 24. SYMS and functions of SMYS as a failure criterion for line pipe

While design codes and pipeline specifications incorporate SMYS directly, and address UTS only indirectly, these results indicate SMYS has little inherent ability to consistently predict failure line pipe behavior. Provided that the UTS or SMTS is known, and is consistently developed in the properties for the line pipe of interest, these results suggest that either parameter better reflects the failure response of the line pipe than does SMYS or functions of SMYS. The UTS defines the average failure pressure, as has been shown in Figure 4. In contrast, SMTS provides a lower bound to the actual failure stress, which is apparent in Figure 25a provided that historic differences in SMTS are accounted for. Evaluation of historic differences in SMTS is motivated in regard to the value of SMTS for Gr B in the current API 5L specifications, which requires SMTS = 60 ksi for grades less than X52. In contrast, a check of SMTS for Gr B in the 1970 API requirements then separate for higher strength and lower strength grades indicates SMTS = 48 ksi for Gr B. The results in Figure 25a suggest that SMTS is a viable conservative measure of failure strength for vintage defect-free line pipe. In turn, this suggests use of the historic values of SMTS for lower-strength grades coupled with current API requirements for higher-strength grades would provide a viable basis for the reference stress when making corrosion predictions – for any vintage of line pipe.

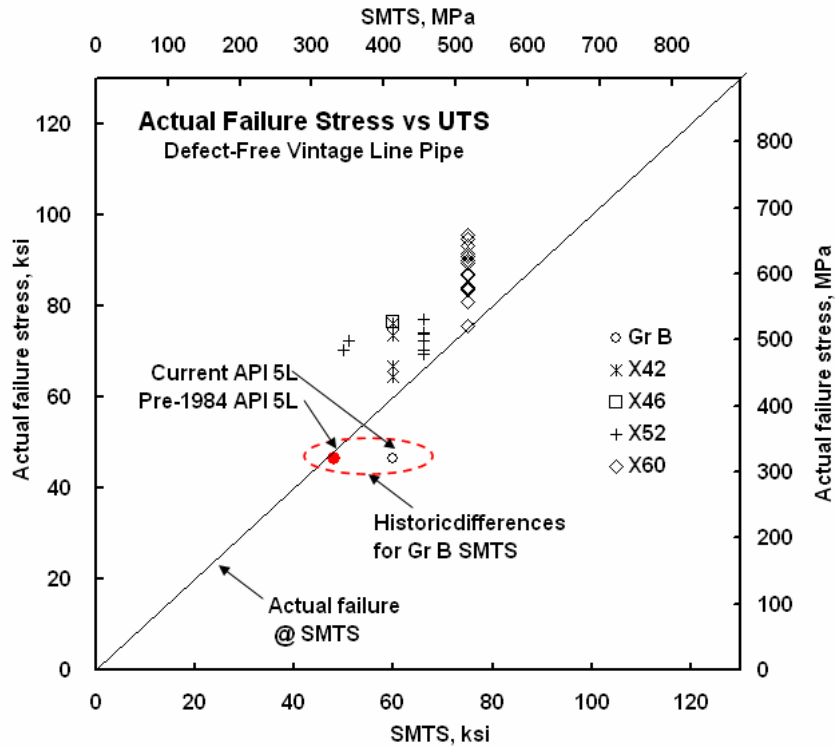
Figure 25b evaluates the utility of SMTS as a reference stress in conjunction with PCORRC in application to the vintage pipeline database culled for repeat-testing, and in light of Figure 25a includes results for Gr A and Gr B line pipe along with results for X-grade line pipe. It is apparent from this predicting naturally occurring corrosion in vintage grades of steel that SMTS provides reasonable predictions for the full database. One result stands out as clearly non-conservative with a few others close to the one-to-one line, all involving Gr B. Otherwise, consistently conservative predictions are achieved for the X-grades, some being quite conservative.

In view of Figures 3 and 4 that indicated the UTS correlated actual failure stress in defect-free line pipe without apparent bias in grade or vintage, one can reasonably conclude that when SMTS is referenced to a code whose vintage is compatible with the application the same will hold for SMTS. As such, the available data indicate that SMTS can be used in 1970s and 1990s criteria without regard to vintage or grade.

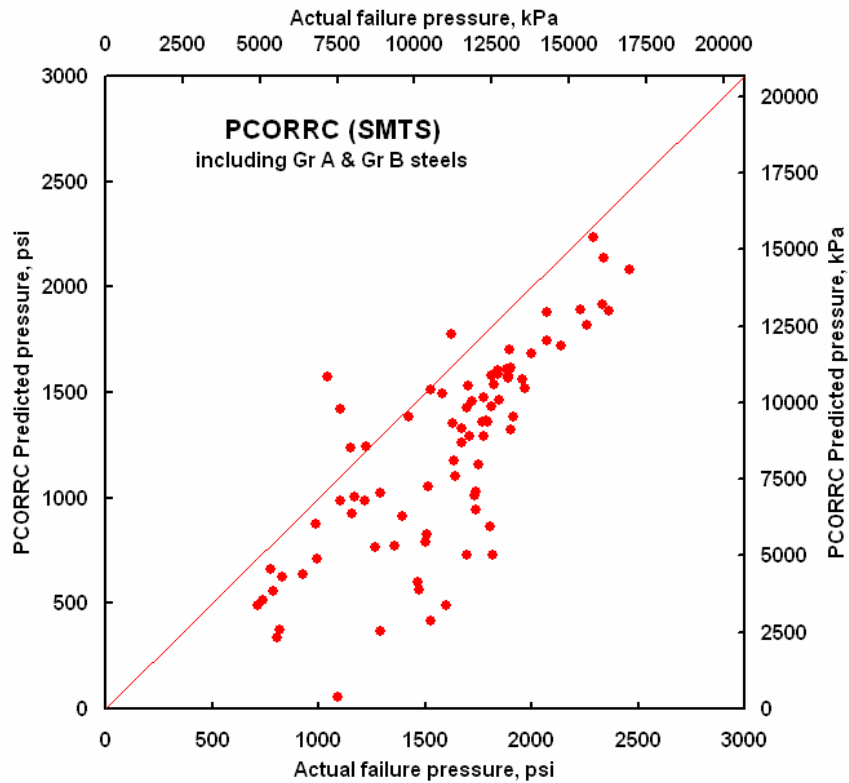
Corrosion Geometry and Constraint Considerations

In light of Figure 9 that uses the UTS as a reference stress, the 1970s and 1990s criteria do not differ in a significant way regarding their evaluation of the effects of corrosion geometry. This outcome was somewhat surprising given that the 1970s criteria calibration of defect geometry commingles its effect with flow-stress, which was anticipated to compromise the calibration of geometry. Nevertheless, as these results do not indicate a significant difference, Modified B31G referenced to SMTS should lead to predictions comparable to that shown in Figure 25b.

Thus, the available results support use of SMTS as the basis for accurate predictions in balance with the usual desire for some conservatism in predicted failure pressure. Except for longer defects, and cases in Figure 25b that involve significant conservatism that earlier were traced to problems in reporting mechanical properties and the size of the corrosion, the results in Figure 5 suggest this limited conservatism should not jeopardize use of these criteria in predicting failing defect size as a function of pressure. In using SMTS, care should be taken to ensure code-based values from current codes reflect the grade and vintage of line pipe involved.



a) actual failure stress vs SMTS for defect-free line pipe



b) SMTS-based PCORRC predictions for the vintage corrosion database

Figure 25. Trends in failure predictions based on SMTS

In regard to Figure 25b, one result stands out as clearly non-conservative with a few others close to the one-to-one line, all involving Gr B. While archival data were not easily located for all cases that lie above the line, results were found in reference to the one result that is significantly non-conservative. These data indicate this failure involves a leak from a deep pit the order about three-quarters through the wall. A sketch in the archives indicates a compound cross-section that is spherical-like over its shallower portion, becoming more conical and terminating in a rather sharp radius. Photographs located to date from the archives are unclear in regard to the exact terminating radius, but the views available and the related data suggest a $\sim 1/16$ -inch to $\sim 1/8$ -inch bottom radius.

Deep spherical to conical pits with a small terminating radius will develop high constraint in comparison to most of the other features noted in the photographs and sketches. In light of the analysis of Task 4, that show significant reduction in apparent fracture initiation and growth resistance due to higher constraint, this feature could be expected to fail at a pressure less than otherwise indicated based on plastic-collapse analysis. For comparisons in the format of Figure 25b, any failure at a pressure less than predicted based on plastic-collapse analysis lies above the one-to-one line in this figure, such that high constraint typical of the subject result could easily account for this missed prediction. It follows that while SMTS is a viable reference stress for blunt defects, where constraint is a factor such predictions will be non-conservative. Significantly, this same corrosion defect also is non-conservatively predicted by Modified B31G, and by a large margin. In this context, constraint is equally problematic for 1970s and 1990s criteria.

Toughness and Residual Stress Considerations

Prior work⁽²⁷⁾ has noted that FSECVP energies as low as ~ 20 ft-lb (27 J) can be found reported for full-scale burst testing of vintage line pipe of the same scope considered in Figure 25. As SMYS is a viable predictor for these results except for the just noted case involving high constraint, one can reasonably state that pipe with FSECVP energies the order of ~ 20 ft-lb (27 J) will also fail by plastic collapse in areas free of constraint and crack-like defects. Indeed, free of areas of high constraint and crack-like features, or high tensile residual stresses, toughness is not a concern. Where crack-like features and constraint cannot be excluded, fracture mechanics analysis that addresses such features should be considered in lieu of either a 1970s or a 1990s corrosion criterion. Finally, for shallow defects the order of 20-percent of the wall thickness and less, failure is typically collapse controlled such that toughness is not a consideration – except where high tensile residual stresses develop. As for cases where cracking is plausible, analyses other than either a 1970s or a 1990s corrosion criterion should be adopted.

Pipeline Service Considerations

The observation that data involving repeat-testing underlay much of the vintage database that was problematic to collapse-controlled predictions is significant. Although such data have populated this database since it was first published, and remained in it through the evolution of Modified B31G and RSTRENG, their history as repeat-test data has never been considered a factor, nor have the implications of pressure reversals observed in such testing been considered. Yet, for some repeat tests one retest cycle in five or more lead to pressure reversals.

Repeat-test cycles involved in developing a corrosion failure database involve very large cycles as compared to typical pipeline service. For example, in many cases the pressure reversals

occurred following pressure cycles from zero to pressures approaching or exceeding 100-percent of SMYS, much like the pressure cycle in a hydrotest or a retest. Nevertheless, the message from such pressure reversals is clear – large-amplitude pressure cycling can nucleate stable tearing and drive other phenomenon such as cyclic hardening or softening that can appreciably change the flow response of the line pipe steel, and do so at otherwise “blunt” defects. It follows that care must be taken in using either 1970s criteria or 1990s criteria in applications to pipelines that experience large or frequent pressure cycling. Analysis of stable tearing and cycle-dependent flow response is possible and should be considered part of any engineering critical assessment and corrosion rehabilitation project. Likewise, if crack-like defects could be present, this possibility should be considered long before analysis to evaluate the effect of metal-loss defects.

Summary for Task Four

Task Four evaluated trends from prior tasks to identify guidelines for the use of 1970s criteria in contrast to 1990s criteria for corrosion assessment involving both predicted failure pressure as well as predicted defect size for use in establishing re-inspection intervals. Some of the key observations that arise from this, which in some ways restate prior conclusions, include:

- SMYS is uncorrelated with the actual failure stress for early as well as modern vintage data, whereas the UTS correlates very well with the actual failure stress, and is free of bias with grade or vintage,
- thus, use of flow-stress in 1970s criteria versus the UTS in 1990s criteria is an essential difference between these criteria,
- SMTS referenced to a standard (e.g., API 5L) whose vintage is compatible with the application is a viable reference stress, and when used in the 1970s and 1990s criteria both were found to be mutually compatible and consistent with the full-scale database,
- when SMTS is used the available data indicate that failure predictions via 1970s and 1990s criteria are comparable and without bias with vintage or grade,
- when the UTS was used as a reference stress, the effects of corrosion geometry were similarly predicted by the 1970s and 1990s criteria,
- consequently, when the 1970s criteria are referenced to SMTS, comparable predictions are anticipated to those of the 1990s criteria, with no need to discriminate one set of criteria as appropriate or better,
- one result stood out in the vintage corrosion database as clearly non-conservative for both the 1970s and 1990s criteria – it involved a leak in Gr B seamless pipe from a deep pit the order of about three-quarters through the wall, whose shape and dimensions indicated high local constraint in comparison to most other corrosion, which is as predicted based on Task 3,
- while SMTS is a viable reference stress for blunt defects, as just noted high constraint leads to non-conservative predictions such that the 1970s and 1990s criteria should not be applied where high constraint develops,
- until further analyses better quantify “high constraint”, corrosion features involving spherical pits within pits, spherical pits whose in-plane size is the order of the wall thickness, and near conical pits should be viewed with concern,

- analysis shows that plastic-collapse based predictions are viable at FSECVP energies the order of ~20 ft-lb (27 J) absent concern for constraint and crack-like defects,
- where crack-like features and constraint or high tensile residual stresses cannot be excluded, fracture mechanics analysis that addresses such aspects should be considered in lieu of either a 1970s or a 1990s corrosion criterion, and
- because of concerns related to crack –like defects and stable tearing within usual corrosion features, applications involving large-amplitude frequent pressure cycling should be avoided unless accompanied by a related engineering critical assessment.

All results indicate that where blunt corrosion free of constraint and crack-like defects is considered, there is no need to discriminate between 1970s and 1990s criteria if they are referenced to SMTS for the vintage of line pipe involved. If the 1970s criteria are referenced to a flow-stress they will embed conservatism without clear value in reducing the likelihood of failure all else being equal, which could promote non-conservative predictions of defect size or re-inspection interval.

Results – Task Five: Full-Scale Demonstration Testing

The first task demonstrated there was little inherent difference in the criteria of the 1970s versus the 1990s except for effects that arise through use of a flow stress whose value was not supported by the empirical evidence or by theoretical considerations. Empirical results for defect-free pipe indicated the UTS correlated with the hoop-stress at failure, which was consistent with plastic-collapse theory. Task Two indicated when idiosyncrasies in the 1970s data, such as use of repeat-testing or problems in characterizing corrosion geometry were addressed apparent differences between these empirical databases disappeared. With the UTS as the reference stress, this empirical database of isolated corrosion features was consistently predicted by both the 1970s and 1990s criteria. Analysis developed in Task Three indicated constraint coupled with lower toughness could lead to non-conservative predictions by UTS-based criteria, but without further quantitative analysis based on the approach formulated could not quantify specific toughness levels where such problems would be a practical concern. Task 4 developed guidelines based on results from the first three tasks, and the parallel study done as part of the cost-share project for this study. From that task, corrosion could be evaluated by plastic-collapse criteria referenced to SMTS for depths less than 30-percent of the wall. For deeper corrosion, where the toughness exceeded the order of 20 ft-lb (27 J) constraint was unlikely a factor. If crack-like defects or defects with high local constraint are involved, or the pipeline experiences large or frequent pressure cycling, care must be exercised prior to using collapse-based criteria referenced to SMTS for depths greater than 30-percent of the wall. Otherwise, Task 4 indicates that SMTS provides rational generally conservative predictions, with no essential difference between criteria from the 1970s and the 1990s.

The present task presents limited testing designed to explore the implications of constraint, crack-like defects, and blunt defects in vintage line pipe for which typically lower-toughness can be anticipated. As crack-like defects and constraint are most common at welds, this task considers corrosion patches sufficiently large to facilitate failure in either the pipe body or at areas where crack-like defects and constraint occur.

Experimental Approach

Features that embody constraint or represent crack-like defects could be simulated via machined defects. However, local residual stresses or possibly unique microstructural features cannot. For this reason, line pipe was sought where such features were likely to occur, on which corrosion patches simulated by machined metal loss could be co-located to those features – albeit with some luck. Vintage single-side arc-welds (SSAW) typically contain shallow planar defects scattered along the inside diameter (ID) as well as occasional volumetric defects that form as the weld is made over a backing bar. Accordingly, simulated patches of metal loss were selectively located over such naturally occurring features. The results presented address the role of crack-like defects and constraint co-located in corrosion such that failure pressure for such circumstances can be contrasted with predictions based on 1970s and 1990s criteria to assess their utility and evaluate the guidelines developed and reported in Task Four.

The SSAW Line-Pipe and its Properties

The full-scale testing was done on 1930s vintage SSAW line pipe that was corroded to an extent that led to replacement, although local reinforcement was equally an option that was not adopted. This pipe was considered an appropriate vehicle for present purposes from two perspectives. First, testing such pipe replicates the process that calibrated the 1970s flow-stress-based criteria for vintage steels, using corroded pipe removed from service. Second, such steels often involve lower toughness at service temperature as compared to today's steels, which if coupled with constraint could promote failure below that predicted by plastic collapse. This circumstance opens the door to constraint effects while it also provides the option for failure at corrosion in the pipe body.

The SSAW seam pipe was nominally 14.25-inch (362-mm) diameter with a 0.254-inch (6.45-mm) thick wall. Based on flattened strap data, the transverse properties for the pipe body showed an AYS of 39.8 ksi (274 MPa) with an average UTS of 56.5 ksi (389 MPa), each based on four replicate tests, giving $Y/T = 0.71$. The measured yield stress for the pipe body is like that anticipated for Gr B, however, the measured value of Y/T is quite high as compared to the average trend for Gr B. This is evident in Figure 26, where bounds on Y/T for Gr B are indicated to typically be $0.45 \leq Y/T \leq 0.70$. Based on axial round bar samples cut from the seam, the seam properties showed an average AYS of 59.0 ksi (407 MPa) with an average UTS of 74.9 ksi (516 MPa), giving a $Y/T = 0.79$. If the cross-weld properties correspond to the axial properties, these results indicate this SSAW is significantly overmatched to the pipe body. In this case, failure controlled by plastic collapse would occur in the pipe body rather than the weld metal, all else being equal. As both the 1970s corrosion criteria and those of the 1990s address failure by plastic collapse, absent the effects of local weld defects or constraint, failure by collapse is anticipated first in the pipe body.

In reference to the measured mechanical properties, failure in a defect-free pipeline is expected at ~2013 psi (13870 kPa) if plastic collapse controls failure. Failure in defect-free pipe based on the flow-stress for B31G is expected at ~1562 psi (10762 kPa) assuming plastic collapse conditions as is implied for use of this criterion. For Modified B31G (or RSTRENG), where plastic collapse controls as implied in using this criterion, failure of defect-free pipe is expected at ~1776 psi (12237 kPa). Finally, for subsequent reference, the pressure corresponding to 100-

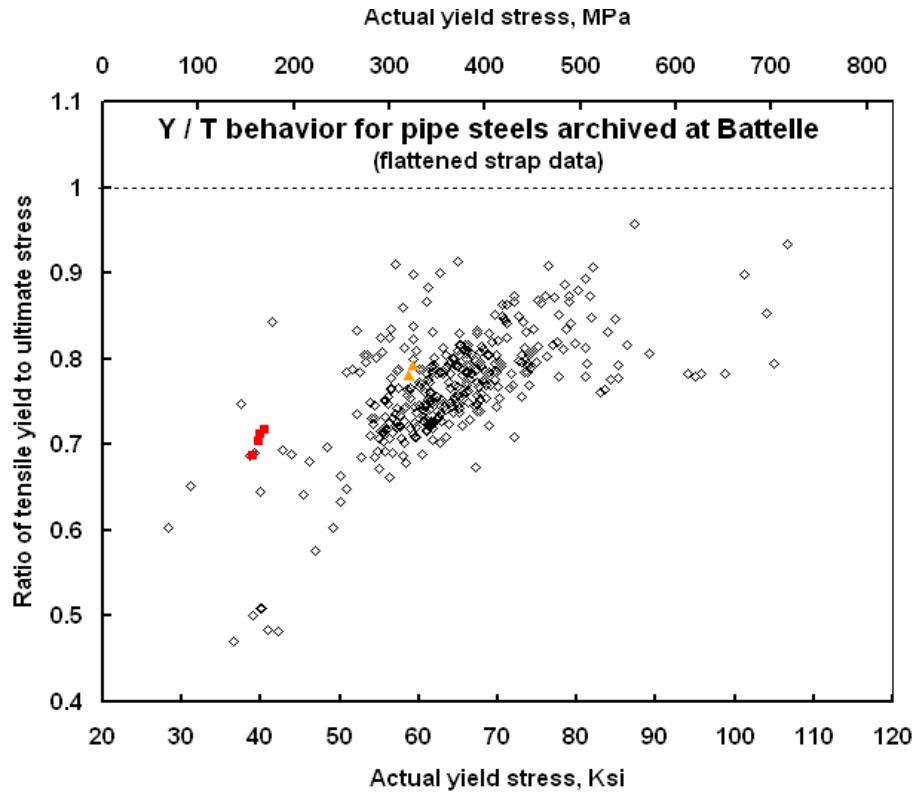


Figure 26. Y/T for the pipe (squares) and weld (triangles) compared to typical trends

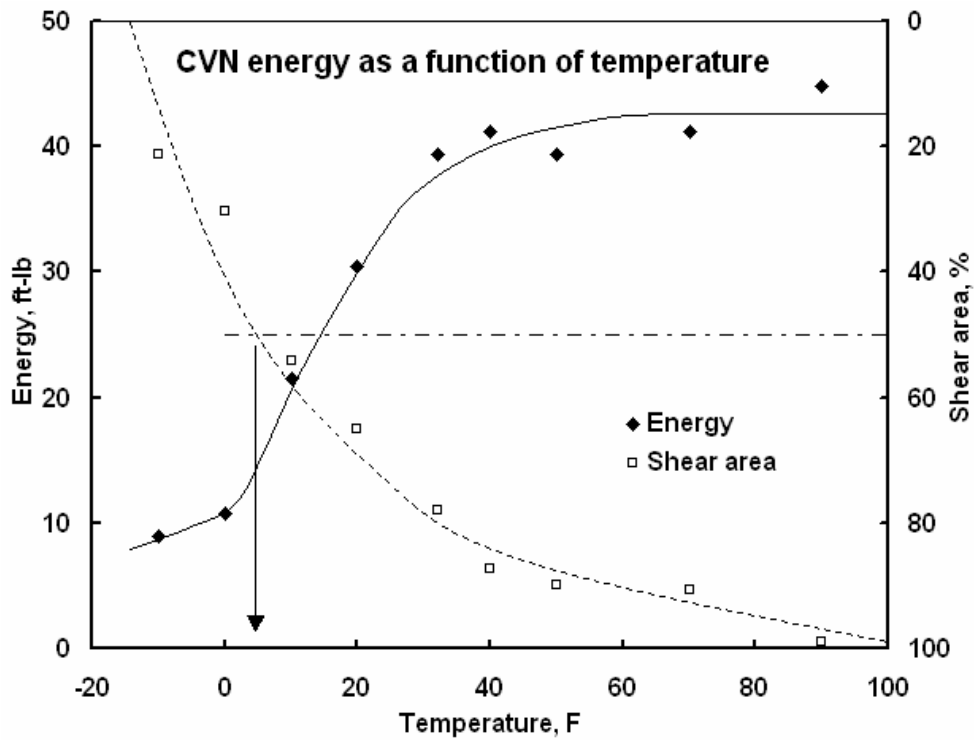


Figure 27. FSE CVN results for the pipe body used in the test vessel

percent of SMYS is ~1420 psi (9783 kPa), (assuming the AYS coincides with SMYS), while the pressure corresponding to the MAOP in service at 72-percent of SMYS is 1022 psi (7042 kPa).

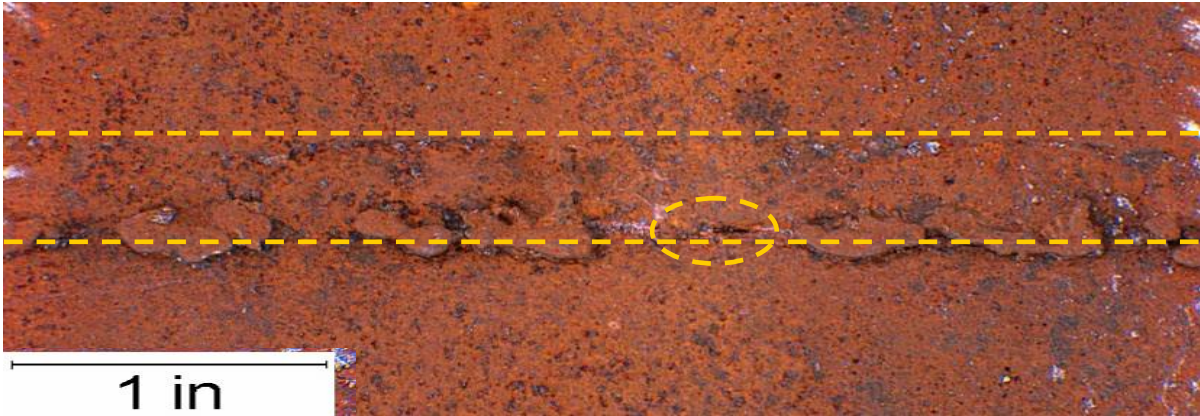
Because failure is anticipated to occur in the pipe body in light of the mechanical properties and collapse-controlled failure, consideration of the fracture properties focused on the pipe body. Further, because circumferential pressure-induced stresses are double those in the axial direction, toughness was characterized in reference to axial cracking along the length of the line pipe. The toughness of the subject line pipe as characterized by CVN impact testing on 0.220-inch (5.6-mm)-thick sub-size specimens is as shown in Figure 27. In this figure, the left-hand axis shows the FSE energy to fail the CVN sample, the right-hand axis shows the percent-shear area, and the x-axis shows the test temperature. Figure 27 indicates that the toughness of the pipe body is quite good, at the order of 42 ft-lb (57 J) FSECVN on the plateau. This FSECVN energy is high compared to typical scenarios that reference “low” toughness that is in such cases the order of 10 ft-lb (13.5 J) or less. The fracture appearance transition temperature (FATT) at 50-percent shear-area (SA) is about 5°F (-15°C), which also is very good as compared to many early vintage steels that show values the order of 100 °F (38°C), or higher. Given these properties, results developed by testing simulated corrosion might for some be considered uncharacteristic of the response of the calibration database of B31G. Likewise, the relatively high toughness would diminish the likelihood for problems anticipated in dealing with “low” toughness steels. For such reasons, some might not anticipate that B31G would under-predict failure pressure – particularly if plastic collapse controls failure.

Line-Pipe Inspection and the Test Pipe

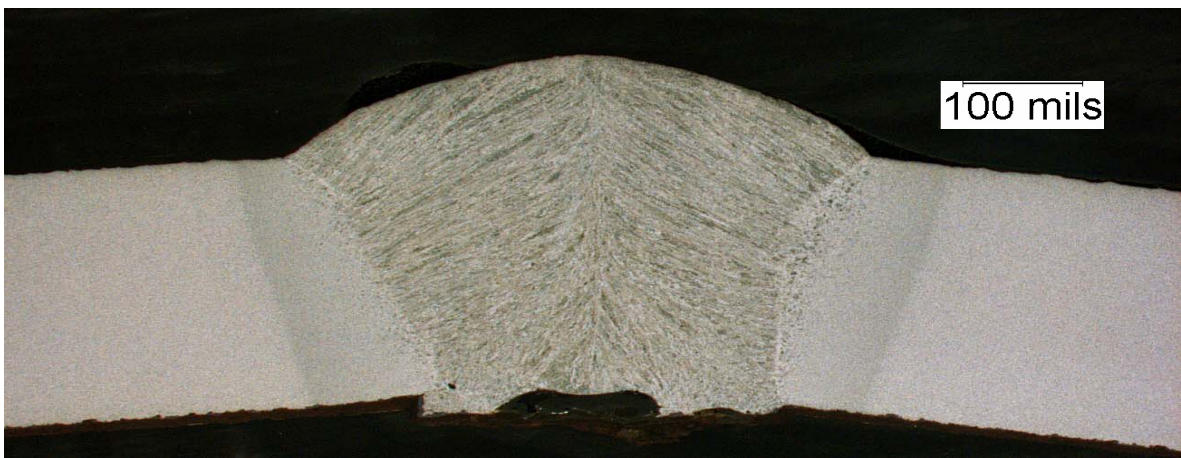
To limit overall concern for seam-related problems or the effects of the corrosion that caused this pipe to be removed from service, the body of the as-received pipe and the seam were visually inspected, and the seam was x-rayed. Areas of the pipe body with deep pit-like corrosion or large areal thinning were marked for reference. Visual examination of the SSAW indicated a rough surface along the ID in the area that lay against the backing bar, which included flash, as is common for such welds. Then the seam was visually inspected for seam defects and seam-related corrosion on the OD, and thereafter the seam was x-rayed.

Figure 28a shows a view typical of the weld along the ID surface, while Figure 28b shows a cross-section view through the weld, with a macro-etch to show the structure. Flash is evident in both parts of Figure 28. The view in part a) indicates the boundaries of the weld by dashed orange lines. A small planar defect that appears to reflect lack of fusion is circled along the lower boundary of the weld. This view also shows the presence of flash along the lower boundary of the weld. The cross-section of the weld indicates features typical of this seam type. The exterior bead is well formed, while the ID shows flash and slight under-fill.

The x-ray inspection was done by a local commercial service that does pipeline-related work, with the film read by Battelle staff whose related experience traces to decades of prior employment in the pipeline industry. Sections containing corrosion that could fail contrary to the purpose of this testing or where seam defects were evident on the film were removed, leaving several “sound” rings of pipe whose lengths were the order of several diameters that were suited to the purposes of this project.



a) view of the ID surface centered along the weld – a defect and flash are evident



b) cross-section showing the structure of the SSAW – flash and slight under-fill are evident

Figure 28. Features typical of the SSAW used in early pipe making



Figure 29. Overview of the three areal defects prior to the first test

The Simulated Corrosion

One ring of sound pipe many diameters long was shipped to the shop where patches of areal corrosion were machined. Three such areal defects were machined – all were centered along the single arc weld (SAW) seam, and were “smooth” bottomed in comparison to typical corrosion. The ring containing the machined patches is shown in Figure 29, along with close-up views of each of the patches shown therein roughly in scale proportion. The defects were machined by a rather small-diameter end mill through a series of axial passes made by a sequential indexing the pipe around its circumference. All defects had a radius somewhat larger than the wall thickness made as the transition from the simulated corrosion into the full thickness. The transition at the corners of the patches likewise had a radius somewhat larger than the wall thickness, as has been typical for machine-simulated corrosion. The machining was done on a numerically controlled system with the actual circumferential pipe shape input along with the desired thickness, and the thickness machined accordingly in an effort to control expectations from this testing. Analysis indicates that where collapse controls failure, areas remote to the transition radius into the full-wall are not likely to fail even with a shaper transition than used. Accordingly, the transition radius is not considered a driver for failure.

All defects were sized according to RSTRENG (equally Modified B31G) to fail at nominally the same pressure targeted at 1346 psi (9274 kPa), which corresponds to a wall stress slightly below SMYS. All defects were 4-inches (102-mm) wide, with lengths and depths varied to produce the target pressure, which meant the shapes and depths differed significantly. The patch that involved the thinnest net wall, labeled #1, was targeted at nominally 70-percent deep, or 0.178 inch (4.52 mm), with a length of 1.6 inches (40.6 mm), such that it was wider than it was long. The second defect labeled #2 was also shorter than it was wide, with a length targeted at 2.6 inches (66 mm) and a depth nominally 50-percent of the wall, or 0.127 inch (3.3 mm). The third defect labeled #3 was targeted at 30-percent deep, or 0.076 inch (1.93 mm), with a length of 10 inches (254 mm), and so was long compared to its width. On this basis, the overall area of these patches increased as the length of the defect along the seam increased.

The sizes of the three defects are summarized in Table 1, along with the projected failure pressure based on RSTRENG (equally Modified B31G). Consistent with the identification in that table and as noted above, the shortest defect is referred to as #1, the next longest #2, and the longest #3. Whereas RSTRENG predicts nominally the same failure pressure for the targeted simulated corrosion, the 1990s criterion collapse-based PCORRC predicts failure at relatively different pressures. For example, PCORRC indicates failure at 1606 psi (11065 kPa) for #1, 1662 psi (11451 kPa) for #2, and 1599 psi (11017) for #3. On this basis, for collapse controlled

Table 1. Defect sizes and projected failure pressures

ID #	Defect Size			Predicted Failure Pressure			
	Length		Depth % wall	RSTRENG		PCORRC	
	inch	mm		Psi	kPa	Psi	kPa
1	1.6	41	70	1348	9288	1606	11065
2	2.6	66	50	1346	9274	1662	11451
3	10	254	30	1348	9288	1599	11017

failure defect #3 should fail first, followed by #1, and thereafter #2. However, as the failure pressures for #1 and #3 are similar, scatter in properties could easily reverse these sequences.

Figure 29 shows an overview of the three defects, axially spaced to avoid interaction. Figure 30 shows a close-up of each of the defects. Note in these views that while they are “smooth-bottomed” by design the machining process leaves some surface discontinuities that are minor in comparison to the roughness associated with corrosion and stress redistribution that occurs on the way to collapse. The weld seam lies across the middle of these defects, all of which are four-inches wide.

For the record, the smallest corrosion patch (#1) lies over a short crack-like high-constraint defect, while patch #2 lies over voids due to porosity in the weld seam that give rise to moderate to high constraint. While such features shown in detail subsequently are not unusual for some vintage welds, they serve the purposes of this project for which the third task targets the effects of constraint.

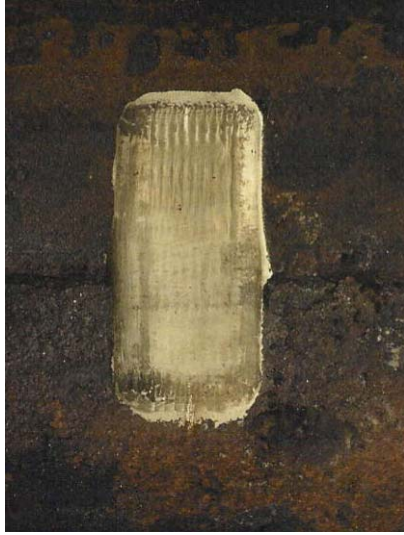
The Experimental Setup

After machining the metal-loss defects, the ring containing the machined defects was welded into a test pipe, which was then end-capped and prepared for pressure testing via nipples welded into both end-caps at an angle of 180° to each other. Figure 31 is a view of the test vessel created by welding the pipe section containing the defects into a test vessel. This view was taken prior to installing the tap for the pressure sensor and the dial gage. Prior to testing, the vessel was tipped slightly such that the end of the vessel with the down-ward facing nipple was slightly lower, with filling at the low end continuing until water drained from the nipple at the high end.

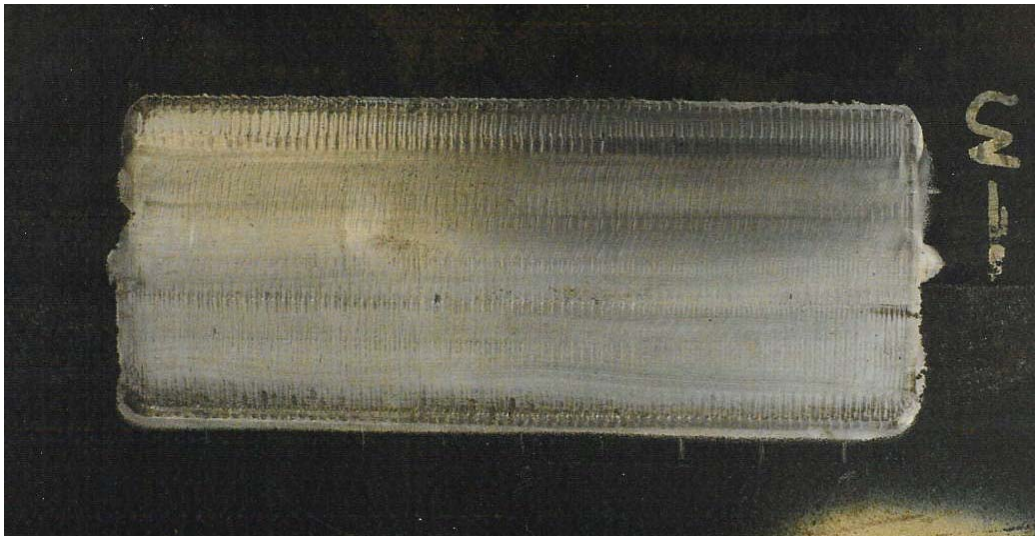
Thereafter, pressure sensors were installed and the vessel pressurized using a motor-driven constant displacement pump. Pressure was monitored visually on a dial gage, and tracked during testing by an analog sensor whose output was continuously recorded. In all cases, transducers were calibrated within the last six months using standards traceable to National Bureau of Standards.

In spite of the rather low FATT, to limit the possibility of a long axial split all testing was done in the summer in the late afternoon. The metal temperature was measured via thermocouple in contact with the pipe and registered digitally. Throughout the testing, the metal temperature was 90 to 93 °F (~33°C). According to Figure 27, at this temperature the pipe steel can be anticipated to show reasonable ductility, although constraint could induce somewhat more brittle response.

The testing involved pressure to failure with periodic brief holds to observe deformation local to the simulated corrosion. These brief holds came at roughly 250-psi (1723 kPa) increments. Testing lasted the order of several minutes, with pressurization at a rate of roughly 100 psi (689 kPa) per minute. Failure for the smallest, deepest defect was a very tight axially oriented leak. The two larger defects also split axially, with the split never favoring the seam in this process. Table 2 presents the actual failure pressures for the three defects identified in Table 1. While the simulated corrosion defects were sized to fail at nominally the same pressure, they actually failed in sequence that corresponded with defect length (or depth), with the shortest (shallowest) defect failing first. After failure, the defect depths were measured to account for the realization that slight out-of-round pipe or other pipe manufacturing variability would offset the efforts to machine constant depth features and achieve nominally comparable failure pressures. Such measurements proved essential, as actual wall thickness varied appreciably as compared to



a) #1 - 1.6-inch long, 70-percent deep b) #2 - 2.6-inch long, 50-percent deep



b) #3 - 10-inches long, 30-percent deep

Figure 30. The three patches of simulated areal corrosion targeted to fail at 1346 psi



Figure 31. Overview of the test vessel prior to adding the pressure transducers

the controlled depth sought in the defect design. RSTRENG predictions based on actual depths also are included in Table 2 normalized in reference to actual failure pressure. The corresponding RSTRENG predicted failure pressures indicate defect #2 should fail first at 1054 psi (7262 kPa), followed by defect #3 at 1143 psi (7875 kPa), with defect #1 failing last at 1387 psi (9556 kPa).

As all three defects were in the same test vessel, the second and third defects to fail (projected to be defect #3 followed by defect #1) would experience prior pressure cycles. Because fatigue due to the effects of such repeated pressure cycles as well as stable tearing leading to pressure reversals could affect a reduced failure pressure as discussed earlier in regard to “repeat-testing,” the effect of such cycles was evaluated. For fatigue or related cycle-dependent processes to be a factor over a life of three cycles, the prior cyclic history would have to cause significant local plastic straining and related damage, or sufficient straining to reduce the toughness because of prior pre-strain effects, or cause cracking in the defects that remained stable. The evaluation of these effects in light of the high toughness and low FATT evident in Figure 27 indicated such effects were not a factor. Accordingly, repeat testing was used in conjunction with plans to excise each failed defect. Details of three independent yet mutually consistent reasons for this decision follow.

First, if the pipe indeed had lower toughness, the presence of the high and moderate constraint in defects #1 and #2 would lead to lower-pressure failures and preclude developing significant strain in the other defects prior to their failure. Small defects existing along the weld considered to provide high constraint can be seen for example in Figure 28a. Such features, which were found along the SSAW at the ID surface, can be anticipated in the test pipe because the weld process in this vintage pipe was imperfect.

Second, by designing all metal-loss defects to fail at nominally the same pressure based on the 1970s criterion Modified B31G, if constraint is a factor then failure is anticipated to occur first in areas of constraint. On this basis, failure is first anticipated through the smallest patch with the thinnest wall, as the seam below this corrosion includes a crack-like high constraint defect. This feature should fail with only limited plastic deformation as local rotation and related bulging in the remaining defects where the heavier wall should resist stretching and bulging. This scenario did indeed develop, with failure of the second and third defects following only limited visual evidence of bulging prior to failure.

Third, if constraint is indeed a factor, the incremental pressure difference to cause failure of the first versus subsequent metal-loss defects is quite large – sufficiently so given the toughness of this steel to preclude local defect growth in a prior cycle. Taken together, these observations indicate the prior cycling caused modest local straining relative to that to cause failure, and occurred absent defect growth in those cycles.

The Results

Comparing the actual failure pressure in Table 2 with that anticipated in light of RSTRENG (equally Modified B31G) indicates the first defect failed well below that predicted, while the larger deeper defects failed at different pressures well above that predicted by RSTRENG (equally Modified B31G). Failure over this range of pressures might be considered by some to be experimental scatter, a conclusion that could be justified based on the extent of the scatter evident in the calibration database for B31G. However, such cannot be justified here, as follows.

First, all defects were located in the same pipe, meaning the variability in properties is small compared to that of the calibration database for B31G. Second, all defects were prepared with the same equipment and practices, and then tested in the same facility by the same staff, which precludes variability driven by differences in testing practices and equipment calibration. And, because they were machined and isolated from each other, there was little difficulty in sizing them. Thus, the significant differences in failure pressure as compared to that anticipated in reference to RSTRENG (equally Modified B31G) reflect fundamentally different causes of failure or factors that control failure, or some combination thereof.

Table 2. Failure conditions versus projected failure response

ID #	Actual Failure Pressure		Failure Mode and Location	Actual / Predicted Failure Pressure		
	psi	kPa		RSTRENG (1.1 SMYS)	PCORRC (UTS)	PCORRC (SMTS)
1	1019	7021	Leak, Seam	0.73	0.63	0.79
2	1408	9701	Rupture, Adjacent to Seam	1.34	0.85	1.06
3	1657	11417	Rupture, Remote	1.45	1.04	1.29

These results show a broad range of predictions achieved by flow-stress-based body criteria in applications to corrosion over this SSAW long seam whose properties indicate failure occurs in the body rather than the seam absent the effects of constraint and local stress raisers. If the under-prediction is associated with seam defects and constraint, then these results validate several aspects of the suggested guidelines.

First, absent constraint or seam defects, failure was found to initiate and grow through-wall remote to the seam weld, as anticipated in light of the seam being over-matched to the body, and did so at a pressure very close to collapse predicted by the UTS. This outcome is fully consistent with the guidelines, which conservatively suggest the use of SMYS in lieu of UTS. Clearly, use of any flow-stress less than SMTS provides an even more conservative prediction. This is evident in predictions based on SMTS that here are conservative by 29-percent for failure in the metal-loss feature free of constraint or crack-like defects.

Second, where moderate constraint develops in the metal-loss #2, SMTS remains a conservative predictor of failure for corrosion in this vintage pipe. Table 2 indicates that with moderate constraint SMTS is conservative by about 6-percent. While the present 1930s vintage line pipe showed properties consistent with the minimum requirements for the UTS as listed by API 5L, because the current requirements were imposed subsequent to much of the construction of the vintage pipeline system it is possible that some line pipe will not satisfy this requirement. Care must be taken therefore to understand the implications of changes in specifications over time, and the certainty those specifications were either applicable as well as achieved. In contrast to the just conservative prediction by SMTS-based PCORRC, note from Table 2 that RSTRENG

(equally Modified B31G) is much more conservative than SMTS-based PCORRC for this situation.

Third, the results in Table 2 clearly show that where high constraint exists at a crack-like defect, the effect of the sharp defect and the locally high constraint lead to failure controlled by fracture mechanics. In contrast to the other cases absent cracking, failure based on SMTS over predicts this situation by more than 20-percent. However, note from Table 2 that RSTRENG (equally Modified B31G) is less conservative than is the SMTS based result. It follows that where crack-like defects are present neither a 1970s criterion nor a 1990s criterion provides conservative predictions. This outcome supports the code prohibition in the use of criteria developed for blunt defects in applications to sharp defects.

Finally, it is noteworthy that RSTRENG (equally Modified B31G) shows a broad range of conservatism for these three failures, even though all were designed by this criterion to fail at nominally the same pressure. It can be argued that this inconsistent provision on conservatism (equally safety margin) reflects application of a corrosion criterion to cases where small moderate to high constraint defects are present. However, the trend to inconsistent margin of safety traces with the 1970s criteria traces directly to the inconsistency evident earlier in SMYS-based predictions of plastic collapse shown earlier in Figure 4. Such inconsistency is also evident in Figure 32, which presents Modified B31G predictions for the same database predicted consistently by PCORRC, as shown earlier in Figure 6a.

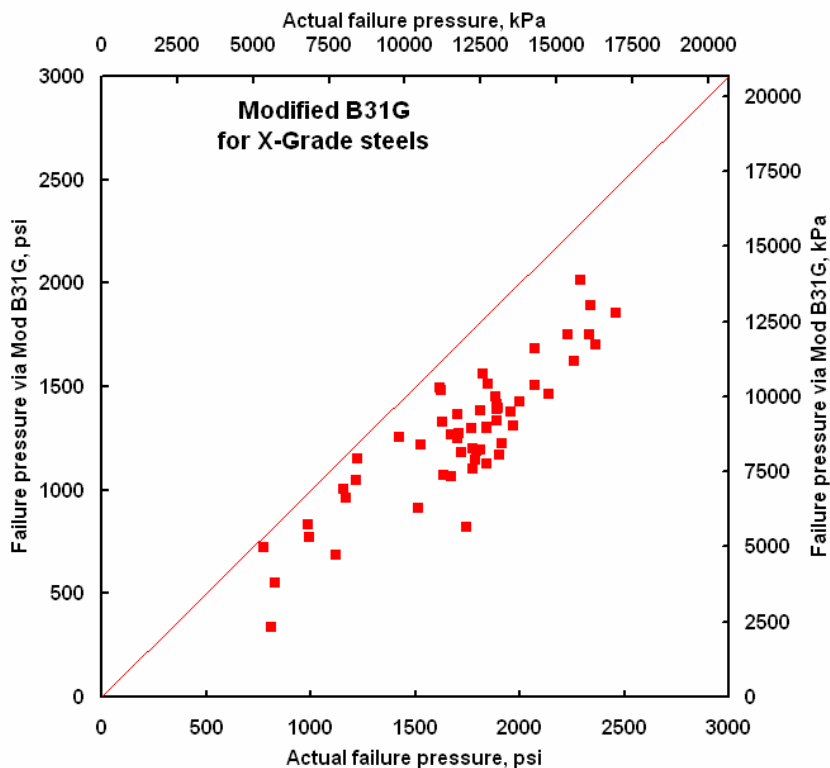


Figure 32. Modified B31G predictions in comparison to PCORRC in Figure 6a

Fractographic Implications of Constraint and Crack-Like Defects

Fractography of each of these failures is useful in understanding differences in factors that controlled each failure, as follows.

Corrosion Defect #1

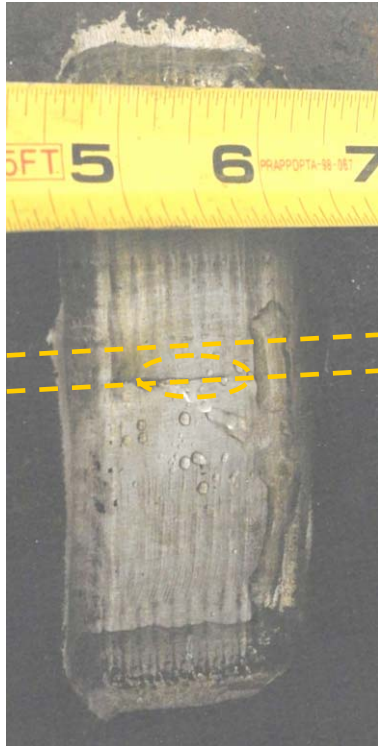
The origin for the leaking (failure) of defect #1 are small planar (crack-like) weld defects whose axial spacing precludes their interaction in this instance. Such defects are evident in the ID view of the SSAW shown earlier in Figure 28a. They can be found along the fracture surface forming at the ID side of the SAW caught in the flash formed between the pipe wall and the backing bar, as illustrated in Figure 33.

Figure 33a shows the defect with the SSAW seam lying between the dashed lines, and the leak path through the net-wall thickness circled toward the mid-width of the defect. After capturing this view, a ring of pipe slightly wider than corrosion defect #1 was cut from the test vessel, and pipe located circumferentially to this corrosion patch was cut away. Figure 33b shows a view of the ID surface that captures the ID origin of the leak path. The width associated with this origin is characteristic of a planar lack of fusion (LOF) weld defect. Tight cracking is located on either side of this LOF feature, which lies toward the mid-width of the simulated corrosion patch.

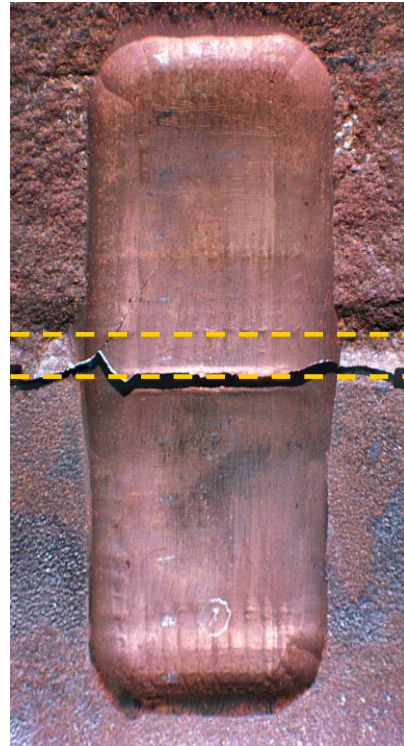
After capturing this view, saw cuts were made from either side of the leak path toward the area where the cracking from the leak path terminates. The ends of the saw-cuts are evident in Figure 33c as the square-ended slots at either side of this crack plane through the leak-path. This figure also shows the leak-path exposed by fracture of the ligament remaining between the ends of saw-cuts made from either edge while the steel remained close to LN₂ temperature. Again, the location of the weld is shown relative to this fracture plane by the dashed lines. In reference to the view in Figure 28b, this leak path and the fracture plane that opens it for study run through the heat-affected zone (HAZ) created in making the SSAW.

Figure 33d shows details of the ID surface along the fracture plane created to open the leak-path for study. The location of the weld is shown in this view by the dashed line, while the leak-path is circled. Note from this view that there are large pieces of flash located at either end of the leak-path. The presence of the LOF feature that served as the ID origin for leak and other similar features is particularly significant for this patch of corrosion because the wall thickness is locally equal to 30-percent of the net wall. Because the wall is locally reduced, nominally shallow root defects (~five to ten-percent of the full wall thickness) that are otherwise inconsequential in the full pipe wall, or in shallower corrosion, become significant in deep corrosion wherein they become about one-third the thickness. Thus, these features have a significant depth relative to the net thickness, and a large strain concentration in this locally thinner wall. As such, while such defects are scattered along the SSAW, such planar features are significant only in the presence of a much reduced wall thickness. It is because such features become structurally significant where corrosion reduces the wall thickness that criteria for blunt metal-loss should not be applied where such cracking might exist, consistent with current code restrictions and the guidelines of Task 4.

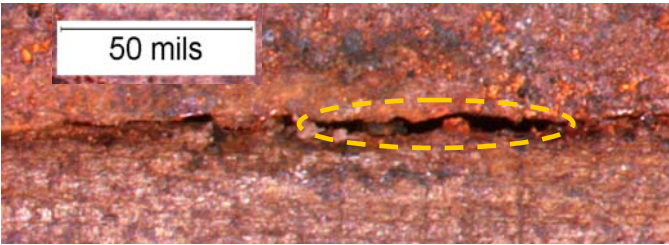
Features local to the origin indicate brittle-like response, with cracking developing on a plane perpendicular to the pipe wall. Such behavior is consistent with the presence of locally high constraint. However, constraint by itself does not drive this failure. Rather, locally high stress intensity develops because the crack-like defect has a depth equal to roughly one-third the wall



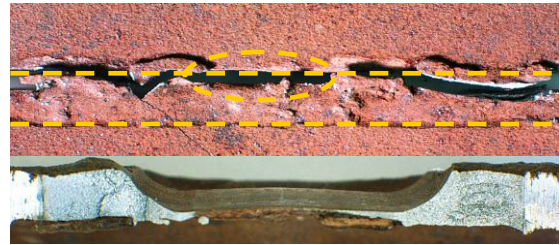
a) view of the leak-path (circled)



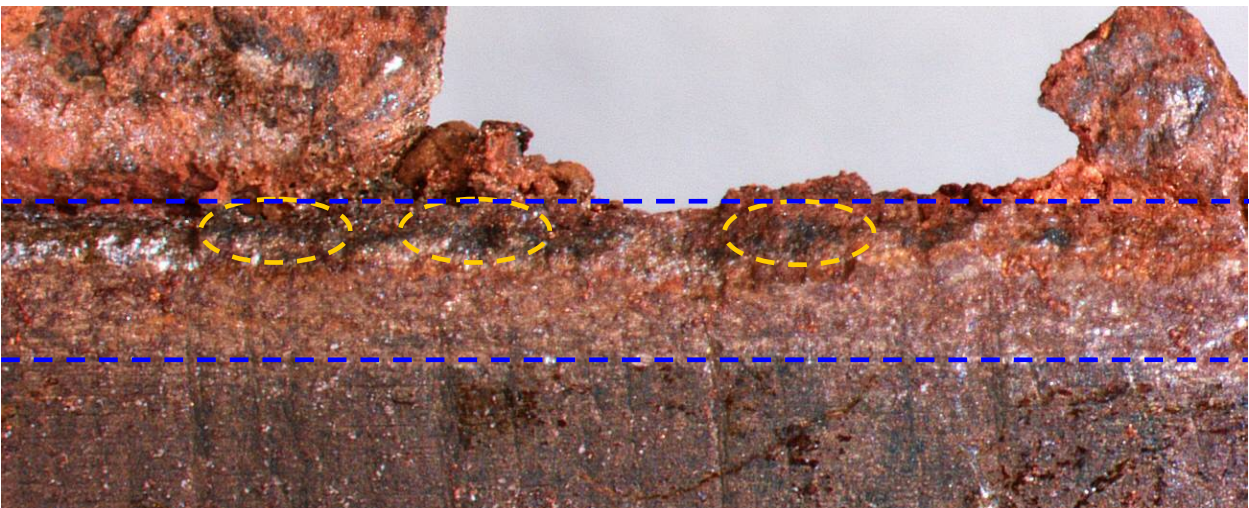
c) view of the leak-path broken-open



b) detail of the leak-path (circled) from the ID



d) details of the leak path and opened crack



e) leak path after opening to illustrate origins (circled) in net wall (dashed lines)

Figure 33. Features of the origins for the leak through corrosion defect #1

thickness. The view in Figure 33e, which shows the net local wall thickness between dashed lines, indicates nested thumbnails immediately surrounding these defects. These nested features indicate cracking nucleated and grew stably from these features, and was locally contained at lower pressures. As the pressure increased the cracking enlarged over a series of steps evident as nested crack fronts that are clearly evident at higher magnification.

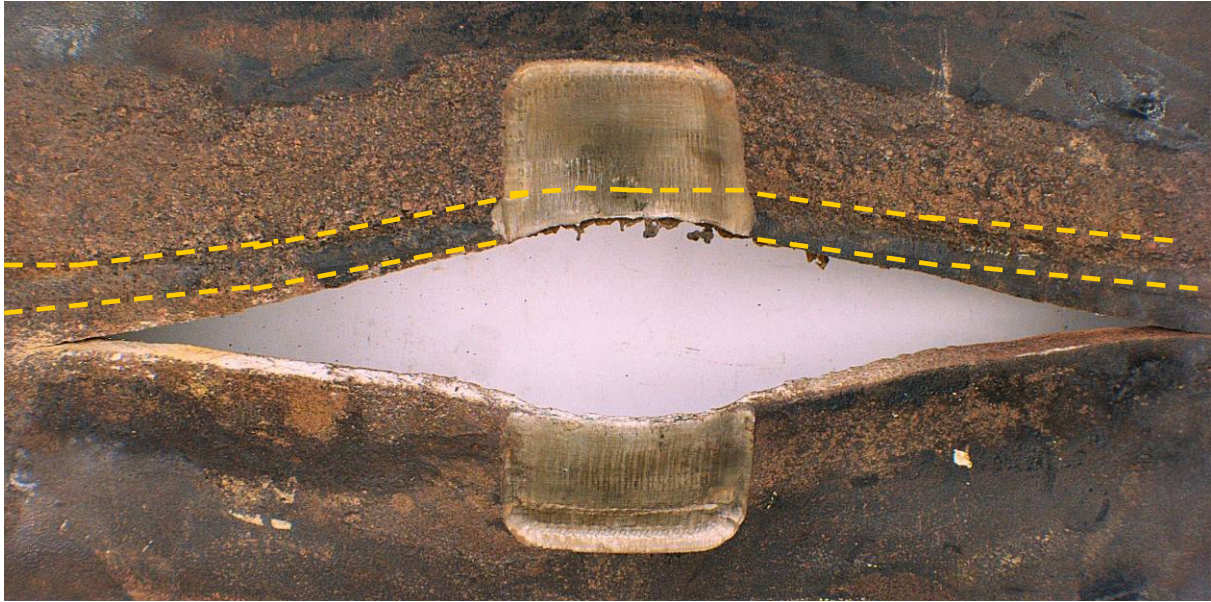
Stable growth such as this is possible in the load (pressure)-controlled line pipe because this nucleation and early growth develops initially under displacement control created by the gradient field local to the LOF features. However, as pressure increases and the crack-tips grow beyond the gradient field of the defects, these thumbnails interact and coalesce axially. This process can continue with stable growth in the local bending field due to bulging as a through-wall leak path forms so long as the toughness is sufficient to contain the cracking. Alternatively, growth can become unstable as a long critical defect length develops through coalescence or through-wall growth. Because such growth is load (pressure) controlled in a pipeline, critical length defects split axially leading to rupture. In the case of defect #1, the wall was breached and the pressure released at the crack tip before the length became critical. Had there been several such crack-like defects located sufficiently close to interact axially, a rupture could have developed.

The crack-like defects in the weld seam serve as local strain concentrations, which when coupled with the high geometric constraint and stress-state induced constraint at and along the tips of these features promotes crack nucleation at pressures less than would occur absent the constraint. Such nucleation and its growth in this scenario are plausible because the reduced toughness of the weld deposit permits it. Had the toughness been locally higher, crack nucleation and or growth would have been deferred to a higher pressure, as higher local strain would have been required to nucleate such cracking and continue its growth to a critical size. On this basis, high stress intensity and constraint at crack-like defects is the root cause of the cracking that leads to this leak, where nucleation and continued growth is facilitated by lower toughness.

Corrosion Defect #2

The origin for the rupture at defect #2 is similar to that for defect #1, except for a few key differences. First, the origin for #2 is small pockets of volumetric defects due to weld porosity as opposed to planar defects. Like the planar defects, these volumetric features were located toward the ID side of the SSAW, in areas where integral flash had formed along the ID surface. These volumetric features are evident in Figure 34. While volumetric rather than planar as was the case for the crack-like origin that caused failure for corrosion patch #1, their shape remains capable of developing constraint – but it does so absent the high local stress intensity that developed because of a planar defect whose depth was the order of one-third the wall thickness. Thus, this failure process involves constraint absent cracking.

Figure 34a presents an overview of the rupture that develops from simulated corrosion defect #2. The location of the weld is roughly indicated in this view by the dashed lines. Note that the origin for the split lies along the weld-seam interface with the body of the pipe, as did the origin for defect #1. While the origin for failure lies along the weld seam, the split does not propagate along this interface but quickly shifts into the pipe body, with growth occurring in a ductile mode on a macroscopic shear plane. That cracking shifts from the weld seam and continues axially into and along the pipe body indicates that the weld seam is locally tougher in this direction than is the body.



a) view of the rupture from the simulated corrosion defect



b) fracture plane and cracking (thumbnail feature in rightmost circle – voids in the other circle)



c) voids and nested thumbnails just visible (spatter from torch cutting also evident)

Figure 34. Features of the origins for the rupture at corrosion defect #2

Porosity that originates failure is evident in Figure 34b, as are small thumbnail features that emanate from the flash where it is attached to the ID of the seam. Some of the porosity was spaced axially such that these features could interact and coalesce. Higher magnification views show this porosity is surrounded by thumbnail features that indicate this cracking initiates and grows stably initially. Such is also the case for the thumbnail feature emanating from the flash interface. Fractography indicates these thumbnails interact and coalesce as the load (pressure) increases, until a through-wall leak path forms or a critical length is reached. In this case, the length of coalesced cracking becomes critical prior to leaking, which means rupture ensues. Where there is only one isolated spot of porosity, or the porosity is spaced to preclude axial interaction, this type of origin could have failed as a leak. The porosity serves as a local strain concentration that when coupled with the high constraint facilitates crack nucleation. Such is possible because the toughness of the weld admits cracking rather than promoting blunting, which would locally drive stress and strain redistribution, as would occur at higher toughness that in turn would sustain higher pressure and more closely approach plastic collapse.

Features local to the origin indicate brittle-like response, whereas continued axial extension was more ductile. As above, had the toughness been higher, cracking would have been deferred to a higher pressure, as higher local driving force would have been required to nucleate or sustain such cracking. On this basis, constraint at porosity facilitates nucleation and growth, but at a pressure higher than where crack-like defects couple with constraint.

Corrosion Defect #3

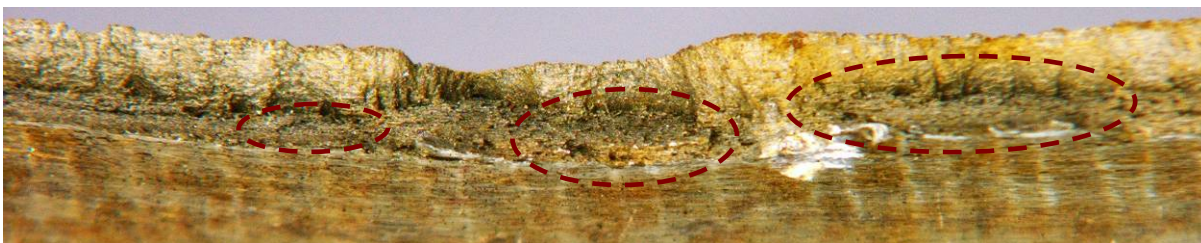
While the origin for failure at defect #2 and defect #1 involved blunt and sharp weld-seam defects, respectively, the failure at defect #3 occurs remote to the weld seam – in spite of the fact that the defect was centered over the seam. While failure occurred remote to the weld, the seam did experience extensive but localized co-linear and co-parallel cracking over an axial distance of a few inches. As evident in Figure 35, the failure involved local cracking apparently starting from or close to the free surface rather than contained well within the thickness as occurs more typically with void nucleation and growth that underlie tensile instability. As such, this failure could reflect a fracture-controlled origin, rather than plastic collapse, which is required for use of RSTRENG (equally Modified B31G), and underlies the formulation of the recently developed corrosion criteria⁷. Consideration of the failure pressure, which occurs at the order of the UTS, indicates failure is collapse controlled.

Figure 35a presents an overview of the rupture that develops from simulated corrosion defect #3. The location of the weld, as is roughly indicated in this view by the dashed lines, lies well remote to the origins for cracking. This is in contrast to the origins for the split in defect #2 or the leak-path in #1 that lay along the weld-seam interface with the body of the pipe. As was the case for the split in defect #2, the split does not propagate toward or along the interface between the seam weld and the body, but rather runs in the pipe body, with growth occurring in a ductile mode on a macroscopic shear plane.

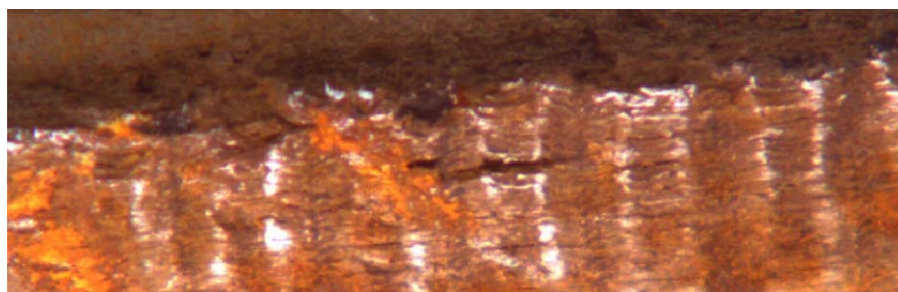
⁷ Crack nucleation occurs along the weld seam here as it did for defects #1 and #2, but this cracking does not control the failure as continuous nucleation also occurs in the root of the radius that forms the simulated corrosion. As longer but shallower cracking becomes critical at pressures less than deeper but much shorter cracking, failure was triggered along the boundary of the corrosion, away from the weld seam.



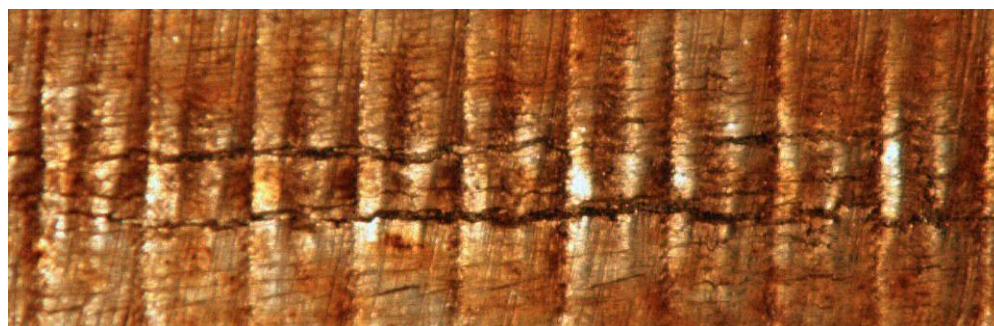
a) view of the rupture from the simulated corrosion defect



b) fracture plane and OD cracking (thumbnail features circled)



b) secondary cracking parallel and adjacent to the fracture plane



c) secondary cracking along, in, and adjacent to the SSAW seam

Figure 35. Features of the origins for the rupture at corrosion defect #3

The view in Figure 35b shows several typical thumbnail shaped features that apparently served as origins. Higher magnification views made after cleaning these features show nested crack fronts that indicate this cracking initiates near the surface and grows stably initially, until a through-wall leak path forms or a critical length is reached. In the case of defect #3, the length became critical prior to leaking, which meant rupture ensued. Absent local defects like porosity or crack-like features, such failures develop absent local strain concentration or the effects of geometric or stress-state induced constraint. Crack nucleation occurs more broadly, representing the fracture resistance of the steel rather than the influence of defects and constraint on those properties. Such cracking is evident in Figure 35c as secondary cracking adjacent to the main fracture plane. Secondary cracking parallel to the main fracture also is evident in the vicinity of the SSAW seam, as shown in Figure 35d. As this cracking shows significant evidence of local stretching, this failure likely reflects a balance between fracture and collapse-controlled failure that the failure pressure shows is dominated by collapse.

Because this failure occurs remote to the weld, it reflects the inherent properties of the steel in the pipe body rather than the potential effects of reduced toughness or constraint associated with the weld. Absent the local effects of defects and constraint associated with the SSAW, and given the presence of incipient cracking along the failure plane and elsewhere, it is likely this failure reflects the transition from fracture-controlled failure to collapse-controlled failure. This likelihood can be evaluated in reference to comparison of the actual failure pressure and that predicted by plastic collapse. Table 2 indicates the failure pressure for this case corresponds well with collapse-based predictions. On this basis, one can conclude fracture did not intervene and that collapse controls this failure. This implies that evidence of crack nucleation and growth as discussed above in reference to Figures 35c and 35d is secondary, being triggered by the large strains developed en route to collapse. These results are consistent with the guidelines presented in Task 4.

Summary for Task Five

Task Five involved testing to evaluate the concepts identified and demonstrate their viability. Full-scale testing whose scope targeted these aspects was designed and completed. Key observations and conclusions that follow from this testing include:

- full-scale testing demonstrates that blunt corrosion overlaid on crack-like defects or areas of high constraint in lower-toughness line pipe can fail at pressures less than that predicted by the 1970s criteria (e.g., RSTRENG) and the 1990s criteria (e.g., PCORRC),
- failure at defects is not triggered by lower toughness, but rather by high local stress intensity or shape or loading that promotes constraint that promotes crack nucleation and growth from the defect,
- for the present, the defects promoting constraint were weld-seam related – but, because natural corrosion includes pitting that develops comparable size and shape, and so equal constraint, care should be taken in characterizing corrosion to identify such features,
- for the present testing, the relative toughness was low enough to admit crack nucleation and growth, such that lower toughness facilitates this failure but constraint and crack-like features are the root cause – where the toughness is high, cracking is deferred to higher pressures that in the limit occur under collapse control rather than fracture control,

- because the value of toughness that facilitates cracking depends on the nature of the defect, one cannot a priori state a toughness level below which such cracking will not occur – but one can identify potential features of concern based on appropriate in-line inspection logs or field digs,
- absent high constraint or crack-like defects, criteria from the 1970s are very conservative even for this vintage line pipe – in contrast criteria from the 1990s are just conservative, whereas all such criteria referenced to SMTS would produce more or less similar results, and
- consideration should be given to additional full-scale testing and related fractographic analysis to better define conditions where constraint are a factor, and to more fully demonstrate the utility approaches that balance conservatism on failure pressure with the need for accuracy in applications to predicting allowable defect sizes.

Summary, Commentary, and Conclusions

As noted in the introduction, corrosion assessment criteria evolved empirically beginning in the 1970s whose applicability restricted their use to line pipe whose toughness was “adequate” or “not significant” in the possible failure of the defect – apparently to ensure plastic-collapse controlled failure. As time passed, it became clear these criteria embedded significant conservatism that remained in spite of modifications to reduce it. Given their roots in plastic-collapse, and motivated by the desire to understand and reduce sources for conservatism, alternative criteria more formally derived in terms of plastic-collapse began to appear in the 1990s. This left the industry with two sets of corrosion assessment criteria that while apparently sharing their roots in plastic collapse led to much different results. The choice of which criterion was appropriate was complicated by the fact that each set of criteria had an extensive validation database. This project has quantitatively evaluated these two sets of corrosion assessment criteria to establish which is valid as a function of characteristic geometric features of the corrosion, as well as the vintage, grade and other metrics of the line pipe and the pipeline’s service and loading. Consideration was given to the mathematical form of these criteria, their “validation” databases, the corrosion geometry, the line-pipe properties, and other factors through use of numerical and analytical techniques and demonstration full-scale testing.

Important observations and conclusions follow first in regard to the demonstration testing, and then through the other elements of the project:

- constraint alone and coupled with crack-like defects affected significant differences in the burst pressure of the test vessels,
- macroscopically blunt corrosion in the presence of very small focused constraint coupled with very small crack-like features can cause failure at pressures much less than predicted by even conservative corrosion assessment criteria (e.g., at 74-percent of an RSTRENG prediction) – this observation supports code restrictions against use of plastic-collapse-based criteria in applications where stress raisers, constraint, or cracking may be present,
- absent constraint effects or where constraint develops in thicker sections and so was less structurally significant, macroscopically blunt corrosion failed at pressures as high as 145-percent of that predicted by the 70s criteria in vintage line pipe, but almost exactly by use of 1990s criteria,

- while a SSAW vintage weld was used to develop constraint features, their shapes and sizes could easily be found in naturally occurring patches of pitting corrosion such that constraint should be a consideration in evaluating metal-loss defects,
- constraint can for earlier vintage steels affect a shift to fracture controlled failure, and so lead to much lower failure pressures – this transition is not due to lower toughness, but rather by high local stress intensity or shape or loading that promotes constraint that promotes crack nucleation and growth from the defect – where the toughness is high, cracking is deferred to higher pressures that in the limit occur under collapse control rather than fracture control,
- all corrosion assessment criteria – whether empirically developed in the 1970s or formulated by trending numerical results in the 1990s had the same form: $S_f = C \cdot S_R \cdot \{f(\text{defect geometry})\}$,
- with this mathematical form, when there is no defect present the term $f(\text{defect geometry})$ is by definition one, which means the product of C and S_R in this function must be equal to the UTS, or empirically equal to the hoop-stress in a burst-test of defect-free line pipe, which was found to equal the UTS,
- the flow-stress adopted for the 70s criteria causes a conservative bias in excess of 25-percent on failure pressure,
- use of an SMYS-based flow stress rather than the UTS is the primary difference between 1970s criteria and 1990s plastic-collapse-based criteria,
- a conservative bias in predicted failure pressure can cause non-conservative predictions in remaining defect size and in re-inspection interval,
- no practical difference exists in the way defect geometry is quantified by the 1970s versus 1990s criteria when UTS is used as a reference stress,
- line-pipe steel fracture resistance is strongly constraint dependent,
- a generic expression for constraint corrected fracture resistance was formulated and validated experimentally at the scale of laboratory specimens and pipelines,
- the divergence between collapse and fracture analysis as a function of toughness and constraint can be used to identify combinations of high constraint and lower toughness that are a practical concern for failure at corrosion,
- SMYS is uncorrelated with the actual failure stress for early as well as modern vintage data, whereas the UTS correlates very well with the actual failure stress, and is free of bias in grade or vintage,
- when the UTS was used as a reference stress, the effects of corrosion geometry were similarly predicted by the 1970s and 1990s criteria,
- consequently, when the 1970s criteria are referenced to SMTS, comparable predictions are anticipated to those of the 1990s criteria, with no need to discriminate one set of criteria as appropriate or better,
- SMTS referenced to a standard whose vintage is compatible with the application (e.g., API 5L) is a viable reference stress, whose use in the 1970s and 1990s criteria produces mutually compatible results consistent with the full-scale database,
- constraint is evident in the full-scale vintage corrosion database as a cause for clearly non-conservative predictions for both the 1970s and 1990s criteria,

- analysis shows that plastic-collapse based predictions are viable at FSECVP energies the order of ~20 ft-lb (27 J) absent concern for constraint and crack-like defects,
- until further analyses better quantifies “high constraint”, corrosion features involving spherical pits within pits, spherical pits whose in-plane size is the order of the wall thickness, and near conical pits should be viewed with concern – of course, crack-like feature or local stress concentration other than due to the metal loss are not addressed by such criteria.
- where crack-like features and constraint or high tensile residual stresses cannot be excluded, fracture mechanics analysis that addresses such aspects should be considered in lieu of either a 1970s or a 1990s corrosion criterion, and
- because of concerns related to crack-like defects and stable tearing within usual corrosion features, applications involving large-amplitude frequent pressure cycling should be avoided unless accompanied by a related engineering critical assessment.

Recommendations

Four recommendations emerge from this work that involve a mix of experiments and analysis to better determine the applicability and utility of corrosion assessment criteria found to be mutually consistent and conservative in reference to SMTS as a reference stress, as follows:

- the divergence between collapse and fracture analysis as a function of toughness and constraint should be used to identify combinations of high constraint and lower toughness that are a practical concern for failure at corrosion,
- better quantify “high constraint” in practical terms that couple the effect of constraint with toughness in reference to specified shapes and sizes of corrosion features that are problematic, might be problematic, or are never problematic in terms of ILI or other parameters,
- some combinations of defect shape and size, including short and deep single defects, are not well characterized analytically, which is also true to some extent for interacting defects – sufficient archival data exist to validate the outcome of such analysis, with the added benefit of better quantifying the role of defect size and shape, and the role of measurement practices in regard to the vintage pipeline corrosion database,
- consideration should be given to additional full-scale testing and related fractographic analysis to confirm conditions where constraint is a factor, and to more fully demonstrate the utility approaches that balance conservatism on failure pressure with the need for accuracy in applications to predicting allowable defect sizes.

References

1. Pourbaix, M., "Thermodynamics of Dilute Aqueous Solutions," PhD Thesis, Technical University Delft, 1938.
2. Faraday, M., "Faraday's (Second) Law of Electrolysis," 1834.
3. Bacon, D. A., "Rehab Projects Use Current Stripping and Coating Procedures," *Oil & Gas Journal*, March 11, 1991.
4. Clark, T. B. and Colwell, J. A., "ECDA Inspections and Excavations," PRCI Catalog No. L52123, July 2005.
5. Anon., "Panhandle Lines," Panhandle monthly employee publication, Volume 21, No. 11, Kansas City, MO, June 1964.
6. Atterbury, T. J. and Duffy, A. R., Battelle correspondence to Texas Eastern Transmission Corporation concerning Project BAT 216, January 1970.
7. Keifner, J. F. and Duffy, A. R., "Summary of Research to Determine the Strength of Corroded Areas in Line Pipe," Battelle Interim Report to Texas Eastern Transmission Corporation, July 1971.
8. Keifner, J. F. and Atterbury, T. J., "Investigation of the Behavior of Corroded Line Pipe," Project 216 Interim Report, February 1971.
9. Keifner, J. F., Duffy, A. R., and Atterbury, T. J., "Optimization of Capability to Predict Remaining Strength," Project 216 – Investigation of the Behavior of Corroded Line Pipe Phase III Report, March 1971.
10. Kiefner, J. F. and Duffy, A. R., "Criteria for Determining the Strength of Corroded Areas of Gas Transmission Lines," Paper T, American Gas Association Operating Section on Transmission Conference, AGA, 1973, pp. T86-T91.
11. B31G American National Standards Institute (ANSI)/American Society of Mechanical Engineers (ASME) B31G "Manual for Determining the Remaining Strength of Corroded Pipelines," 1984.
12. Kiefner, J. F. and Vieth, P. H., "A Modified Criterion for Evaluating the Remaining Strength of Corroded Pipe," Final Report on Project PR 3-805 to the Pipeline Research Committee, December 1989.
13. Kiefner, J. F., Vieth, P. H., and Roytman, I., "Continuing Validation of RSTRENG," Pipeline Research Supervisory Committee, A.G.A. Catalog No. L51689, 1996; see also Vieth, P. H. and Kiefner, J. F., "RSTRENG User's Manual and Software," A.G.A. Catalog No. L51688 and L51688A, March 1993.
14. Coulson, K. E. W. and Worthingham, R. G., "Standard Damage-Assessment Approach is Overly Conservative," *Oil and Gas Journal*, April 9, 1990, and "New Guidelines Promise more Accurate Damage Assessment," *Oil and Gas Journal*, April 16, 1990.
15. Chouchaoui, B. A., Pick, R. J., and Yost, D. B., "Burst Pressure Predictions of Line Pipe Containing Single Corrosion Pits using the Finite Element Method," OMAE-92, 11th International Conference on Offshore Mechanics and Arctic Engineering, Calgary Alberta, June 7, 1992.
16. Hopkins, P. and Jones, D. G., "A Study of the Behavior of Long and Complex-Shaped Corrosion in Transmission Pipelines," British Gas plc, OMAE-92-1004, ASME, 1992.

17. Fu, B. and Kirkwood, M. G., "Determination of Failure Pressure of Corroded Linepipes Using the Nonlinear Finite Element Method," Pipeline Technology, Vol. II, R. Denys, Ed., Elsevier Science B V, 1995, pp. 1-12.
18. Ritchie, D. and Last, S., "Burst Criteria of Corroded Pipelines – Defect Acceptance Criteria," EPRG/PRC 10th Biennial Joint Technical Meeting on Line pipe Research, Cambridge, UK, April 18-21, 1995, paper No.32.
19. Smith, M. Q. and Grigory, S. C., "New Procedures for the Residual Strength Assessment of Corroded Pipe Subjected to Combined Loads," First International Pipeline Conference (IPC 1996), Calgary, ASME, June 1996, pp. 387-400.
20. Batte, A. D., FU, B., Kirkwood, M. G., and Vu, D., "A New Method for Determining the Remaining Strength of Corroded Pipelines," 16th International Conference on Offshore Mechanics and Arctic Engineering (OMAE 1997), ASME, Yokohama, April 1997.
21. Leis, B. N. and Stephens, D. R., "An Alternative Approach to Assess the Integrity of Corroded Line Pipe – Part I: Current Status," Volume 4, 7th International Offshore and Polar Engineering Conference, Honolulu, HI, May 1997, pp 624-634.
22. Leis, B. N. and Stephens, D. R., "An Alternative Approach to Assess the Integrity of Corroded Line Pipe – Part II: Alternative Criterion," Volume 4, 7th International Offshore and Polar Engineering Conference, Honolulu, HI, May 1997, pp 635-641.
23. Stephens, D. R., Leis, B. N., Kurre, J. D., and Rudland, D. L., "Development of an Alternative Failure Criterion for Residual Strength of Corrosion Defects in Moderate- to High-Toughness Pipe," Battelle report to PRC International, PRCI Catalog Number L51794, January 1999.
24. Bjornoy, O. H., FU, B., Sigurdsson, G., Cramer, E. H., and Ritchie, D., "Introduction and Background to DNV-RP-F101 – Corroded Pipelines," International Conference on Offshore and Polar Engineering, ISOPE'99, Brest, France, 1999.
25. Stephens, D. R. and Leis, B. N., "Development of an Alternative Criterion for Residual Strength of Corrosion Defects in Moderate- to High-Toughness Pipe," International Pipeline Conference 2000, Calgary, IPC00-0019, 2000.
26. Jones, C. L., Fu, B., Stephens, D., and Ritchie, D., "Improved Methods for Assessment of Remaining Strength of Corroded Pipelines," Project Number: PR-273-9803, Catalog Number: L51878, April 2002.
27. Leis, B. N., Clark, E. B., Zhu, X. -K., and Galliher, R. D., "Guidelines for Assessing Corrosion Associated with Girth and Long-Seam Welds," PRCI Catalog Number L52009, October 2004.
28. Anon., ASME Code Supplement on Integrity Management for Pressure Piping, ASME B31.8S, Revision 1, 2002.
29. Anon., Code of Federal Regulations, Title 49-Transportation, Part 192 and Part 195.
30. Anon., "ASME Code For Pressure Piping, B31: B31.4 Liquid Petroleum Transportation Piping Systems and B31.8 Gas Transmission and Distribution Piping Systems," 2002.
31. Anon., "Specification for Line Pipe," API Specification 5L, 2004.
32. Anon., "Fitness-for-Service," API 579, January 2000.

33. Wilkowski, G., Stephens, D., Krishnaswamy, P., Leis, B., and Rudland, D., "Progress in Development of Acceptance Criteria for Local Thinned Areas in Pipe and Piping Components," *Nuclear Engineering and Design*, Vol. 195, pp 149-169, 2000.
34. McGehee, W. B., "Maximum Allowable Operating Pressure Background and History," Attachment E, June 1998, pp. E3 - E12 in Shires, T. M. and Harrison, M. R., "Development of The B31.8 Code and Federal Pipeline Safety Regulations: Implications for Today's Natural Gas Pipeline System," GRI-98/0367, December 1998.
35. Neil, B. G., The Plastic Methods of Structural Analysis, Chapman and Hall Ltd., Great Britain, 1963.
36. Anon., Plastic Design of Braced Multistory Steel Frames, American Institute of Steel Construction, American Iron and Steel Institute, New York, NY, 1968.
37. Yukawa, S., "ASME Nuclear Code Applications of Structural Integrity and Flaw Evaluation Methodology," in Structural Integrity Technology, ASME, 1979, pp. 29-38: see also Marshall, P. W., "Strategy for Monitoring, Inspection and Repair for Fixed Offshore Platforms," in Structural Integrity Technology, ASME, 1979, pp. 97-110.
38. Maxey, W. A., Kiefner, J. F., Eiber, R. J., and Duffy, A. R., "Ductile Fracture Initiation, Propagation and Arrest in Cylindrical Vessels," ASTM STP 514, American Society for Testing and Materials, Philadelphia, PA, 1972, pp. 70-81.
39. Shih, C. F., German M. D., and Kumar, V., "An Engineering Approach for Examining Crack Growth and Stability in Flawed Structures," G. E. Report No. 80CRD205, August 1980.
40. Schwalbe, K.-H., et al, "EFAM ETM 97 – The ETM Method for Assessing the Significance of Crack-Like Defects in Engineering Structures," GKSS 98/E/6, 1998.
41. Kiefner, J. F., Rosenfeld, M. J., Maxey, W. A., Vieth, P. H., and Orban, J. E., "Rationale for Corroded Pipe Removal Priorities," to Texas Eastern Gas Pipeline Company, June 30, 1988.
42. Fu, B. and Batte, A. D., "Advanced Methods for the Assessment of Corrosion in Linepipe," Health and Safety Executive Summary Report, HSE Books, OTO 1999-051, 1999.
43. Sigurdsson, G., Cramer, E. H., Bjornoy, O. H., Fu, B., and Ritchie, D., "Background to DNV-RP-F101 – Corroded Pipelines," Proceedings of the 18th International Conference on Offshore Mechanics and Arctic Engineering, ASME, (OMAE 1999), Newfoundland, July 1999.
44. Bjornoy, O. H., Sigurdsson, G., and Cramer, E. H., "Residual Strength of Corroded Pipelines, DNV Test Results," Tenth International Conference on Offshore and Polar Engineering (ISOPE 2000), Seattle, WA, May 2000.
45. Anon., DNV-RP-F101, "Corroded Pipelines," Det Norske Veritas, 1999.
46. Leis, B. N., private communication with O. H. Bjornoy during prepublication commentary on Reference 45, 1998.
47. Kiefner, J. F. and Zelenak, P. A., "Comparison of the Accuracy of Nine Methods for Determining the Remaining Strength of Corroded Line Pipe," Final Report to Winmar Consulting Services, October 2002.
48. Leis, B. N., private communication with Bin Fu, British Gas, 2001.
49. Kiefner, J. F., Maxey, W. A., and Eiber, R. J., "A Study of the Causes of Failures of Defects That Have Survived a Prior Hydrostatic Test," NG-18 Report No. 111, November 1980.

50. Keshevan, S., "Some Studies on the Deformation and Fracture of Normalized Mild Steel Under Cyclic Conditions," PhD Thesis, University of Waterloo, 1967.
51. Pope, D. H., Dziejewski, D., and Frank, J. R., "Recent Advances in Understanding Microbiologically-Influenced Corrosion in the Gas Industry, and New Approaches to Mitigation", AGA Distribution and Transmission Conference, Los Angeles, 1990.
52. Joyce, J. A. and Link, R. E., "Effects of Constraint on Upper Shelf Fracture Toughness," Fracture Mechanics: 26th Volume, ASTM STP 1256, American Society for Testing and Materials, Philadelphia, pp.142-177, 1995.
53. Joyce, J. A. and Link, R. E., "Application of Two Parameter Elastic-Plastic Fracture Mechanics to Analysis of Structures," *Engineering Fracture Mechanics*, **57**, pp.431-446, 1997.
54. Neimitz, A., Dzioba, I., Galkiewicz, J. and Molasy, R., "A Study of Stable Crack Growth Using Experimental Methods, Finite Elements and Fractography," *Engineering Fracture Mechanics*, Vol. 71, pp.1325-1355, 2004.
55. Dodds, R. H., Anderson, T. L., and Kirk, M. T., "A Framework to Correlate a/W Effects on Elastic-Plastic Fracture Toughness," *International Journal of Fracture*, Vol. 48, pp. 1-22, 1991.
56. O'Dowd, N. P. and Shih, C. F., "Family of Crack-Tip Fields Characterized by a Triaxiality Parameter – I: Structure of Fields," *Journal of the Mechanics of Physics and Solids*, 39, pp.989-1015, 1991, and "Family of Crack-Tip Fields Characterized by a Triaxiality Parameter – II. Fracture Applications," *ibid*, 40, 1992, pp.939-963.
57. Yang, S., Chao, Y. J. and Sutton, M. A., "Higher-Order Asymptotic Fields in a Power-Law Hardening Material," *Engineering Fracture Mechanics*, 45, 1993, pp.1-20.
58. Chao, Y. J., Yang, S. and Sutton, M. A., "On the Fracture of Solids Characterized by One or Two Parameters: Theory and Practice," *Journal of the Mechanics of Physics and Solids*, 42, 1994, pp.629-647.
59. Kim, Y., Zhu, X. -K. and Chao, Y. J., "Quantification of Constraint Effect on Elastic-Plastic 3D Crack Front Fields by the J-A2 Three-Term Solution," *Engineering Fracture Mechanics*, 68, 2001, pp.895-914: see also Chao, Y. J., Zhu, X. -K., Lam, P. S., Louthen, M. R. and Iyer, N. C., "Application of the Two-Parameter J-A2 Description to Ductile Crack Growth," ASTM STP 1389, G. R. Halford and J. P. Gallagher Eds., American Society for Testing and Materials, 2000, pp.165-182.
60. Chao, Y. J., Zhu, X. -K., Kim, Y., Lam, P. S., Pechersky, M. J. and Morgan, M. J., "Characterization of Crack-Tip Fields and Constraints for Bending Specimens under Large-Scale Yielding," *International Journal of Fracture*, 127, 2004, pp.283-302.
61. Shen, G., Tyson, W. R., Glover, A., and Horsley, D., "Constraint Effects on Linepipe Toughness," 4th International Conference on Pipeline Technology, Oostende, Volume 2, May 2004, pp.703-720.
62. Rice, J. R. and Rosengren, G. F., "Plane Strain Deformation Near a Crack Tip in a Power Law Hardening Material," *Journal of the Mechanics of Physics and Solids*, 16, 1968, pp.1-12.
63. Hutchinson, J. W., "Singular Behavior at the End of a Tensile Crack in a Hardening Material," *Journal of the Mechanics of Physics and Solids*, 16, 1968, pp.13-31.

64. Chao, Y. J. and Zhu, X. -K., "J-A2 Characterization of Crack-Tip Fields: Extent of J-A2 Dominance and Size Requirements," *International Journal of Fracture*, 89, 1998, pp.285-307: see also Chao, Y. J. and Zhu, X. -K., "Constraint-Modified J-R Curves and Its Applications to Ductile Crack Growth," *International Journal of Fracture*, 106, 2000, pp.135-160.
65. Glover, A. G., "Small and Full Scale Fracture of Thick Section Girth Weldments," PRCI Project PR-140-512, PRCI Cat. L51533, March 1987.
66. Pisarksi, H. G. and Wifnall, C. M., "Fracture Toughness Estimation for Pipeline Girth Welds," Proceedings of the 4th International Pipeline Conference, Calgary, September 2002.
67. Hippert, E., Dotta, F. and Ruggieri, C., "Structural Integrity Assessment of Pipelines Using Crack Growth Resistance Curves," Proceedings of the 4th International Pipeline Conference, Calgary, September 2002.
68. Pavankumar, T. V., Chattopadhyay, J., Dutta, B. K. and Kushwaha, H. S., "Transferability of Specimen J-R Curve to Straight Pipes with Through-wall Circumferential Flaws," *International Journal of Pressure Vessels and Piping*, 79, 2002, pp.127-134.
69. ASTM E 1820-01, "Standard Test Method for Measurement of Fracture Toughness," American Society for Testing and Materials, West Conshohocken, PA, 2004.
70. Schwalbe, K. H., Cornec, A. and Baustian, K., "Application of Fracture Mechanics Principles to Austenitic Steels," *International Journal of Pressure Vessels and Piping*, Vol. 65, 1996, pp. 193-207.
71. Anon., "ABAQUS Standard User's Manual (version 6.4)," Hibbitt, Karlsson, and Sorensen, Inc., Pawtucket, RI, USA, 2004.
72. Chao, Y. J. and Zhang, L., "Tables of Plane Strain Crack Tip Fields: HRR and Higher Order Terms," Me-Report, 97-1, Department of Mechanical Engineering, University of South Carolina, 1997.
73. Lam, P. S., Chao, Y. J., Zhu, X. -K., Kim, Y. and Sindelar, R. L., "Determination of Constraint-Modified J-R Curves for Carbon Steel Storage Tanks," *Journal of Pressure Vessel Technology*, Vol. 125, 2003, pp.136-142.
74. Leis, B. N., Brust, F. W., and Scott, P. M., "Development and Validation of a Ductile Flaw Growth Analysis for Transmission Line Pipe," A. G. A. Catalog No. L51543, June 1991.
75. Leis, B. N. and Thomas, T. C., "Line-Pipe Property Issues in Pipeline Design and in Re-Establishing MAOP," 6th Pipeline Congress and International Exposition, PEMEX, Conference CD – Risk Section, Paper ARC-17, Mexico, 2001.
76. Leis, B. N., "Hydrostatic Testing of Transmission Pipelines: When It Is Beneficial and Alternatives When It Is Not," PRCI Final Report PR 3-9523, 2002.